NTNU

Norwegian University of
Science and Technology

The Effect of Small-Scale Heterogeneities on the Gas Distribution in the Tubåen Formation through Upscaling of CO_2-Brine Relative Permeability

Sofie Annesdotter Svartdal Berge

Petroleum Geoscience and Engineering
Submission date: June 2017
Supervisor: Per Arne Slotte, IGP
Co-supervisor: Philip Ringrose, IGP

Norwegian University of Science and Technology
Department of Geoscience and Petroleum

Abstract

The Tubåen Formation in the Norwegian Sea is an aquifer and was used by Statoil ASA as the injection reservoir for CO_2 separated from produced gas at Snøhvit in the time period between April 2008 until it was abandoned in April 2011. The CO_2 injection and plume development is currently described with a simulation model using only one set of isotropic, un-scaled flow functions, i.e. the potential for a more accurate simulation model is great. This thesis investigate how upscaled flow functions affect the dynamic behaviour in the reservoir. Different upscaling techniques are used and compared by looking at how they affect the CO_2 plume development in the formation. All models used in this thesis are the property of Statoil ASA.

Lithofacies models with small scale hetereogeneities typical for the Tubåen formation, Wavy and Flaser, are made to fit each of the zones in Tubåen before the flow functions are upscaled in the models using the upscaling techniques *Capillary Equilibrium* and *Viscous Limit*. The upscaling is performed by the Upscaling Module in the open source software *Open Porous Media*. The resulting relative permeability curves clearly show that the small scale heterogeneities and upscaling technique affect the two-phase flow. In the final step the upscaled flow functions are used in various combinations as input in the full scale simulation model of the Tubåen Formation. A set of models with various combinations of upscaled flow functions are made to be able to distinguish between geology effects in the reservoir and relative permeability effects on the CO_2 distribution. All models with upscaled curves are also compared to the *Basecase* with a single set of isotropic, un-scaled flow functions.

The results are that small scale geological heterogeneities, demonstrated by Wavy and Flaser bedding, are found to greatly affect the development of the plume, and most so Wavy bedding. The choice of upscaling technique, *Capillary Equilibrium* or Viscous Limit, is also found to be of great importance for the CO_2 distribution - especially in the gravitational dominated period after injection stop. The Capillary Equilibrium option shows a greater impact on the relative permeability curves than the Viscous Limit option, but both lead to reduced vertical relative permeability of CO_2.

Besides the upscaling work itself, the process of creating relative permeability curves for upscaling and adjusting the lithofacies models and the full scale model are described in detail.

Sammendrag

Tubåenformasjonen i Norskehavet er et vannreservoar som i tidsrommet April 2008 - April 2011 ble brukt av Statoil ASA for injisering og lagring av den adskilte CO_2-strømmen ved prosessering av produsert naturgass fra Snøhvit-feltet.

Den dynamiske oppførselen til den injiserte CO_2-en blir i dag beskrevet med en simuleringsmodell som bruker ett sett isotropiske, ikke-skalerte relative permeabilitets- og kapillærtrykkskurver - det er med andre ord et stort forbedringspotensiale. Denne masteroppgaven undersøker om relativ permeabilitet oppskalert med ulike oppskaleringsteknikker påvirker modelleeringen av gassplumen. Alle modellene brukt i oppgaven tihører Statoil ASA.

Lithofacies-modeller med småskala heterogeniteter typisk funnet i Tubåenformasjonen, Wavy og Flaser, blir justert for etter de ulike sonene i Tubåen før relativ permeabilitetskurvene blir oppskalert i både *Kapillær Likevekt* og *Viskøs Grense*. Oppskaleringen blir utført i oppskaleringsmodulen til programvaren *Open Porous Media*. De oppskalerte relativ permeabilitetskurvene viser klart at småskalaheterogeniteter og oppskaleringsmetode påvirker to-fase-strømningen. Til slutt blir de oppskalerte kurvene brukt i ulike kombinasjoner i fullskalamodellen av Tubåen. Modellene er satt sammen for å kunne skille geologieffekter og effekten av oppskalert relativ permeabilitiet. Alle modellene med oppskalert relativ permeabilitet blir sammenlignet med en *Basecase* med ett sett isotropiske, ikke-skalerte relative permeabilitets- og kapillærtrykkskurver.

Konklusjonen er at småskalaheterogeniteter, demonstrert av Wavy og Flaser, i stor grad påvirker hvordan gassen fordeler seg i reservoaret, spesielt Wavy som i stor grad reduserer strømningssevnen i vertikal retning. Valg av oppskaleringsmetode, Kapillær Likevekt eller Viskøs Grense, viser seg også å være viktig for CO_2-utspredelsen - spesielt i perioden etter injeksjonsstopp når modellen blir kjørt under påvirkning av bare tyngdekraften. Det er vist at Kapillær Likevekt-metoden har større påvirkning på relativ permeabilitetskurvene enn Viskøs Grense-metoden, men begge metodene fører til redusert vertikal relativ permeabilitet for CO_2.

I tillegg til oppskaleringsdelen, blir prosessen med å lage relativ permeabilitet- og kapillærtrykkskurvene som brukes i oppskaleringen forklart, samt hvordan lithofacies-modellene og fullskalamodellen ble justert.

Aknowledgement

This Master's thesis written in my 10th semester at the Department of Petroleum Engineering and Applied Geophysics at The Norwegian University of Science and Technology marks the end of the Master of Science program with specialization in Reservoir Technology and Petrophysics. The thesis was written in co-operation with Statoil ASA and I would like to thank them for letting me work with real data and models currently being used by the company.

I would like to thank my co-supervisor Prof. Philip Ringrose who came up with the idea for the thesis and my main supervisor, Assoc. Prof. Per Arne Slotte, for guidance throughout the semester.

Trondheim, 2017-06-10

Sofie A. Svartdal Berge

Contents

List of Figures

List of Tables

Chapter 1

Introduction

The gas produced from the Snøhvit natural gas field in the Norwegian sea originally contains about 5-8% CO_2 - which get separated from the sales gas before the liquefaction process at the onshore LNG plant at Melkøya.

Since April 2008 large volumes of CO_2 has been transported back from the LNG plant and re-injected into the sub-surface. The injection reservoir at Snøhvit was originally the shallow Tubåen formation where injections started April 18, 2008, but an evaluation of fall-off pressures, updated reservoir models and analysis of the rock mechanical strength of the reservoir lead to the reservoir being abandoned in April 2011.

The reservoir is situated in three fault blocks located in the Hammerfest Basin and consists of Lower to Middle Jurassic sandstones. The Snøhvit Field, which Tubåen is a part of, is located in an elongated E-W trending fault block system located in the Hammerfest Basin in the western Barents Sea, at 71° north. CO_2 (Statoil ASA (2010); Hansen et al. (2013)).

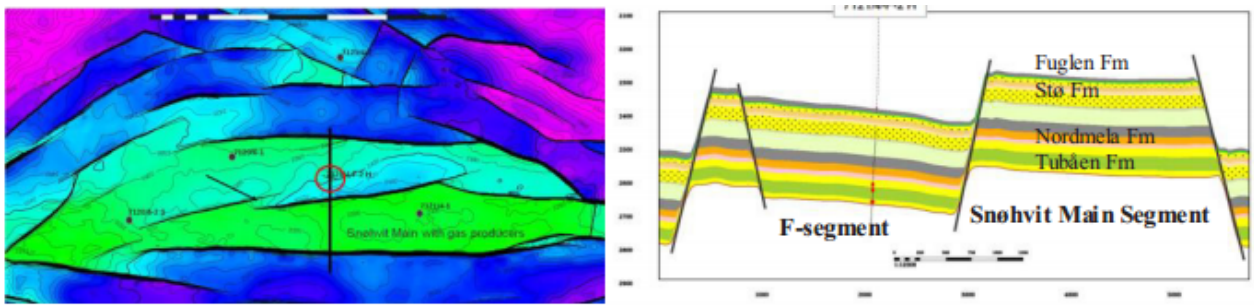

Figure 1.1: Location of injection well F-2H in Tubåen and cross-section indicated by black line to the left, and the cross-section N-S to the right.

The Tubåen formation consists of a number of different sandstone facies, between thin layers of mudstones and siltstones. The geology is a result of the field being an early Jurassic deltaic to fluvial sandstone sequence. Quarts cementation contributes to highly variable

cementation patterns, in addition to the reservoir being quite compartmentalized with many faults leading to a high occurrence of lateral and vertical permeability barriers. The highest permeability is found in the lowermost Tubåen 1 zone where the well intersects a fluvial channel. This unit is of very good quality for storing CO_2 (Hansen et al., 2013).

Statoil ASA is currently modelling the CO_2 injection and plume development in Tubåen with a simulation model using only one set of isotropic, un-scaled flow functions, i.e., the potential for creating a more accurate simulation model is great.

Objective of the Thesis

The objective of this thesis is to investigate the effect of small scale heterogeneities on the plume development in the Tubåen Formation.

The objective is met through applying different upscaling techniques on lithofacies models to upscale CO_2-brine relative permeability. The effect of upscaling is tested by applying the upscaled relative permeabilities in a full scale model of the Tubåen Formation and comparing the resulting fluid distribution.

Approach

1. Create multi-phase flow functions (relative permeability and capillary pressure).

2. Upscale the multi-phase flow functions in lithofacies models using different upscaling techniques.

3. Implement the upscaled flow functions in the full scale simulation model to investigate effects on the CO_2 plume development.

Structure of the Report

Chapter 2 covers how the Tubåen formation is subdivided into zones, and the process of defining average reservoir properties per zone based on core plugs, well logs and tabulated values from Statoil's *Snøhvit CO2 Tubaen Fm. Storage Capacity and Injection Strategy Study.*

Chapter 3 describes how the *Relative Permeability Input Files* for the upscaling step were created, starting with the fitting of relative permeability curves using Corey Correlation.

Chapter 4 covers how the lithofacies models are altered to fit the reservoir properties of Tubåen, before the process of upscaling flow functions from laboratory scale to lithofacies scale is described. The resulting upscaled flow functions are presented and commented.

Chapter 5 is first covering, in detail, how properties from the current Eclipse 300 compositional simulation model used by Statoil were transferred to a simulation model better fit for the purpose of analyzing the effect of incorporating small scale heterogeneities in the flow functions. The second part of the chapter explains how new, full scale, simulations models are created with various variations of upscaled relative permeability.

Chapter 6 is the Results and Discussion chapter, where the results from running full scale simulation models with variations of upscaled flow functions are discussed and compared to the *Basecase*.

Lastly, Conclusions and Recommendations for Further Work are covered in **Chapter 7**.

Chapter 2

The Tubåen Fm; Reservoir Properties

2.1 Evaluation of Reservoir Properties: Tubåen Fm. Study

Statoil's *Snøhvit CO_2 Tubåen Fm. Storage Capacity and Injection Strategy Study* from 2010 describes the Tubåen Fm. and present the results from coring, pressure measurements and well logs. The report was supplied by co-supervisor Prof. Philip Ringrose. In the Study the Tubåen Formation is sub-divided into five zones where the three lowermost zones are perforated. Table 2.1 present the range of estimated permeability and porosity values per perforated zone based on measured and calculated logs (CPI, Computer Processed Interpretation) in the Study. The lowermost zone (Tubåen 1, T1) is the zone of highest permeability and porosity.

Table 2.1: The well data from 7121/4-F-2H perforation intervals in Tubåen (Statoil ASA, 2010).

Zone	Depth (MD)	H (MD)	ϕ (Core)	k (Core)	ϕ (Log)	k (Log)	kH product
Tubåen 3	2736-2743m	7m	10-18%	7.7-450mD	15-16%	100-400mD	2400mD.m
Tubåen 2	2748-2759m	11m	9-11%	0-197mD	10%	10-50mD	550mD.m
Tubåen 1	2784-2794m	10m	No Core	No Core	20%	4000mD	40000mD.m

2.2 Setting Goal Reservoir Properties per Zone

Using the right permeability and porosity values is important for the accuracy of this work. The current simulation model used for Tubåen Fm. - to be described in Chapter 5 - has reservoir properties outside the range of reservoir properties in Statoil's Study, and therefore a decision was made to use the Statoil Study as the base for creating a **new set of values**

for each zone. The new set of values for the reservoir properties of the different zones in Tubåen, hereafter called the *goal values*, will be used to calibrate the lithofacies models in Chapter 4, and the full scale model in Chapter 5. The Statoil Study is assumed to be the most reliable source, compared to the simulation model without explanations to the values used.

Table 2.1 tabulate in what range the permeability and porosity of the three perforated zones are estimated. The kH product together with the measured depth was used to back-calculate the permeability value needed to reach the kH product tabulated. This gave the permeability values given in Table 2.2.

Table 2.2: Using tabulated kH and the height of each zone to find a goal value for permeability.

Zone	Depth (MD)	H (MD)	kH product	k=kH/H
Tubåen 3	2736-2743m	7m	2400mD.m	342.9mD
Tubåen 2	2748-2759m	11m	550mD.m	50mD
Tubåen 1	2784-2794m	10m	40000mD.m	4000mD

The study present Well logs of GR/DENS/NEU/RT run over the full Tubåen interval used to create the estimated ranges of reservoir properties. By closer inspection of the measured and calculated logs (CPI), the properties of zone 2 showed to be very varying. The lowermost part of T2 is evaluated as shale with an associated low porosity and permeability, while the well logs show that the upper part have a much greater permeability than the average of zone T2 tabulated in Table 2.2 using the kH product and height of zone.

Figure 2.1 shows permeability estimates calculated from the MDT pressure measurements, as well as measurements from core plugs, and give an idea of the permeability distribution within each of the perforated zones. Nearly the full Tubåen Fm. interval was cored, but only 4 core plugs were taken from T1. These core plugs showed permeability in the 3-12 Darcy range and porosities greater than 20% - but as the number of cores is low, these values may not be representative for the whole zone.

For the accuracy of the simulation model, it was decided to split zone T2 into the shaley T2_2 and the sandstone interval T2_1. The permeability of T2_1, T4 and T5 was decided approximately by comparing the KLOGH-curves in Panel 8 of the well logs, see Figure 2.2. The original and new zone-division and permeability goals per zone are presented in the same figure.

Table 2.3 tabulate the reservoir property values that will be used as goal values for each zone in Tubåen when altering lithofacies and full scale models in Chapter 4 and 5. Zone T2_2 is defined as a shale zone, and given characteristic properties equal to the ones set for mud

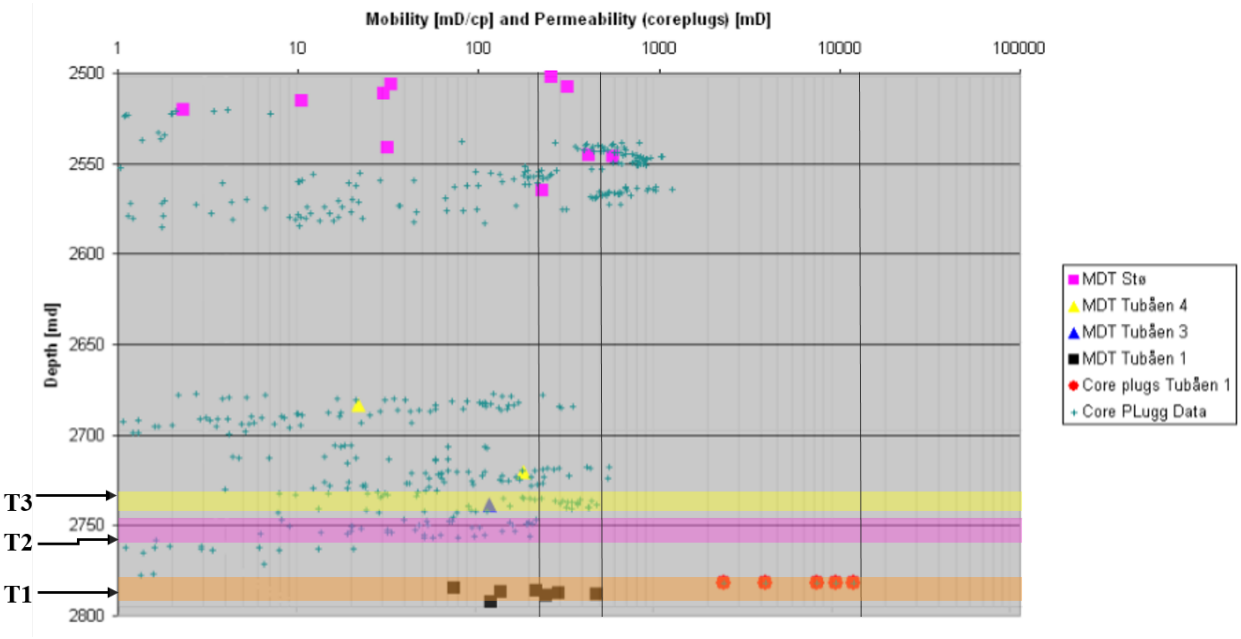

Figure 2.1: Adjusted Figure 10 from (Statoil ASA, 2010). The mobility measured by the MDT tool is compared with the permeability measured on core plugs for the 7121/4-F-2H well.

Table 2.3: Defined Reservoir Properties per layer to be used for the calibration of Lithofacies beddings and Full Scale models.

Defined for the thesis:	Tubåen 5	Tubåen 4	Tubåen 3	Tubåen 2_1	Tubåen 2_2	Tubåen 1
Avg. Permeability, k	340mD	30mD	343mD	232mD	0.1mD	4000mD
Avg. Porosity, ϕ	12%	7%	14%	11%	5.01%	20%

layering in the lithofacies models (to be discussed further in Chapter 4). The goal porosity values were chosen based on Table 2.1 and Figure 2.2.

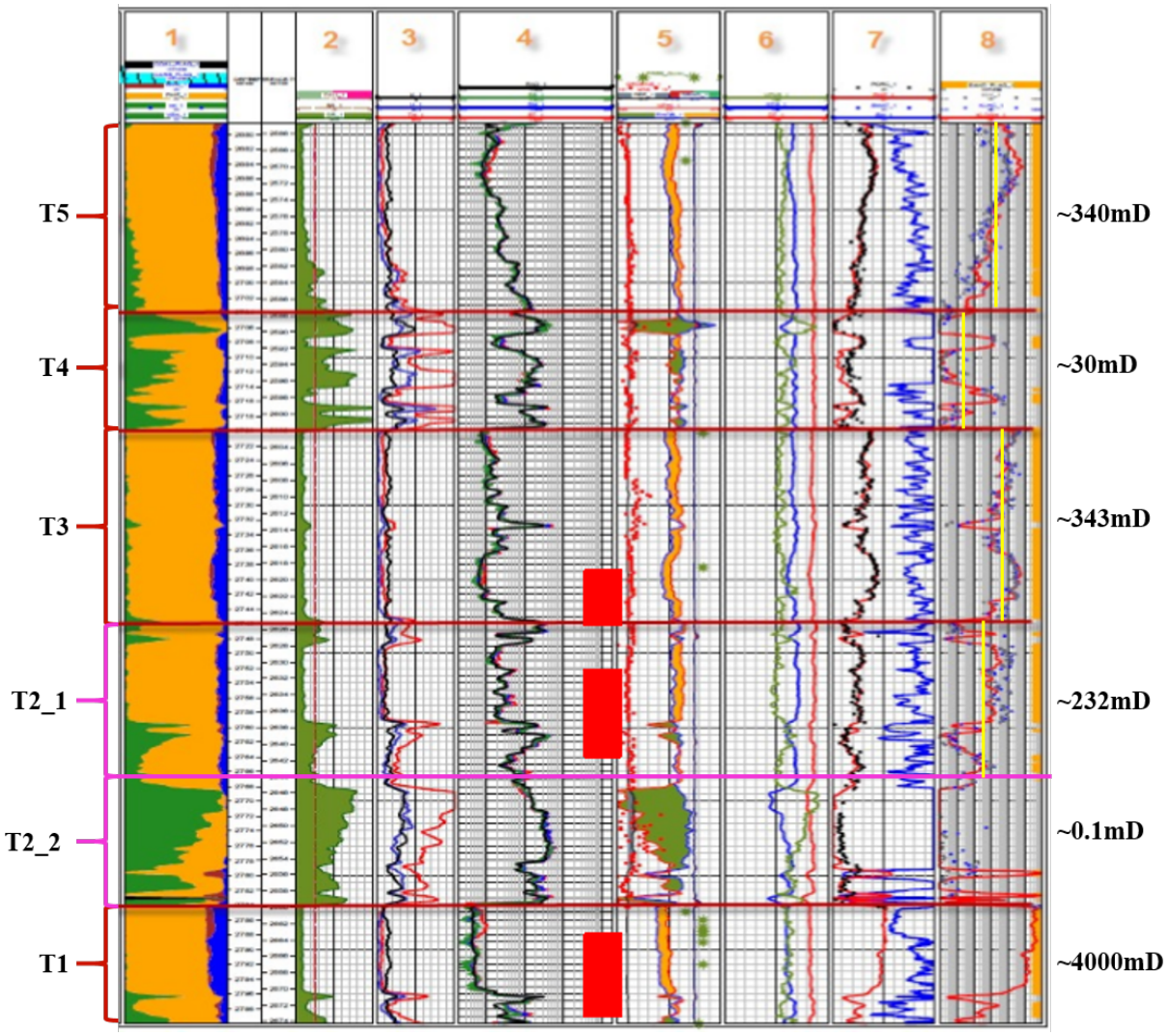

Figure 2.2: CPI log from the Tubåen Fm. of the F-2 well. Panel 1) green-shale, orange-sand, red-irreducible oil, blue-water, Panel 2) green-GR, red-calliper, Panel 3) black-calcium, blue-uranium, red-thorium, Panel 4) resistiviy logs, Panel 5) red point-core plug density, red curve-NPHI, blue-RHOB, Panel 6) green-VPVS, blue-dts, red-dt, Panel 7) black dit-core porosity, red-PHIF, blue-SW, Panel 8) orange-sand flag, grey dot-KLV, blue dot-KLH, red curve-KLOGH. The zonation of Tubåen Fm. is given to the far left, and the defined average permeability values per zone to the far right (altered model from Statoil ASA (2010))

Chapter 3

Relative Permeability Input Files

Upscaling relative permeability curves starts with *having* a set of relative permeability curves to upscale. This chapter covers how Rock Input Files, consisting of water saturation, relative permeability of water and CO_2 and the corresponding J-function, are created. The Rock files are the basis for all of the upscaling work, and should therefore be as accurate as possible. In the current Eclipse 300 simulation model of Tubåen is only one set of drainage relative permeability and capillary pressure tables supplied. These tables consist of few data points, and the capillary pressure is especially poorly defined. By using given parameters for a Sandrock sample, hereafter called *TubåenHigh*, typical for the Tubåen formation (supplied by Prof. Philip Ringrose, Statoil), can Corey Correlation be used to create more detailed flow functions for the Rock Input Files. The parameters given are; initial and residual water saturation, relative permeability endpoints, pore size distribution and fitting parameter C'.

To increase the accuracy of the relative permeability upscaling, the input curves are adjusted according to a rock sample typical for the Tubåen formation. Analysis of the sandstone sample will make the basis for all the Rock Input files, as the *assumption* is that all the layers in the Tubåen formation have the same relative permeability relationship between CO_2 and water as well as the same curvature of the Capillary Pressure function at the laboratory scale.

Table 3.1 shows the characteristics the *new* and adjusted relative permeability curves are built with. Using these, the new curves are made with Corey Correlation to match the curvature of the current curves used in the Eclipse 300 simulation model.

Table 3.1: Measured data for *TubåenHigh*

	k	ϕ	S_{wc}	S_{wrg}	C'	$1/\lambda$	σ
	mD	%	fraction	fraction	-	-	mN/m
TubaenSand	2000	20	0.3	0.4	1.4	0.667	35*

*Surface tension (σ) was not supplied. How it was decided is described in Section 4.5. C' is a constant incorporating σ (surface tension), and λ is the pore-size distribution index. S_{wc} is the connate water saturation and S_{wrg} is 1-S_{rg}, i.e. 1 - residual gas saturation.

The original relative permeability curves used in the current full scale simulation model of the Tubåen Fm. are given in Table 3.2.

Table 3.2: Original input relative permeability tables in the current full scale simulation model of Tubåen.

S_w fraction	k_{rw} mD	Pc Bar	S_g fraction	k_{rg} mD	P_c Bar
0	0	0	0	0	0
0.3	1.00E-06	0	0.116	1.00E-03	0
0.411	4.00E-03	0	0.247	6.00E-03	0
0.502	1.10E-02	0	0.276	1.70E-02	0
0.569	4.50E-02	0	0.335	3.90E-02	0
0.665	1.00E-01	0	0.341	7.80E-02	0
0.724	1.58E-01	0	0.498	1.52E-01	0
0.753	2.03E-01	0	0.589	2.00E-01	0
0.834	3.17E-01	0	0.691	4.00E-01	0.1
1	1	0	0.7	1*	0.2
			0.75	1*	0.3
			0.8	1*	0.5
			0.85	1*	1
			0.9	1*	4
			1	1	10

3.1 Fitting New Relative Permeability Curves

3.1.1 Corey Correlation

Two-phase *characteristic curves* couples the relative permeabilities and capillary pressure. These characteristic curves need to draw the relative permeability functions between 'end-points' - the points at which the flow rate of one phase becomes insignificant - as the total fluid mobility of a two-phase system is less than for a single-phase system. The endpoints are typically estimated from core measurements in the lab, but there does not exist physically fixed endpoint values, they are, among other, dependent on phase pressure and temperature (Reynolds and Krevor, 2015). The most common functions used for relative permeability are the Corey exponent functions, also called the *Corey Correlation*:

$$k_{rnw} = k^{\circ}_{rnw} \left(1 - S_{wn}\right)^{C_{nw}} \tag{3.1}$$

$$k_{rw} = k^{\circ}_{rw} \left(S_{wn}\right)^{C_{w}} \tag{3.2}$$

Where the endpoint relative permeabilities are defined as:

$$k^{\circ}_{rw} = k_{rw} \,@\, \left(1 - S_{nwr}\right) \tag{3.3}$$

$$k^{\circ}_{rnw} = k_{rnw} \,@\, \left(S_{wc}\right) \tag{3.4}$$

Where k°_{rw} and k°_{rnw} are the endpoint wetting relative permeability and the endpoint non-wetting relative permeability, respectively. C_w and C_{nw} are the Corey exponents for the wetting and the non-wetting phase (Ringrose and Bentley, 2015). Water is the wetting phase in Tubåen.

Ringrose et al. (1993) used the Corey exponent functions for relative permeability together with a generalized equation for capillary pressure (3.8) obtained by rearranging the dimensionless Leverett J-function (3.5), and the exponential relationship introduced by Brooks and Corey (3.6).

$$J(S_w) = \frac{P_c}{\sigma}\sqrt{\frac{k}{\phi}} \tag{3.5}$$

$$J(S_w) \propto S_{wn}^{-1/\lambda} \tag{3.6}$$

Equating equation (3.5) and (3.6) gives:

$$\frac{P_c}{\sigma}\sqrt{\frac{k}{\phi}} = C S_{wn}^{-1/\lambda} \tag{3.7}$$

Where C is a constant. This can be rewritten as:

$$P_c = C' S_{wn}^{-1/\lambda}\sqrt{\frac{k}{\phi}} \tag{3.8}$$

Where C' is a constant incorporating σ (surface tension) and the initial constant C, and λ is the pore-size distribution index.

The original input data for relative permeability and capillary pressure in the E300 simulation model is tabulated in Table 3.2. The Corey Correlation uses data from Table 3.1 to create relative permeability functions fitting the limited set of data points supplied in the current simulation model. The original relative permeability values are compared to the relative permeability values obtained from the use of different Corey exponents, and the exponents are chosen to minimize the total square difference for all the data-points. Table 3.3 shows an excerpt of the trial and error approach to find the best fit of Corey exponents by comparing the associated square difference. The highlighted values are the ones chosen and used in the Corey Correlation Equation 3.1 and 3.2, giving the new relative permeability curves seen in Figure 3.1 for *SandHigh*. The corresponding capillary pressure curve was then made for relative permeability of water and gas using Equation 3.8. The J-function was created using Equation 3.5. The end-points calculated for TubåenHigh are tabulated in Figure 3.4.

Table 3.3: Fitting Corey exponents for *TubåenHigh*

C_w	$(k_{rw,original} - k_{rw,SandHigh})^2$	C_g	$(k_{g,original} - k_{g,SandHigh})^2$
6	0.00133608	2.5	0.36351520
5.89	**0.00120308**	2.4	0.36342345
5.85	0.09323131	**2.39**	**0.36342341**
5.5	0.10577763	2	0.36522911

Table 3.4: Calculated end-points for TubåenHigh

	k°_{rw}	k°_{rg}
TubaenSand	0.51	0.4175

3.1.2 End-point Scaling

Using the Corey Correlation method with exponents found by trial and error for the *TubåenHigh*, a set of synthetic rock data for a lower permeability sandrock, called *TubåenLow*, is created. Typical end-point relative permeability values, endpoint water saturation values, absolute permeability, porosity and the C' and λ were chosen by Prof. Philip Ringrose, Statoil, and tabulated in Table 3.5. With a lower absolute permeability, as here for *TubåenLow*, the connate water saturation will naturally be higher.

Based on this data, the *TubåenHigh* data is saturation endpoint-scaled to create synthetic rock data for *TubåenLow* (Reynolds and Krevor, 2015). The result is shown in Figure 3.2,

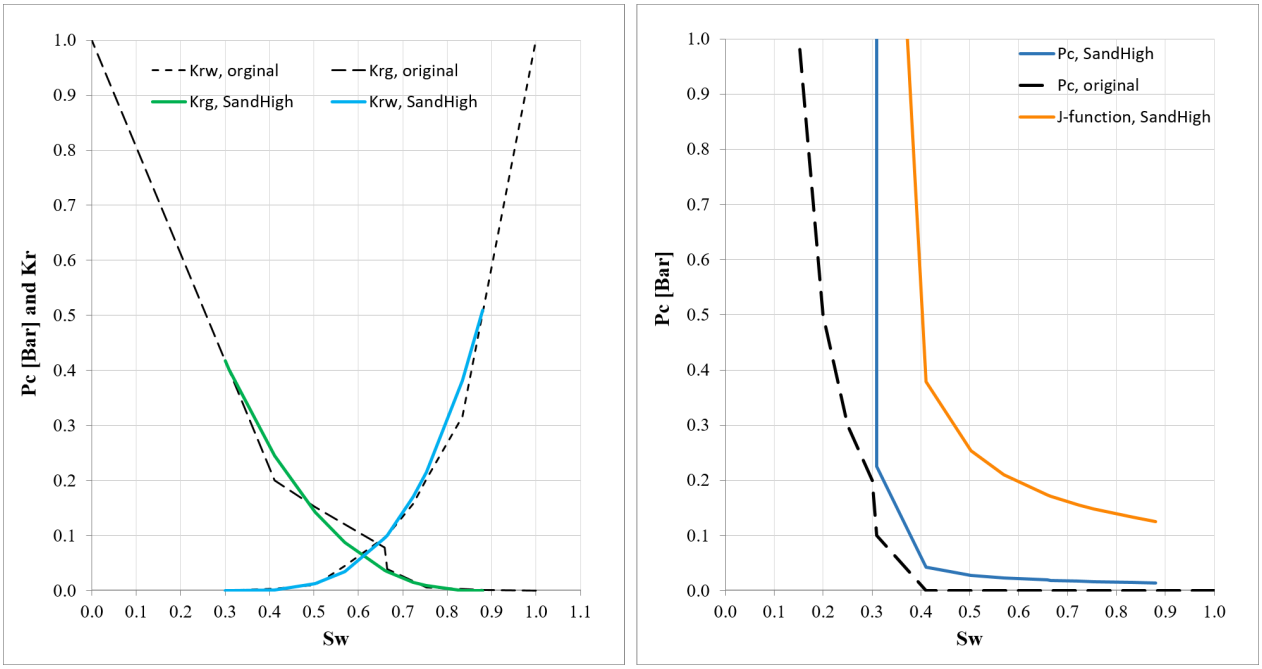

Figure 3.1: *TubåenHigh*: Left hand side: the new relative permeability curves are fitted using Corey Correlation and given endpoints. Right hand side: the original and new capillary pressure curve plotted together with the created J-function.

Table 3.5: Rock Data for *TubåenLow*

	k mD	ϕ fraction	S_{wi} fraction	S_{wrg} fraction	k°_{rw} fraction	k°_{rg} fraction	C' -	$1/\lambda$ -	IFT mN/m
SandLow	100	0.15	0.4	0.88	0.7	0.4	1.2	0.5	35

together with the curves from *TubåenHigh*. The new curves reflect the given parameters in 3.5.

3.1.3 Rock Input Files

The Rock Input Files consist of water saturation, relative permeability of water and CO_2 and the corresponding J-function, tabulated in 3.6. The next chapter describes how the Rock Input Files are assigned to the three different layering types in two lithofacies models. The data from *TubåenHigh* and *TubåenLow* are hereafter called *SandRock* and *MudRock*, respectively.

The layering types are present in the lithofacies models to be used; two sands and one mud. The *MudRock* data are used for the mud layering type in the lithofacies models, while *SandRock* is used for both of the sand layering types.

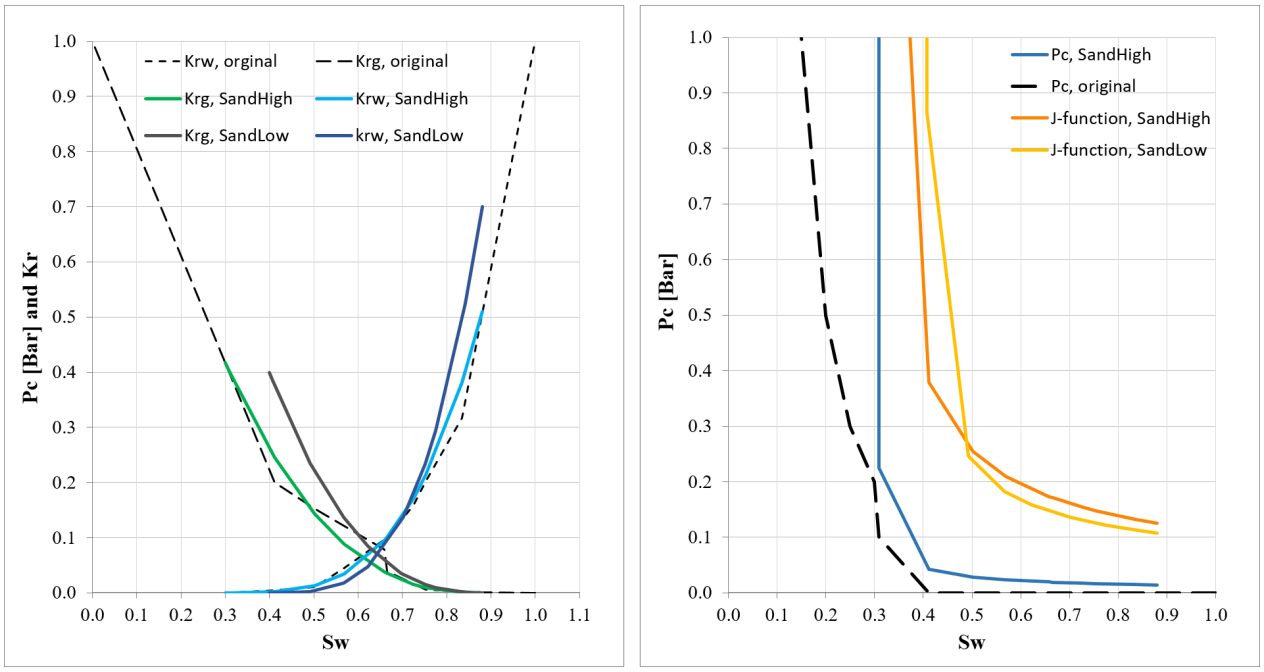

Figure 3.2: *TubåenLow*: The new relative permeability curves, capillary pressure and J-function are creating with saturation end-point scaling.

Table 3.6: Input Rock Files, SandRock and MudRock

SandRock - used for Sand1 and Sand2 in the lithofacies models			
S_w	k_{rw}	k_{rg}	J-function
fraction	mD	mD	-
4.000E-01	0.000E+00	4.000E-01	1.622E+10
4.000E-01	0.000E+00	4.000E-01	1.622E+10
4.074E-01	3.258E-07	3.847E-01	8.647E-01
4.919E-01	2.146E-03	2.352E-01	2.462E-01
5.672E-01	1.745E-02	1.372E-01	1.825E-01
6.226E-01	4.756E-02	8.422E-02	1.582E-01
6.971E-01	1.306E-01	3.585E-02	1.369E-01
7.021E-01	1.384E-01	3.346E-02	1.358E-01
7.509E-01	2.338E-01	1.501E-02	1.260E-01
7.749E-01	2.947E-01	8.974E-03	1.219E-01
8.419E-01	5.242E-01	7.086E-04	1.123E-01
8.800E-01	7.000E-01	0.000E+00	1.077E-01
8.800E-01	7.000E-01	0.000E+00	1.077E-01

MudRock - used for Mud in the lithofacies models			
S_w	k_{rw}	k_{rg_2}	J-function
fraction	mD	mD	-
3.000E-01	0.000E+00	4.175E-01	6.283E+09
3.000E-01	0.000E+00	4.175E-01	6.080E+09
3.090E-01	2.374E-07	4.015E-01	2.023E+00
4.110E-01	1.564E-03	2.455E-01	3.786E-01
5.020E-01	1.271E-02	1.432E-01	2.539E-01
5.690E-01	3.465E-02	8.790E-02	2.098E-01
6.590E-01	9.515E-02	3.742E-02	1.730E-01
6.650E-01	1.008E-01	3.493E-02	1.711E-01
7.240E-01	1.704E-01	1.566E-02	1.549E-01
7.530E-01	2.147E-01	9.367E-03	1.482E-01
8.340E-01	3.819E-01	7.396E-04	1.328E-01
8.800E-01	5.100E-01	0.000E+00	1.257E-01
8.800E-01	5.100E-01	0.000E+00	1.257E-01

Chapter 4

Upscaling Flow Functions

This chapter covers how the flow functions, k_{rw}, k_{rg} and P_c, are upscaled from laboratory scale to lithofacies scale using the Upscaling Module in OPM.

Concept of Upscaling Relative Permeability

Upscaling of grid properties is a means to preserve the heterogeneities from the smaller scale. Petrophysical properties of a reservoir are often determined at laboratory scale - a scale to fine to use for full scale reservoir simulation where grid blocks easily can have dimensions >100m to reduce the computational cost.

Some properties are easy to upscale (like porosity, which is a volumetric property), while *permeability* is challenging being an intrinsic property. Upscaled permeability should induce the same flow as the fine-scale permeability, i.e. the effective permeability of a coarse grid block should yield the same flow as the equivalent fine-scale grid blocks it is representing.

The accuracy of reservoir models is highly dependent on the relative permeability curves, as relative permeability is one of the fundamental parameters controlling flow in porous media (Krause and Benson, 2015). The upscaled relative permeability should incorporate the impact of small-scale heterogeneity on the reservoir flow.

The use of lithofacies models is the first step in the upscaling process. In this work, the lithofacies models are used as framework for upscaling relative permeability from the laboratory measurement scale (core plugs of $\sim$ 3cm diameter) to the scale of the lithofacies models ($0.5\times0.5\times0.5$m). The idea is that this upscaling step results in the effect of small-scale heterogeneities getting incorporated in the upscaled relative permeability.

The Upscaling Module in the Open Porous Media (OPM) software (see Appendix A) can upscale relative permeability and capillary curves using a flow-based steady-state approach. The module is designed for one or two-phase flow and lithofacies models described by Eclipse corner point grids.

In this study, the objective is to investigate the effect of upscaling CO_2-brine relative permeability using different steady-state upscaling techniques. To do so, the Upscaling module of the OPM software is used to create upscaled relative permeability tables using end-member upscaling techniques on lithofacies models. The upscaled relative permeability curves will then, in Chapter 5, be assigned to specified areas of the Tubåen formation model in a number of combinations.

4.1 The Balance of Forces

There are three interacting fluid forces that together with the properties of the porous medium control two-phase flow. These are the viscous, capillary and gravitational forces. A set of dimensionless scaling groups (force ratios) is widely used to estimate the relative dominance of each force at given conditions (Reynolds and Krevor (2015); Virnovsky et al. (2004); Ringrose et al. (1993)). Spatial dimensions are included in all three ratios, implicating that a coarsening of the grid will alter the force balance. For the same rock system the flow behaviour will differ between a gravity-dominated, viscous-dominated or capillary-dominated flow regime. The *balance of forces* concept is a framework for understanding which scales most affect a particular flow process.

The viscous/capillary ratio:

$$\frac{\text{Viscous}}{\text{Capillary}} = \frac{v_x \, \Delta x \, \mu_{nw}}{k_x \, (dP_c/dS)} \tag{4.1}$$

The gravity/capillary ratio:

$$\frac{\text{Gravity}}{\text{Capillary}} = \frac{\Delta\rho \, g \Delta z}{(dP_c/dS)} \tag{4.2}$$

The viscous/gravity ratio:

$$\frac{\text{Viscous}}{\text{Gravity}} = \frac{v_x \Delta x \ \Delta y \mu_{nw}}{\Delta\rho \, g \, \Delta z} \tag{4.3}$$

Where Δx, Δy and Δz are spatial dimensions in the horizontal (x and y) and vertical direction (z), μ_{nw} is the viscosity of the non-wetting phase, v_x is the Darcy velocity (where $v_x = q/\Delta y \Delta z$) in the x direction, k_x is the permeability in the x direction, $\Delta\rho$ is the fluid density difference, (dP_c/dS) is the capillary pressure gradient with reference to saturation, and g is the gravity constant. The system performance should, in principle, remain unchanged if the

ratios are kept fixed (for given multiphase functions; k_{rg}, k_{rw}, P_c). The ratios are particularly important to model flow behaviour at the small-scale (pore-scale) in heterogeneous systems. The flow behaviour at this scale usually is the starting point of the upscaling procedure of creating flow functions for reservoir grid blocks (Ringrose et al., 1993) - as it is in this thesis where the work starts at the pore-scale/laboratory scale.

In the following work, different upscaling techniques will be tested on the same lithofacies models to compare the effect of force balance on upscaling relative permeability. Two-phase relative permeability curves will be upscaled from pore-scale (laboratory measurements) in different lithofacies beddings using extreme-limits, before the upscaled curves are transferred to full scale simulation models.

4.2 Steady-State Upscaling Techniques

After generating fine-scale relative permeability curves in Chapter 3, the upscaling of the curves can be carried out using either a dynamic or steady-state method. Steady-state methods assume an unrealistic "ideal" flow behaviour - unchanging in time - whilst dynamic methods attempt to capture the "true" flow behaviour. The dynamic methods are computationally more expensive compared to steady-state methods which are quick and simple to implement (Nilsen et al. (2011); Ringrose and Bentley (2015)).

A reservoir flow is in steady-state when the saturation in each grid block is constant with time, leading to an altered form of the continuity Equation 4.4 where the time-dependent term $\frac{\partial(\phi S_i)}{\partial t}$ is neglected:

$$\frac{\partial(\phi S_i)}{\partial t} + \nabla \cdot (\mathbf{v}_i), \quad \frac{\partial(\phi S_i)}{\partial t} = 0 \quad \Longrightarrow \quad \nabla \cdot (\mathbf{v}_i) = 0 \tag{4.4}$$

$$P_c = P_{nw} - P_w \tag{4.5}$$

Three common steady-state upscaling techniques are based on the idea that one should consider the ratios of the forces controlling flow; the gravitational, capillary and viscous forces. At the extreme limits, either capillary, gravitational or viscous forces dominate, and make up three common upscaling techniques;

- **The Capillary Equilibrium (CE)**: Assumes that capillary pressure is spatially invariant throughout the geometry and completely controls the saturations. Applied pressure gradients are assumed to be zero or negligible.

- **The Viscous Limit (VL)**: Assumes steady-state flow at a given, constant fractional flow. Capillary pressure is assumed to be zero.

- **The Gravity-Capillary Equilibrium (GCE)**: Similar to CE, but the capillary pressure controlling the saturations is only spatially invariant in the horizontal direction, while it is adjusted according to pressure changes due to gravity forces in the vertical direction.

The reality will lie somewhere within the triangle drawn between the three extreme-limits. For the same rock system the flow behaviour will be different for a viscous-dominated, capillary-dominated or gravity-dominated flow regime. The appropriate scale-up technique to use depends on the scale of the heterogeneities one is trying to capture, as well as the relative dominance of one force over the other at that scale. Factors affecting the force ratios, and under which conditions the techniques are appropriate, are previously discussed.

The focus in this thesis: CE and VL

This thesis focus on the two extreme cases of viscous-dominated flow and capillary-dominated flow in the *absence of gravity* - an approximation evaluated and considered acceptable at small scale by Virnovsky et al. (2004). The Upscaling Module in the open source software Open Porous Media is used for the upscaling of relative permeability in this thesis.

4.2.1 The Capillary Equilibrium (CE)

The capillary equilibrium method is considered applicable at small length-scales where the assumption is that when the flood is capillary dominated, the fluids can be in capillary equilibrium over *small distances*. In capillary equilibrium, the capillary pressure is assumed to be constant throughout the geometry and to completely control the saturations, whilst the applied pressure gradient given by $\nabla(\rho_i g z)$ is neglected – meaning that all flow in and out of each grid cell is assumed to be governed only by the capillary pressure curve.

According to Morrow et al. (1965), the condition for capillary equilibrium state in a reservoir is a steady-state situation where the fluid distribution is independent of time, causing no mass transfer by pressure difference. For the reservoir to fulfill the criteria, the flow rate needs to be zero, in which case there will be no pressure gradient across the model to create an effective permeability. However, in application of the theory, the assumption is that if the injection rate is reasonable low, the saturations will not change appreciably over short time intervals and we may assume that capillary equilibrium holds approximately (Pickup and Stephen, 2000).

When using the CE technique for upscaling, the underlying assumptions of the method are applied to the governing equations for each phase in each direction, for each rock type. Then a directional averaging over rock types makes upscaled and directional flow curves that can be used as input in reservoir models. The steps of the method are listed by several authors, among others: Pickup and Stephen (2000); Ringrose and Bentley (2015); Christie (2001); Pickup et al. (1996).

4.2.2 The Viscous Limit (VL)

For the viscous limit (VL) method, the assumptions are that the capillary pressure and gravity are negligible, so that saturations are determined purely by the distribution of the absolute permeability in the domain. Both large length-scales and high flow rates favor viscous forces, as can be seen from the force ratio, Equation 4.1. At steady-state, when neglecting capillary pressure and gravity, the expression for fractional flow of the non-wetting phase (CO_2) and water is reduced to a simple relationship between the relative permeabilities and phase viscosities;

$$f_{nw} = \frac{q_{nw}}{q_t} = \frac{k_{rnw}/\mu_{nw}}{k_{rnw}/\mu_{nw} + k_{rw}/\mu_w} \tag{4.6}$$

$$f_w = \frac{q_w}{q_t} = \frac{k_{rw}/\mu_w}{k_{rnw}/\mu_{nw} + k_{rw}/\mu_w} \tag{4.7}$$

With the assumption that the non-wetting phase, CO_2, is injected into the model with a uniform fractional flow over the boundary and that the relative permeabilities are isotropic, then the fractional flow will be uniform throughout the model. In this case, the constant fractional flow determines the water saturation distribution, and the relative permeability curves can be determined by finding the effective total mobility at enough fractional flows. The steps of the method are listed by Pickup and Stephen (2000), among others.

It must be noted that the fractional flow over the coarse block boundary is assumed to be uniform - which is an unlikely situation. But, Pickup and Stephen (2000) and Kumar et al. (1996), among others, present test results showing that the approximation can be made without compromising the results too much. As mentioned, the method assumes isotropic permeability. If the relative permeabilities instead are anisotropic, the fractional flows are constant along *streamlines*, which in general are not parallel to the coordinate axes. This problem can be solved by assuming the fractional flow to be constant in one direction at the time to calculate the effective relative permeability for each direction separately (Pickup et al. (2000); Kumar et al. (1996)). The method is then expanded to account for anisotropy

in the relative permeability, and produce directional effective relative permeability curves. This is the option which will be used for the upscaling described in this thesis.

4.2.3 Transition between Capillary and Viscous Dominance

The mentioned end-member cases of the fluid system under steady-state will in most cases not represent the real fluid flow in a porous media. The reality will lay somewhere inside the triangle created by the three extreme limits. Capillary number and other dimensionless groups have been used in many systematic studies investigating the response of CO_2-brine relative permeability to changing reservoir conditions and to validate the steady-state method (Benson et al., 2013) .

When coarsening the grid from fine-scale, the transition from capillary to viscous-dominated flow will not necessarily occur at the same capillary number for all rock types, but be dependent on the specific heterogeneity in the medium. Virnovsky et al. (2004) found the typical transition from a capillary limit to a viscous limit to be with a capillary number in the range $10^{-1} < N_c < 10^2$. The capillary number defined and used by Virnovsky et al. (2004) is the ratio of viscous to capillary pressure drop on the heterogeneity scale;

$$N_c = \frac{H}{|\Delta P_c(f_w)|}\frac{\Delta P}{L} \tag{4.8}$$

Where L [m] and H [m] are length scales in the principal and transverse directions of flow, respectively; the viscous component is given by the pressure drop ΔP [Pa], and the difference in capillary pressure $\Delta P_c(f_w)$ [Pa] represent the capillary forces. From the capillary number Equation 4.8, it is clear that viscous forces dominate at larger length-scales, higher flow velocities, and higher fluid viscosities. Supercritical CO_2 is a low-viscosity fluid, which from the expression favour capillary forces, but for the area in the immediate vicinity of the injection well, the flow rate is high - which favor viscous forces.

Reynolds and Krevor (2015) find that a transition from capillary dominated flow to viscous dominated flow can be expected around $N_c \approx 10-75$, depending on the fluid saturation.

Several definitions of the "capillary number" exists, and Jonoud and Jackson (2008) state that; *"For systems with heterogeneity, a capillary number that compares viscous fluid velocities in a principal direction (e.g., along the length of a rock core) to capillary-driven flow transverse to this is a key measure of the importance of capillary and permeability heterogeneity in the system"*. This is sometimes referred to as a *transverse* capillary number, $N_{c,T}$. A commonly used transverse capillary number is defined by Zhou et al. (1997) and Yokoyama

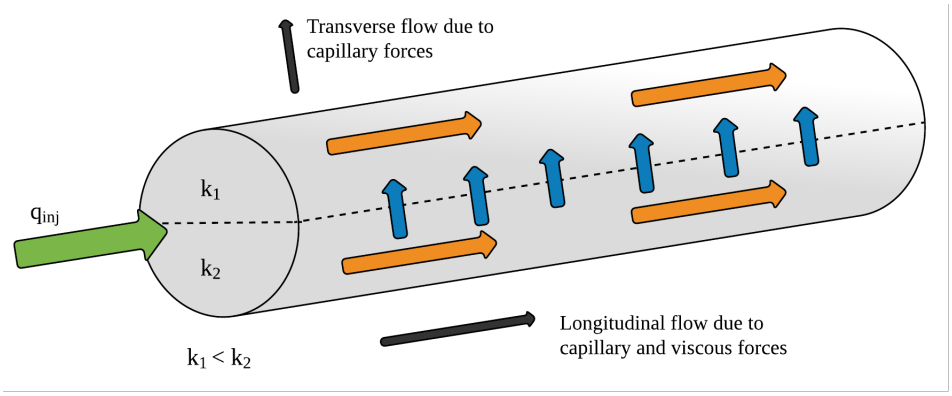

Figure 4.1: Transverse and longitudinal flow in a core with a simple layered heterogeneity in absolute permeability, $\boldsymbol{k}$. Figure based on illustration in Reynolds and Krevor (2015)

.

et al. (1981) as;

$$N_{c,T} = \frac{H^2 q_{inj} \mu_{inj}}{L p_c^* k_T} \tag{4.9}$$

Where P_c^* [Pa] is characteristic capillary pressure, k_T[m^2] is the permeability in the transverse direction, $\boldsymbol{v}_t$ [m/s] is the total fluid velocity in the principal direction, and μ_{inj} [Pa s] is the viscosity of the injected fluid. If considering a drainage displacement of water by CO_2 in a simple two-layered core (Figure 4.1), then for a high transverse capillary number, $N_{c,T} >> 1$, viscous forces dominate the flow resulting in longitudinal flow in both layers of the core equally. A low transverse capillary number, $N_{c,T} << 1$, would however imply dominance of capillary forces driving fluid flow in the transverse direction, causing water to migrate into the low permeability layers of a water-wet rock. The result is an increased invasion of water in the low permeability layers, a capillary redistribution phenomenon called crossflow that is not accounted for in the capillary number defined by Virnovsky et al. (2004). However, Reynolds and Krevor (2015) find the capillary number N_c to be more beneficial than the transverse capillary number, $N_{c,T}$, as it does not need defined directionality of the capillary heterogeneity.

The scope of this thesis is to compare the *effect* on the CO_2 plume development in a full scale simulation model using relative permeability curves upscaled in the extreme limits of force balance, but does not cover a thorough inspection of the validity of the techniques. Even though the capillary numbers are not going to be related to the upscaling of CO_2 and water in this thesis, discussing them is important. They build up the understanding of the end-member techniques.

not the validity of the techniques. Therefore, the capillary number is not looked into, but

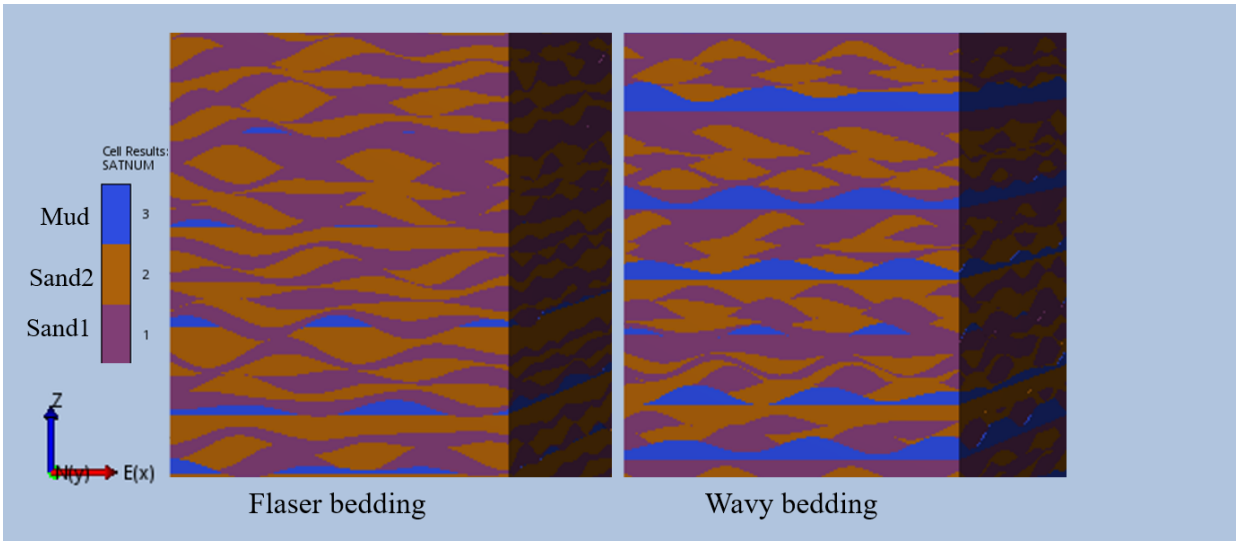

Figure 4.2: Visualization of the two beddings; Flaser and Wavy. Sand2 has higher permeability and porosity than Sand1.

is interesting for further and more detailed work.

4.3 Lithofacies Models Used for Upscaling Relative Permeability

Two models of bedding types relevant to the Tubåen formation are provided by Statoil and describe two heterolithic beddings; Flaser and Wavy. These are characteristic for the Tubåen Formation, and generated to give a detailed characterization of the subsurface systems.

The Flaser bedding is characterized by alternating rippled sand and discontinuous mud layers created by the deposition of mud on previously existing sand ripples. Wavy bedding is similar, but with thicker, more horizontally continuous mud layers than in Flaser bedding (Martin, 2000). From Figure 4.2 can it clearly be seen that Wavy bedding has more coherent mud layers in the horizontal direction compared to Flaser bedding.

4.4 Altering the Lithofacies Models

Wavy and Flaser are used as the ”body” for the first step of upscaling relative permeability, and need therefore be representative of Tubåen. It is established that the bedding *structures* are characteristic for the Tubåen formation, but the models need altering of the reservoir properties.

Layering Types

The original models of Flaser and Wavy each have six layering types, or *regions*. The distribution and characteristics of these were found by importing the saturation function region numbers (SATNUM), permeability and porosity data to Matlab from the grid files. Matlab script D.1 was used to calculate the average permeability and porosity (of the active cells) in the layering types, see Table 4.1.

Table 4.1: Original Layer Types in Wavy and Flaser.

	Flaser			Wavy		
Layer:	k [mD]	ϕ [frac]	% in layer	k [mD]	ϕ [frac]	% in layer
Flood Sand1	100	0.25	19.59	100.40	0.25	19.59
Flood Sand2	150	0.30	19.28	150	0.30	19.28
Flood Mud	0.01	0.05	8.57	0.01	0.05	8.57
Ebb Sand1	100	0.25	22.19	100	0.25	22.19
Ebb Sand2	150	0.30	20.92	150	0.30	20.92
Ebb Mud	0.01	0.05	9.44	0.01	0.05	9.44

The original data show that two and two of the specified layering types have identical or almost identical average permeability and porosity. The number of layering types was therefore reduced from six to three in both models, resulting in two sand layers and 1 mud layer after layering types with the same or similar permeability and porosity were combined in the adjusted models. Table 4.2 gives an overview of the new layering with the average permeability and porosity values, and percentage occurrence in Wavy and Flaser.

Table 4.2: Restructured Layer types in the Lithofacies Models

		Flaser			Wavy		
New layer:	Combined of:	k [mD]	ϕ [frac]	% in layer	k [mD]	ϕ [frac]	% in layer
Sand1	Ebb and Flood Sand1	100.10	0.25	32.18	100.10	0.25	27.43
Sand2	Ebb and Flood Sand2	150.00	0.30	31.03	150.00	0.30	26.55
Mud	Ebb and Flood Mud	0.01	0.05	36.78	0.01	0.05	46.02
Tot. Avg. Permeability and Porosity:		102.03	23.41	-	76.51	18.81	-

The next step was to alter the average permeability and porosity values of each layering type to make the lithofacies models more representative of the Tubåen Fm. The total average permeability and porosity of both models were scaled in accordance with the values discussed and defined per zone (a total of six zones) in the Tubåen Formation in Section 2.2. The properties were scaled to match one zone in Tubåen at a time, making a total of 6 models per bedding type. The goal was to get average permeability and porosity values matching the tabulated values, while maintaining the clear separation in averages between

Sand1 and Sand2. Table 4.4 gives an overview of the scaled zones in Wavy and Flaser. The mud layer was kept as original or carefully scaled as a means to preserve the effect of mud in the model.

Two alternatives were evaluated for scaling the permeability and porosity values in Wavy and Flaser, namely;

1. Scale the permeability and porosity values within each layer by multiplying all values with a constant, i.e. shifting the values.

2. Making each layering type homogeneous with a new set of permeability and porosity values matching the goal average value.

Alternative 1 maintains the original heterogeneity within the layer types as the cells in each layer are multiplied by a scaling factor, i.e. only "shifted". Alternative 2 is the easiest and quickest option, but the heterogeneity is lost. Therefore, Alternative 1 was chosen, as the effect of loosing the heterogeneity within the layers at the bedding scale was unknown.

Permeability and Porosity

The biggest part of altering the lithofacies models was adjusting the permeability and porosity, see Matlab script D.2. Table 4.4 present the original and scaled average properties for each bedding in each zone of Tubåen together with the goal values repeated here in Table 4.3.

Table 4.3: Defined Reservoir Properties per layer to be used for the calibration of Lithofacies beddings and Full Scale models.

Defined goal Avg.:	Tubåen 5	Tubåen 4	Tubåen 3	Tubåen 2_1	Tubåen 2_2	Tubåen 1
Permeability, k	340mD	30mD	343mD	232mD	0.1mD	4000mD
Porosity, ϕ	12%	7%	14%	11%	5.01%	20%

Complete tables of how every layering type per bedding and zone were scaled are found in Appendix B. After scaling the permeability and porosity of each layering type in each Tubåen zone, the scaled permeability and porosity tables were exported into new grid files for each zone. This meant six new grid files per lithofacies model, thus making a total of twelve new grid files.

Table 4.4: Scaled and Original Permeability and Porosity Averages in Wavy and Flaser

Tubåen-5			Tubåen-4			Tubåen-3		
Model	k_{avg} [mD]	ϕ_{avg} [%]	Model	k_{avg} [mD]	ϕ_{avg} [%]	Model	k_{avg} [mD]	ϕ_{avg} [%]
Flaser	340.07	11.92	Flaser	30.13	7.03	Flaser	343.41	14.00
Wavy	336.46	12.06	Wavy	30.02	7.14	Wavy	342.97	13.58
Goal	340.00	0.12	Goal	30.00	0.07	Goal	343.00	0.14

Tubåen-2_1			Tubåen-2_2			Tubåen-1		
Model	k_{avg} [mD]	ϕ_{avg} [%]	Model	k_{avg} [mD]	ϕ_{avg} [%]	Model	k_{avg} [mD]	ϕ_{avg} [%]
Flaser	232.66	11.11	Flaser	0.10	5.01	Flaser	4023.87	19.89
Wavy	232.05	10.82	Wavy	0.10	5.01	Wavy	3996.60	19.87
Goal	232.00	11	Goal	0.10	0.0501	Goal	4000.00	20.00

Comments to Tables in Appendix B:

- Flaser in T5 and T3 stand out as two models which could have been scaled with greater care. The permeability ratio between the two sands has been greatly altered giving a higher permeability difference. The new permeability ratio is assumed to affect the upscaling result.
- Zone T1 is highly permeable, and has been made close to homogeneous.

4.5 Upscaling Relative Permeability in OPM

After making Wavy and Flaser grid files with adjusted permeability and porosity per Tubåen zone, the models were ready for being used as the body for upscaling relative permeability of CO_2 and water.

The Upscaling module of the OPM software can be used to create upscaled relative permeability tables using end-member upscaling techniques. Three end-member upscaling techniques were tested; Capillary Equilibrium (CE), Viscous Limit (VL) and Gravity-Capillary Equilibrium (GCE) - described in Chapter 4.2. Although three techniques were tested, only two will be discussed further in this thesis, as the GCE technique did not give logical output from OPM. It seems to be some error in the program and/or the bedding models. The upscaling option is currently being looked into by Statoil.

Simulation Options

The Upscaling module does only specify water-oil systems, which means that the gas specifications must be entered for oil. The upscaling is not affected by this.

Table 4.5: Simulation options in CE and VL.

Capillary Equilibrium		Viscous Limit		
Boundary Condition	*Surface Tension*	*Boundary Condition*	*Water Viscosity*	*Gas Viscosity*
Fixed	35 dynes/cm	Fixed	0.00036 Pa s	0.0000578 Pa s

Rock Input Files

The lithofacies bedding models are built with isotropic permeability. Therefore, the Rock Input Files are given in the isotropic permeability input format with water saturation, relative permeability of water, k_{rw}, relative permeability of CO_2, k_{rCO2} and J-function, respectively (Wiki.opmproject.org, 2017).

The upscaling module in Open Porous Media requires a Rock Input File for each layering type in Flaser and Wavy. In Chapter 3 it is explained how Rock Input Files with fine-scale relative permeability and J-function were created based on core data, the original curves and Corey Correlation. The sand layering types, *Sand1* and *Sand2*, are given the Input file "SandRock", while *Mud* is given the end-point scaled table, "MudRock". The exception is for zone T1, where the SandRock Input File is used for all layering types due to the high permeability and porosity of the zone. The finalized Rock Input Files are tabulated in Table 3.6.

Boundary Condition

OPM gives the option of using either fixed, periodic or linear boundary condition when upscaling. Periodic boundary condition is recommended for simulations in OPM, but did not work. Neither did linear boundary condition, and the problem is looked into by the developers, founded by Statoil.

reported to Statoil. A list of the specifications of each boundary conditions is given underneath. The option of fixed boundary condition was used in this thesis, mainly because it was the only condition working.

- **Fixed boundary conditions**: Pressure is set to 1 on the inflow and 0 on the outflow sides (X− and X+ for the X direction), and no-flow Neumann conditions are used on the other sides. This corresponds to boundary condition f on the command line, and produces diagonal tensors.
- **Linear boundary conditions**: Pressure is set to 1 on the inflow and 0 on the outflow sides, and linear (from 1 down to 0) Dirichlet conditions are used on the other sides.

This corresponds to boundary condition l on the command line, and produces a full tensor, which may not be symmetric however.

- **Periodic boundary conditions**: Modified periodic Dirichlet conditions are set on all sides. On the inflow side the pressure is set to (1 + the outflow side pressure), and on the other sides pressure is set to be everywhere equal to its periodic neighbour (on the opposite side). This corresponds to boundary condition p on the command line, and produces a full, symmetric tensor. This is the recommended boundary condition for simulations in OPM.

Surface Tension

Surface tension of CO_2-brine needs to be specified for upscaling in the Capillary Equilibrium option. Surface tension is a decreasing property with increasing pressure, while increasing with increasing temperature and salinity.

Bachu and Bennion (2009) investigate the Dependence of CO_2-brine interfacial tension on aquifer pressure, and the tables in this paper could be used to find the approximate surface tension to use for Tubåen. To do so, water salinity, reservoir temperature and pressure prior to injection are taken from the paper of Pham et al. (2011) covering the Tubåen formation.

- Water Salinity: 168 g/l $\approx$ 2.8747 mol/kg
- Reservoir Temperature: $\sim$ 98 °C
- Initial Reservoir Pressure: $\sim$ 265 Bar $\approx$ 26.4 Mpa

Table 4.6: Surface Tension

Water Salinity	Reservoir Temperature	Initial Reservoir Pressure	$\Longrightarrow$	Surface Tension
168 g/l $\approx$ 2.8747 mol/kg	$\sim$ 98 °C	$\sim$ 265 Bar $\approx$ 26.4 MPa		$\sim$ 35 mN/m

Using these values, the Surface Tension was found to be $\sim 35\ mN/m$.

Viscosity

The full scale Eclipse 300 model was run to find the viscosity of brine (constant), and a relationship between pressure and viscosity for CO_2. This relationship was somewhat linear. For the upscaling, viscosity corresponding to a pressure of 300 Bar is used - this is the approximate pressure near the injection well while injecting CO_2.

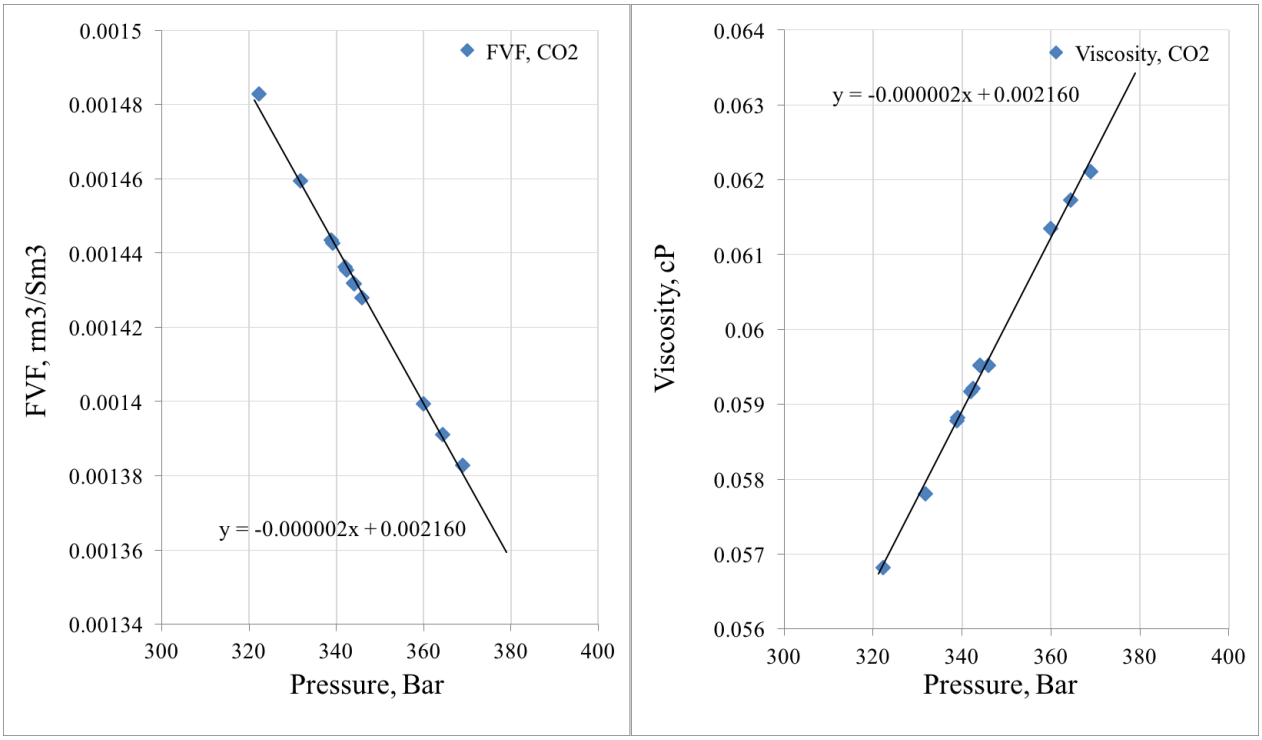

Figure 4.3: Viscosity of CO_2 vs. pressure from a run of the original E300 model.

The relationship between pressure and viscosity for CO_2 is found in Figure 4.3, whilst the chosen viscosities of brine and CO_2 for a reference pressure of 300 Bar are listed underneath:

- μ_{CO_2} @ 300 Bar = 0.0578 cP
- μ_{brine} @ 300 Bar = 0.36 cP

4.6 Results

The result from upscaling relative permeability for the three perforated zones of Tubåen in the two lithofacies Wavy and Flaser using the two extreme limit techniques Viscous Limit and Capillary Equilibrium are given here. OPM gives output in water-oil format, and the plots were made without changing from the ”oil” nomenclature to ”gas” nomenclature. Therefore, the plots will read relative permeability of CO_2 as *oil*. The upscaled directional relative permeability curves are compared to the *SandRock* Input curve, see table 3.6. The *MudRock* Input curve is not included in the comparison to limit the number of curves, but is plotted togeterher with *SandRock* in Figure 4.4. *SandHigh* corresponds to *Sand* in Figure 4.5, 4.6 and 4.7, while *SandLow* corresponds to the Mud layering type in the lithofacies beddings.

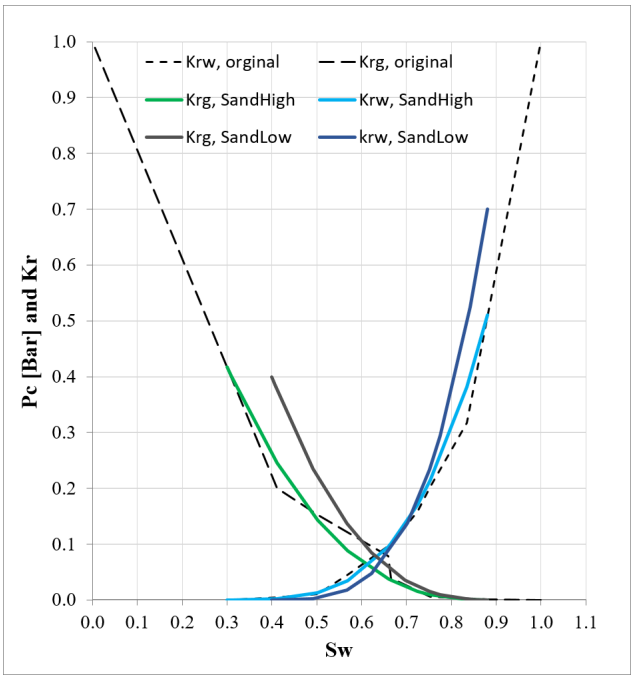

Figure 4.4: Input relative permeability curves for upscaling in beddings in OPM.

Table 4.7: Restructured Layer types in the Lithofacies Models

Layer:	Flaser	Wavy
Sand1	32.18%	27.43%
Sand2	31.03%	26.55%
Mud	36.78%	46.02%

Table 4.7 repeat the percentage distribution of layering types in Wavy and Flaser bedding

The results presented here consist of the upscaled relative permeability and capillary pressure curves plotted for the three perforated zones, and the upscaled permeability tensor supplying the k_v/k_h relationship between the directional, single phase permeabilities.

The original and scaled reservoir properties (scaled to match the values tabulated in Table 2.3) per zone, bedding and layering type are found in Appendix B.

4.6.1 Tubåen Zone T3

Results from upscaling relative permeability in Wavy and Flaser bedding with average reservoir properties corresponding to zone T3 in Tubåen.

The VL option is expected to yield an upscaled curve somewhere between the two input curves (plotted in Figure 4.4). The upscaled relative permeability curves in VL show little to

no variation from the original input of *SandHigh* (presented as "$K_{rw}, Sand$" in the plots) when upscaled in Flaser bedding, but in Wavy bedding, the z-directional relative permeability of water has increased in the region of two-phase flow. The Wavy bedding has a higher content of *Mud*, and it is therefore natural that the upscaled relative permeability curves in Wavy bedding are more affected by the *Mud* input curves than Flaser bedding which is built with less of the *Mud* layering type.

The lower right plot shows that relative permeability upscaled in Wavy bedding with the CE option have a very limited two-phase flow range in the z-direction. The vertical relative permeability of CO_2 is zero or close to zero until almost reaching the connate water saturation. The curvature means that vertical flow of CO_2 is limited to the when the drainage process has reduced the water saturation to almost connate water saturation. The upscaled relative permeability curves are a result of how the CE option pushes for capillary equilibrium between the layers within the bedding. Tubåen is a natural aquifer and water-wet, and the water is drawn towards the lower permeable layers. The CO_2 does on the other hand get very restricted mobility in the low permeable layers compared to water. The effect is alternating zones with almost single-phase flow of water in mud layers. The effect of the CE option is greatest in Wavy bedding, explained by the bedding having continuous horizontal layers of *Mud*. Flaser also have a quite high content of mud, but not in continuous layers. Using the upscaled curves from CE in Wavy bedding as input in the full scale model should result in less segregation of the gas plume and rather a more unified and extensive plume.

The upscaled curves in Flaser bedding with the CE option do not show the same behaviour as in Wavy bedding. As mentioned, the main difference between Wavy and Flaser bedding is the content and distribution of *Mud*. The *Mud* layering does not form continuous horizontal layers in Flaser bedding, and therefore does not create the same barriers to vertical flow.

Table 4.8: Vertical over horizontal permeability ratio in T3.

Bedding	$\mathbf{k_v/k_h}$
Flaser	0.177
Wavy	0.0021

The k_v/k_h ratios, see Table 4.8, substantiates the effect of bedding type on the vertical flowability. The ratio will be used to scale the z-directional permeability in the layer of the full scale simulation model.

4.6.2 Tubåen Zone T2-1

Results from upscaling relative permeability in Wavy and Flaser bedding with average reservoir properties corresponding to zone T2_1 in Tubåen.

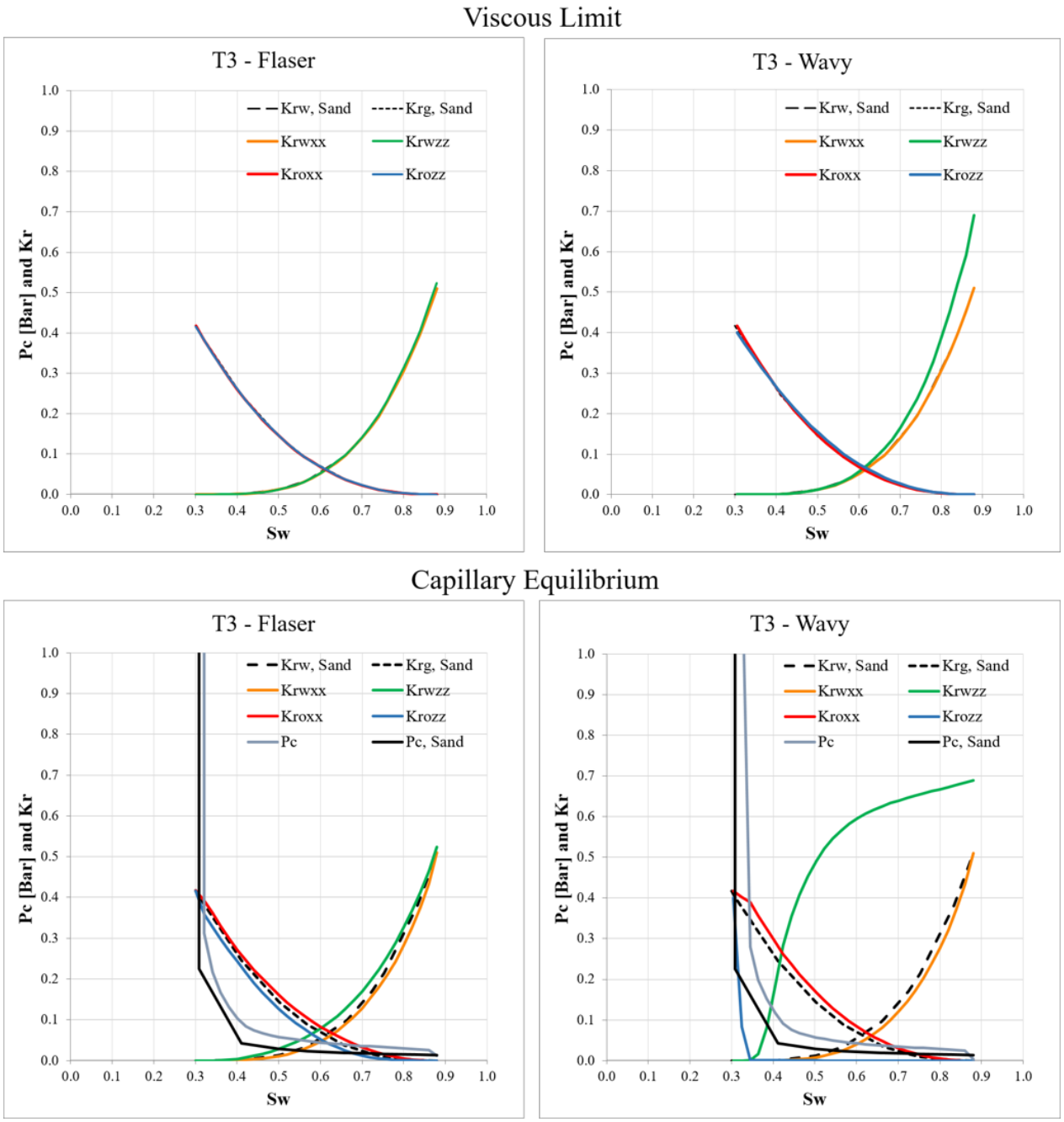

Figure 4.5: Relative Permeability and Capillary Pressure Upscaled in Capillary Equilibrium, and Relative Permeability upscaled in Viscous Limit.

The upscaled relative permeability curves in both VL and CE are very similar to those in zone T3, see Figure 4.9. The upscaling of relative permeability in Flaser bedding failed with the CE option. Several attempts were made without success. For the implementation of uspcaled relative permeability curves in the full scale model, the input curves for *SandRock*

will be used for T2_2 in the absence of upscaled curves.

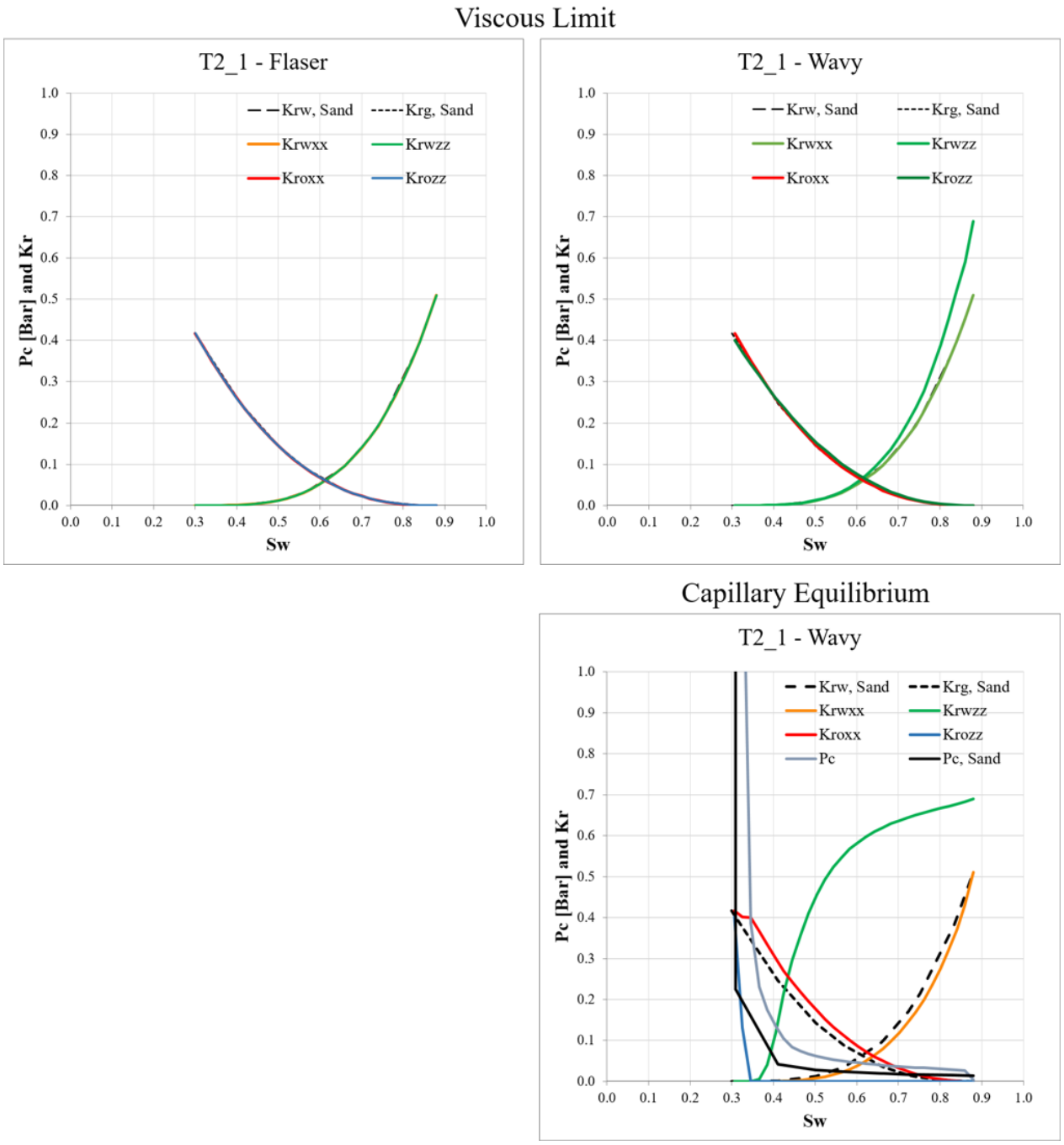

Figure 4.6: Relative Permeability and Capillary Pressure Upscaled in Capillary Equilibrium, and Relative Permeability upscaled in Viscous Limit. Upscaling in capillary limit of zone T-2_1 failed.

The k_v/k_h ratio is higher in T2_1 than in T3. A reasonable explanation to this is the permeability ratio between the layering types within Wavy and Flaser bedding in the two zones. After closer inspection, it was found that when adjusting the permeability in Flaser

Table 4.9: Vertical over horizontal permeability ratio in T3 and T2_1.

	$\mathbf{k_v/k_h}$	
Bedding	$T3$	$T2\_1$
Flaser	0.177	0.180
Wavy	0.0021	0.0030

bedding zone T3, the permeability ratio between the two sands was altered. This mistake may have affected the vertical over horizontal permeability ratio in T3. See Appendix B for the scaling factors used on each layering type.

4.6.3 Tubåen Zone T1

Results from upscaling relative permeability in Wavy and Flaser bedding with average reservoir properties corresponding to zone T1 in Tubåen.

The upscaled curves in Flaser and Wavy bedding, with the VL option, show little to no variation from the original input of *SandHigh* (presented as "$K_{rw}, Sand$" in Figure 4.7). In CE, the effect in both Wavy and Flaser is similar to the effect observed for Flaser bedding in CE for zone T3. The z-directional relative permeability of CO_2 is less for Wavy than for Flaser, but not to the same extent as in T3. A reasonable explanation to the smaller effect on the curves is the high permeability and porosity in T1.

The upscaled vertical and horizontal permeabilities are not differing by much, giving a k_v/k_h ratio close to 1.

Table 4.10: Vertical over horizontal permeability ratio in T3, T2_1 and T1.

	$\mathbf{k_v/k_h}$		
Bedding	$T3$	$T2\_1$	$T1$
Flaser	0.177	0.180	0.861
Wavy	0.0021	0.0030	0.811

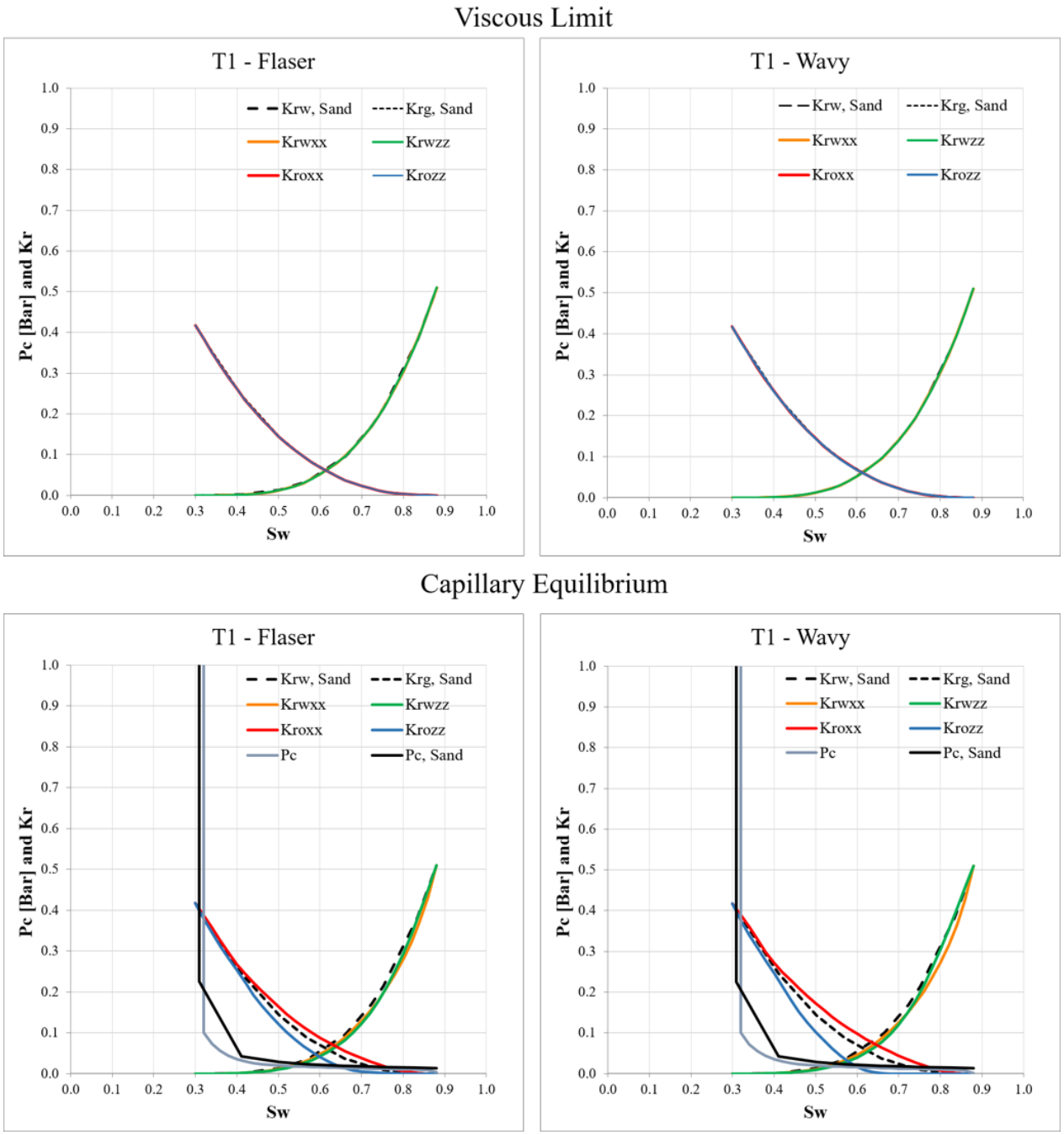

Figure 4.7: Relative Permeability and Capillary Pressure Upscaled in Capillary Equilibrium, and Relative Permeability upscaled in Viscous Limit.

Chapter 5

Running Full Scale Simulation Models

The last upscaling step is to transfer the relative permeability tables from the upscaling in different beddings to the full scale simulation model of the Tubåen formation. Two full field models were made available by Statoil; one Eclipse 300 compositional model of the entire Snøhvit field (which includes Tubåen) and one Eclipse 100 black oil model for Tubåen.

The most up-to-date and detailed model of the Tubåen formation is the 3-phase E300 compositional model using the Network option covering the Snøhvit natural gas development in the Barents sea. The model is history matched up until July 3, 2010 with production forecast up until January 1, 2020. The period from 3. July 2010 to January 1, 2020 simulate how the gas plume moves when only gravitational forces affect the flow.

5.1 Altering the E100 Model

The Tubåen section of the model has one CO_2 injection well, named F-2H. The injection is under group control, causing the composition of the injected gas in Tubåen to be dependent on the produced gas from the other sections in the field. The black oil model in E100 has a better grid resolution than the E300 model of Tubåen.

The E300 model is the model currently used by Statoil, but considering all the wells are linked, the model is over-complicated and unfavourable to use for the comparison of upscaling techniques of relative permeability of brine and $CO2_2$ at Tubåen - not at least because it is difficult to alter and adjust a compositional model. The Eclipse 100 black oil model of the Tubåen formation is, though less accurate, more suitable for the scope of this thesis. A decision was made to use the E300 model as a guideline, and create a local grid refinement around the injection well in E100 with the same size and properties as the Local Grid Refinement (LGR) used around the well in the E300 model. This way, any spatial differences in permeability and porosity are transferred - as well as all other reservoir properties linked to the grid blocks. The E100 model was modified from being a

3-phase model to being a 2-phase model for water and gas. The first step was to create the "Basecase" in E100, i.e. without upscaled relative permeability.

Adjusting the Basecase Model

Creating a Basecase model for the Tubåen Fm. is the first step, and the process starts with looking at the properties set around the injection well in the E300 model, and how these can be transferred to the E100 model.

5.1.1 How LGR4 in E300 is Transferred to E100

Several grid refinements are made in the Tubåen section of the E300 model. Local grid refinements are used to increase accuracy in defined areas of a grid. Having the same accuracy in the entire model would mean an unnecessary high run-time, and is generally not expedient in large models. Such a LGR, named LGR4, is surrounding the injection well at Tubåen (well F-2H), and increases the accuracy of the simulation in the area where gas is injected and stored. The grid dimensions for LGR4 are $\sim 85 \times 85 \times 10$m in the E300 model, and the refinement is covering the area most relevant for analyzing the plume development and migration of gas and will therefore be the area of focus throughout this paper.

LGR4 enables a higher precision and differentiation of reservoir properties in the area. This is ultimately to get a more realistic picture of the injection site in order to better understand where the gas is flowing and accumulating. LGR4 is made in the original layer 15 - the lowermost layer in the model where the F-2H well is perforated. The refinement replaces $I : 101 - 133,\ J : 141 - 150$ and $K : 15 - 15$ with a refined grid with the dimensions $I : 1 - 99,\ J : 1 - 30$ and $K : 1 - 20$. The placement of the injection well F-2H in the main grid is $I : 118,\ J : 144$ - which corresponds to $I : 50,\ J : 11$ in the refined grid.

The refinements in the xy-plane are 3×3, i.e. every grid block is refined into nine cells. In the x-direction, this means going from 33 to 99 grid blocks, while going from 10 to 30 grid blocks in the y-direction. In the z-direction, layer 15 is refined into 20 layers. Starting from the top of LGR4, the first four layers, 1-4, represent the uppermost zone of the LGR, T-5. The next four layers, 5-8, represent T-4, and so forth. Well F-2H is perforated in layer 9-20, i.e. T-3, T-2 and in the lowermost zone; T-1.

The LGR is divided into five zones of four layers each, but as previously concluded, the T2 interval with high shale content is better modelled as a separate zone. The zone division is discussed in Chapter 2.2, and resulted in a splitting of T-2 into T-2_1 and the more shaly T-2_2. For LGR4, this means that instead of 4 layers in T-2, it is now 2 layers in T-2_1 and 2 layers in T-2_2.

LGR4 in E300 refines the grid in all directions from 3×10×1 to 99×30×20. In the E100

model, however, the grid is *originally* more refined in the vertical direction and sufficiently refined in the xy-plane by the dimensions $\sim 50 \times 54 \times 20$m in the main grid. A result of the dimensions in the E100 model is that the LGR to be made and placed around the injection well does not need refinements in the xy-plane. However, refinements are needed in the vertical direction and each of the five layers are refined into four - making a total of 20 layers and reducing the z-directional dimension to $\sim 4m$. The LGR, hereafter named *LGR4* also in the E100 model, will therefore cover 99×30×5 grid blocks in the main grid and refining them into 99×30×20. LGR4 in E100 is a exact copy of LGR4 in the E300 model and placed at: $I : 241 - 339$, $J : 57 - 86$ and $K : 1 - 5$, with the well placed at $I : 50$, $J : 11$. The reason for making a LGR in E100 with the same dimensions as LGR4 in the E300 model was that it made it easier to transfer properties from E300. The dimensions in the LGR becomes $\sim 50 \times 54 \times 4$m, i.e. smaller grid blocks than in the original LGR4 in the E300 model.

5.1.2 Permeability and Porosity

Permeability and porosity values are given as special input data for the LGR in the correct dimensions of $99 \times 30 \times 20$. The permeability in the Basecase is modelled as isotropic, but with a the z-direction scaled according to the vertical versus horizontal permeability ratio, the k_v/k_h relationship. From the E300 model, this ratio is set to 0.1.

Matlab was used to import the permeability and porosity tables from LGR4 to calculate the average permeability in each zone, for then to find the scaling factors necessary for matching the original data to the goal values defined per zone. See Matlab script D.3 and D.4. Table 5.1 list the original and scaled average permeability in the x-direction, PERMX, and the original and scaled average porosity, PORO. The permeability in the z-direction is scaled proportionally with PERMX, as the k_v/k_h relationship is constant.

Table 5.1: Original (in E300) and scaled PERMX and PORO averages for each zone.

	PERMX			PORO		
Zone	Original mD	Scaling factor k -	Scaled mD	Original %	Scaling factor ϕ -	Scaled %
T5	31.29	10.40	340	20	0.59	12
T4	29.24	1.14	30	25	0.28	7
T3	4.99	60.56	343	8	1.84	14
T2_1	20.12	12.61	232	22	0.5	11
T2_2	21.18	0.01	0.1	22	0.23	5
T1	881.10	4.53	4000	26	0.77	20

5.1.3 Relative Permeability

The SATNUM (Saturation function region numbers) keyword is of special interest in this work, as it assigns the relative permeability tables to each grid block in the main grid. In the E300 model, the Tubåen formation is supplied with *one* set of water and CO_2 relative permeability tables. The unscaled curves from SandRock, Table 3.6 are used in the Basecase.

The injection period is from April 18, 2008 until April 12, 2010, and the simulation then runs to January 1, 2020 to simulate the plume migration caused by gravitational forces only. During the injection period, the injection is stopped between August 14, 2009 and January 4, 2010. When stopping the injection of CO_2 in the Tubåen Fm., an aquifer, the drainage process of gas displacing water is replaced by an imbibition process of water displacing gas and an hysteresis effect should be evident. Incorporating the effect of hysteresis is discussed in *Further Work* in Chapter 7.

5.1.4 Other Properties

PVT (pressure, volume, temperature) properties for the gas, Formation Volume Factor and Viscosity as a function of pressure, was created based on the output from a full run of the original and history matched E300 model, see Figure 5.1 for the plots.

Several properties linked to the LGR are defined in the main grid, such as SATNUM mentioned above. To extract these, Matlab script D.3 was written to target the correct cells of the main grid in E300; $33\times10\times1$ elements from $I : 101-133$, $J : 141-150$ and $K : 15-15$, and expand the matrix to $99\times30\times5$ elements in order to cover the corresponding area in the main grid of the E100 model. Next, these values from the E300 model were transferred to the correct location in the main grid of the E100 model.

5.1.5 Adding a Second LGR

When doing a test run of the Basecase with the transferred LGR4, the refined area was found to be a *little* to small to capture the full extension of the plume towards the last years of simulation. After the injection period, the simulation is run for about 10 years with only the gravitational forces to create equilibrium between the phases. In this time period, the gas plume is migrating towards higher elevation (north in the model) due to the density difference between water and gas. To make sure the plume movement is captured by a refined area with adjusted permeability, porosity and relative permeability tables, a LGR identical to LGR4 was placed on the north-side of LGR4. The second LGR is named LGR4_2.

The area outside LGR4 and LGR4_2 is not altered, but remains as in the original E100 model. The basis for this decision, is that the injected gas will not reach outside the LGRs

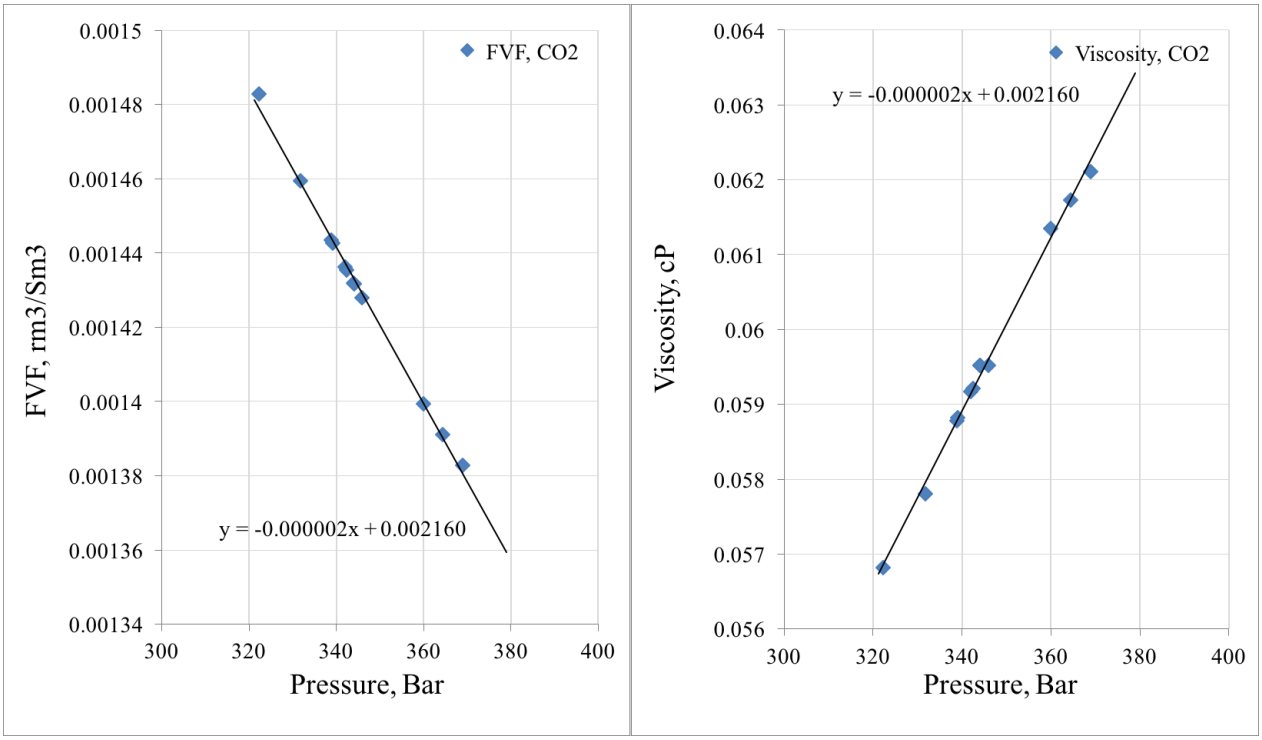

Figure 5.1: FVF for CO_2 vs. pressure and viscosity of CO_2 vs. pressure from a run of the original E300 model.

in the injection period, or the 10 years of only gravitational equilibrium, which is the time frame this thesis covers. Only the area inside the LGR is therefore interesting as this is the area where the effect of different upscaling techniques and combinations of these are visible. It can be discussed that the refined area can ”feel” for example pressure effects from outside the LGR, but such effects are assumed to be negligible and will not be discussed further.

5.2 Model 0: Basecase

The Basecase is created to have a basis for comparison assimilating the model of Tubåen which is currently used by Statoil, the E300 model. This model does not have upscaled nor directional relative permeability curves, but uses the set of permeability curves from a typical sandstone, *SandRock* in Table 3.6. The model is as described in Section 5.1.

Relative permeability

Only one set of relative permeability tables are used for the LGRs, see Table 5.4. The tables are almost the same as in the Rock Input File for *SandRock* used for the first upscaling step in OPM (Table 3.6), but with corresponding capillary pressure tabulated instead of J-function

and smaller modifications to fit the Eclipse input guidelines. The tables were fitted using Corey Correlation, see Chapter 3.

The Basecase will be used as the basis for comparison when models with upscaled, anisotropic relative permeability tables are tested in Section 5.3. A few keypoints are important about the Basecase, for later to compare it with models using upscaled relative permeability curves;

1. Only one set of relative permeability tables is used for water and CO_2.
2. The relative permeability tables are not upscaled.
3. The relative permeability is isotropic, i.e. the same in x, y and z-direction.
4. The k_v/k_h relationship is the same in all layers, and equals 0.1.

5.3 Full Scale E100 Models with Upscaled Relative Permeability

New full scale models are created with various variations of upscaled relative permeability. In Chapter 4, the different upscaled relative permeability tables are presented. The upscaling of relative permeability was performed for each zone in Tubåen (T5, T4, T3, T2_1, T2_2 and T1) in both Wavy bedding and Flaser bedding, using both Capillary Equilibrium upscaling and Viscous Limit upscaling. The k_v/k_h relationship corresponding to the upscaled curves was used to alter the z-directional permeability in the LGR, and the SATNUM table needed alterations, see Matlab script***. The upscaling work resulted in twelve new relative permeability tables upscaled in capillary limit, and twelve new relative permeability tables upscaled in viscous limit.

The first four models with upscaled relative permeability

- **Model 1: Rel.perm. upscaled in Flaser bedding, Capillary limit**
  The model was given upscaled relative permeability tables from upscaling in Flaser bedding using the CE option. The z-directional permeability in each layer was scaled by the upscaled k_v/k_h ratio.
- **Model 2: Rel.perm. upscaled in Flaser bedding, Viscous limit**
  The model was given upscaled relative permeability tables from upscaling in Flaser bedding using the VL option. The z-directional permeability in each layer was scaled by the upscaled k_v/k_h ratio.

- **Model 3: Rel.perm. upscaled in Wavy bedding, Capillary limit**
  The model was given upscaled relative permeability tables from upscaling in Wavy bedding using the CE option.The z-directional permeability in each layer was scaled by the upscaled k_v/k_h ratio.

- **Model 4: Rel.perm. upscaled in Wavy bedding, Viscous limit**
  The model was given upscaled relative permeability tables from upscaling in Wavy bedding using the VL option. The z-directional permeability in each layer was scaled by the upscaled k_v/k_h ratio.

These four models will mostly be used to investigate the effect of small scale heterogeneities on the full scale simulation. Keeping it simple, using *one* upscaling method at the time, is important to be able to clearly distinguish between the effect of upscaling in different beddings, geology effect, and the effect of using different upscaling techniques. The relative permeabilities upscaled in each bedding and each upscaling limit are tabulated in Appendix C.

The last 2 models with upscaled relative permeability

The last 2 models are a bit more complex. A set of cut-off values for permeability is used to classify each grid cell as either *Well Sorted Sand*, *Flaser bedding*, *Wavy bedding* or *Mud*. The cut-off values are determined based on a histogram of the permeability values (x-direction) in LGR4, see Figure 5.2. Table 5.2 tabulate the cut-off values. The k_v/k_h relationship corresponding to the upscaled curves assigned by the cut-off values was used to alter the z-directional permeability in the LGR, see Matlab script***. The result of using permeability cut-offs, is that we end up having areas with permeability upscaled in Flaser bedding, Wavy bedding, and areas where the relative permeability curves are unscaled - a mix of relative permeability curves are used.

- **Model 5: Rel.perm. upscaled in Mixed bedding, Capillary limit**
  The model was given a mix of upscaled relative permeability tables in Wavy or Flaser with the CE option, or unscaled tables for *Well Sorted Sand* or *Mud*. The z-directional permeability in each layer was scaled by the corersponding upscaled k_v/k_h ratio.

- **Model 6: Rel.perm. upscaled in Mixed bedding, Viscous limit**
  The model was given a mix of upscaled relative permeability tables in Wavy or Flaser with the VL option, or unscaled tables for *Well Sorted Sand* or *Mud*. The z-directional permeability in each layer was scaled by the corersponding upscaled k_v/k_h ratio.

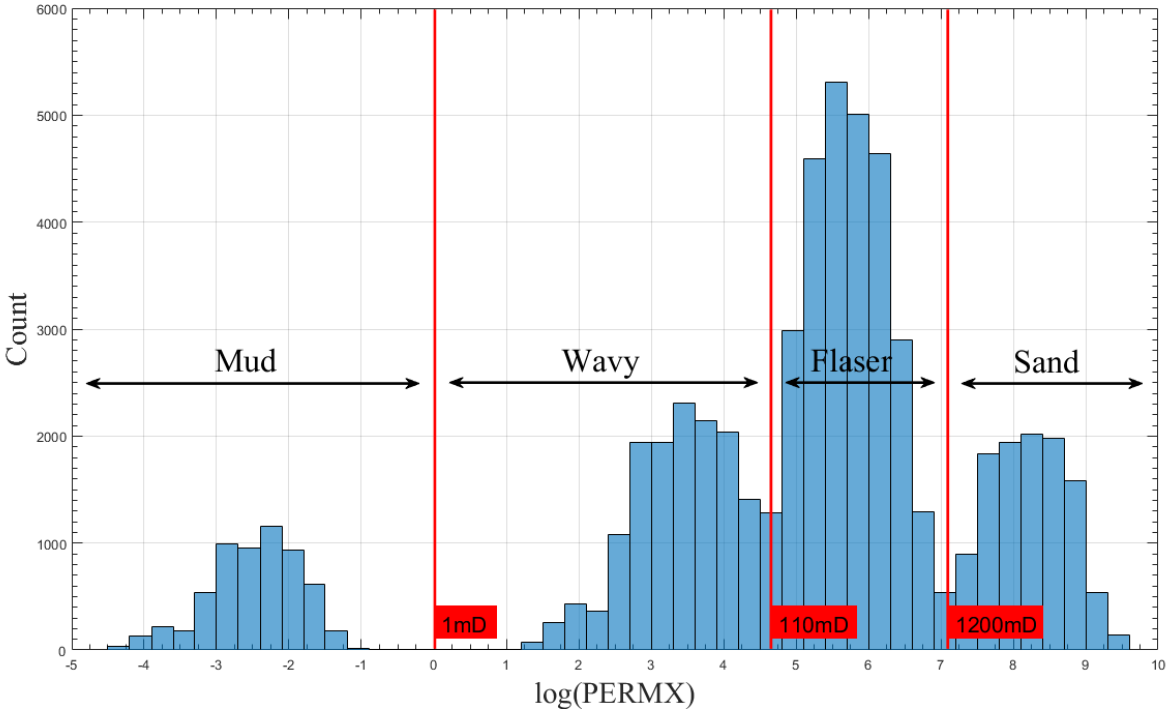

Figure 5.2: Histogram of permeabilities in LGR4, determining cut-off values.

Table 5.2: Permeability cut-off values and categories

Cut-offs:	Mud $<$ *1mD* $<$ Wavy $<$ *110mD* $<$ Flaser $<$ *1200mD* $<$ Well Sorted Sand

Table 5.3 gives an overview of SATNUM, saturation numbers, for saturation tables (relative permeability and capillary pressure) when using cut-off values. For T2_2 in Flaser bedding with the CE option, the upscaling in OPM failed. Therefore, the relative permeability and capillary pressure table for *Well Sorted Sand* is used for Flaser in this zone. The same numbering of relative permeability tables is used for both the CE and the VL option - the SATNUM numbering.

Table 5.3: Overview of SATUM numbers for cut-off models.

Zone	Mud	Wavy	Flaser	Well Sorted Sand
T5	6	8	7	5
T4	6	10	9	5
T3	6	12	11	5
T2_1	6	14	13(5)	5
T2_2	6	16	15	5
T1	6	18	17	5

The idea behind using cut-off values is that the two bedding types, Wavy and Flaser,

are typically found in different zones of a reservoir. As commented in Chapter 4 and seen from Table 4.2, Wavy bedding contains more mud than Flaser bedding and it is therefore natural to assign Wavy to the lower permeability areas in the model. Tubåen is a highly channelized formation where the use of such permeability cut-off values may be important for the accuracy of the gas distribution.

Grid cells with permeability value categorized as either *Well Sorted Sand* or *Mud* are assigned unscaled relative permeability tables from the creation of Input Rock Files in Chapter 3 - they are given the *SandRock* and *MudRock* relative permeability tables, respectively (Table 5.4). The tables are almost the same as in the Rock Input File for Sand and Mud used for the first upscaling step in OPM (Table 3.6), but with corresponding capillary pressure tabulated instead of J-function and smaller modifications to fit the Eclipse input guidelines.

For T2_1, the upscaling failed with Flaser bedding. SATNUM 13 is therefore assigned the relative permeability table from unscaled *SandRock*, SATNUM 5.

Table 5.4: Unscaled relative permeability and capillary pressure tables for Full Scale models.

SandRock - used for *Well Sorted Sand*

Water			CO_2		
S_w fraction	k_{rw} mD	P_c Bar	S_g fraction	k_{rg} mD	P_c Bar
3.000E-01	0.000E+00	2.300E-01	0.000E+00	0.000E+00	0
3.090E-01	2.374E-07	2.253E-01	1.200E-01	0.000E+00	0
4.110E-01	1.564E-03	4.218E-02	1.660E-01	7.400E-04	0
5.020E-01	1.271E-02	2.829E-02	2.470E-01	9.370E-03	0
5.690E-01	3.465E-02	2.337E-02	2.760E-01	1.570E-02	0
6.590E-01	9.515E-02	1.928E-02	3.350E-01	3.490E-02	0
6.650E-01	1.008E-01	1.907E-02	3.410E-01	3.740E-02	0
7.240E-01	1.704E-01	1.725E-02	4.310E-01	8.790E-02	0
7.530E-01	2.147E-01	1.651E-02	4.980E-01	1.430E-01	0
8.340E-01	3.819E-01	1.479E-02	5.890E-01	2.460E-01	0
8.800E-01	5.100E-01	1.400E-02	6.910E-01	4.020E-01	0
1.000E+00	1.000E+00	0.000E+00	7.000E-01	4.180E-01	0

MudRock - used for *Mud*

Water			CO_2		
S_w fraction	k_{rw} mD	P_c Bar	S_g fraction	k_{rg} mD	P_c Bar
4.000E-01	0.000E+00	4.000E-01	0.000E+00	0.000E+00	0
4.074E-01	3.258E-07	3.731E-01	1.200E-01	0.000E+00	0
4.919E-01	2.146E-03	1.062E-01	1.581E-01	7.090E-04	0
5.672E-01	1.745E-02	7.875E-02	2.251E-01	8.970E-03	0
6.226E-01	4.756E-02	6.824E-02	2.491E-01	1.500E-02	0
6.971E-01	1.306E-01	5.907E-02	2.979E-01	3.350E-02	0
7.021E-01	1.384E-01	5.859E-02	3.029E-01	3.580E-02	0
7.509E-01	2.338E-01	5.436E-02	3.774E-01	8.420E-02	0
7.749E-01	2.947E-01	5.259E-02	4.328E-01	1.370E-01	0
8.419E-01	5.242E-01	4.844E-02	5.081E-01	2.350E-01	0
8.800E-01	7.000E-01	4.648E-02	5.926E-01	3.850E-01	0
1.000E+00	1.000E+00	0.000E+00	6.000E-01	4.000E-01	0

Chapter 6

Results and Discussion

The results from running the Full Scale Models described in Chapter 5 are presented and discussed in this chapter. The plume development and what causes the development to differ between the models are the focus and will be discussed together with the results. The results were originally meant to be compared to seismic plume data, but the data was unfortunately not supplied before the deadline of this project. Instead, the models will be commented based on the effect of bedding and upscaling limit on the gas distribution.

6.1 Results and Discussion

6.1.1 Joint Characteristics of the Models

All models have the same permeability in the horizontal direction, porosity and depth. These properties are presented for the top of the Tubåen 1 zone - layer 17. Zone T1 was chosen as it is the zone of highest permeability and porosity, and therefore the best injection zone. The general properties for Model 0-6 are presented in Figures 6.1, 6.2, 6.3 and 6.4.

The perforated intervals in all models are zone T3, T2_1 and T1. It should be noted that the visualization software, ResInsight, interpret a two-phase system as oil-water, which is why the legend reads SOIL and not SGAS for gas saturation in all saturation tables and Figures to follow.

The permeability map (xy-plane) shows that T1 has N-S trending channels with even higher permeability than the rest of the high-permeability zone. Injection well F-2H is placed just on the edge of one of these channels with an area of lower permeability to the west, and higher permeability to the N-E. The permeability distribution in the zone is expected to affect the gas distribution, i.e. from the permeability map alone, it should be expected to see the CO_2 spreading and accumulating more on the N-E side of the injection well. The porosity distribution, especially evident with the area of lower porosity west of the injection,

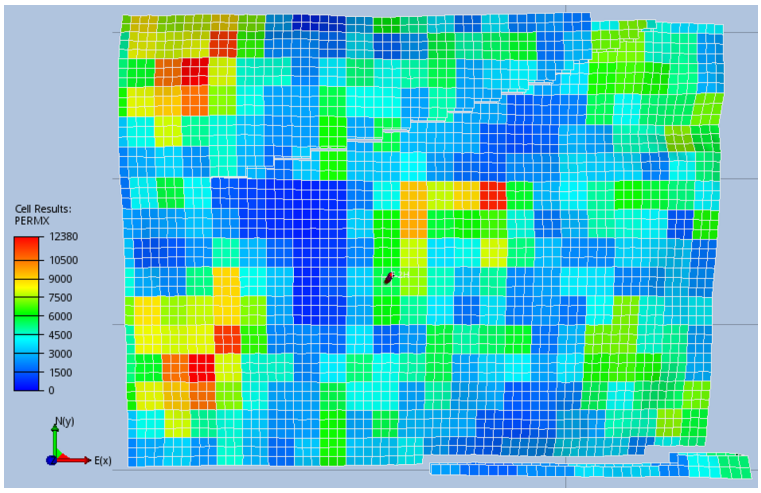

Figure 6.1: Permeability distribution in the xy-plane for top of T1 - layer 17.

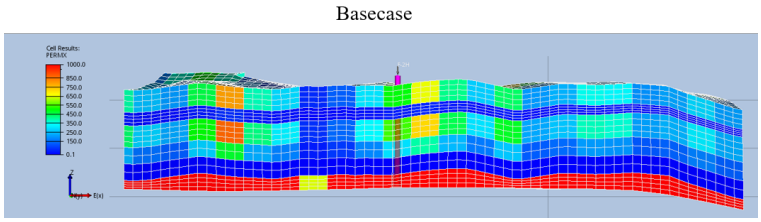

Figure 6.2: W-E cross-section of the permeability distribution in the xy-plane for the Basecase.

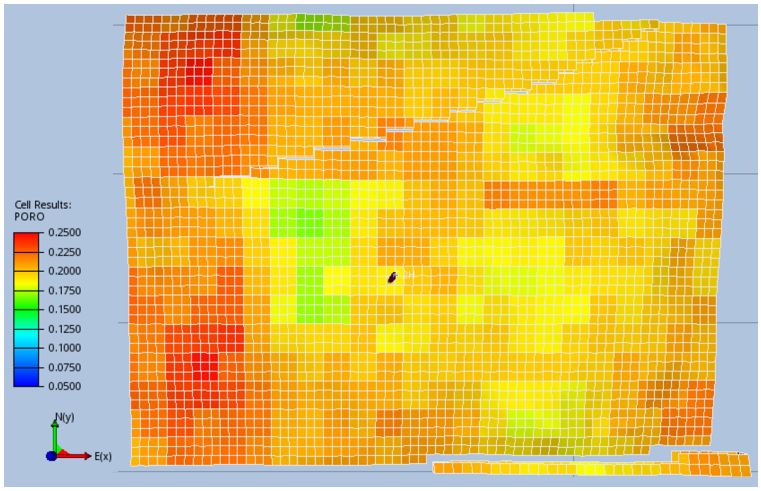

Figure 6.3: Porosity distribution in the xy-plane for top of T1 - layer 17.

coincides with the permeability map. For the gravitational dominated period, i.e. after history matching and the well is closed, the gas is expected to find a migration path towards higher elevation due to the density difference between injected CO_2 and the water in the aquifer. Higher elevation is seen north and west of the injection well.

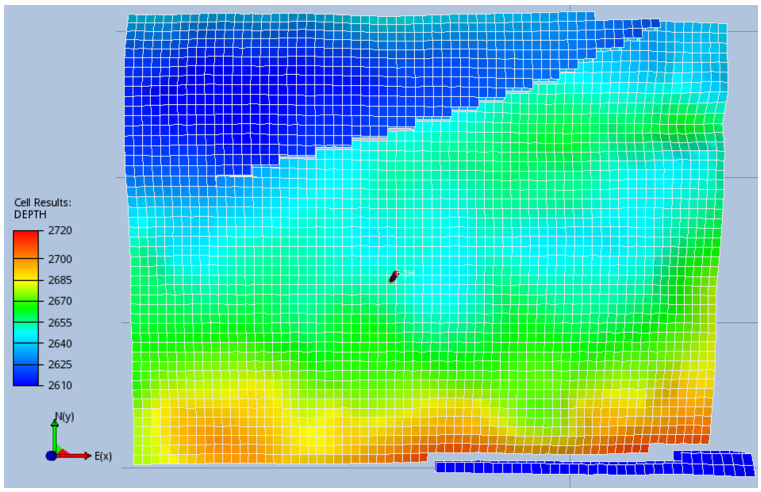

Figure 6.4: Depth Map from top of T1 - layer 17.

In the paper by Singh et al. (1981) it is discussed how CO_2 storage is most likely dominated by capillary and gravity forces. The effect of gravitational forces at the small scale was tried tested with the Gravity Capillary Equilibrium option in OPM, but the method failed and produced illogical output. The capillary equilibrium method is assumed to be the preferred method for upscaling relative permeability of CO_2 and brine, but it is nevertheless interesting to compare the effect of capillary forces with the effect of viscous forces.

6.1.2 Model 0: Basecase

The results from running Model 0, the Basecase, with one set of unscaled relative permeability tables are given in Figure 6.5. Having an unscaled relative permeability curve as input, effectively means that the formation is given relative permeability as if it was homogeneous. For this reason, it is expected to see a plume development more affected by the geology than the relative permeability.

The gas saturation topmap shows that in the xy-plane, the gas spreads quite uniformly during the injection period, but slightly more to the east. This coincides well with the permeability and porosity distribution showing better reservoir properties (higher permeability and porosity) to the east (Figure 6.1 and 6.3). An interesting result is the little pier to the east of the injection well at the end of injections. A natural thought is that the pier correlates to a zone of higher permeability and porosity, but by looking at Figure 6.6, there is not an obvious correlation to the reservoir properties. The most likely explanation is the difference in elevation. The pier coincides well with a more elevated area. If the pier is a result of this height difference, then that means the gravitational forces are driving the plume upwards.

A cross-section W-E through the well shows how the gas segregates in the injection period, seen by the non-uniform shape of the plume. The gas saturation increases towards the higher

layers, and a gas cap is created at the top of T3, with a modest migration into the T4 zone. Zone T2 is split in T2_1 and T2_2 (see Chapter 2), where T2_2 (layer 15 and 16) is of very low permeability and porosity and acts as a barrier for vertical flow between T1 and T2_1.

After injection stop, in the gravity driven equilibrium period from end of injections until end of simulation January 1, 2020, the segregation continues and the gas migrates predominantly in the N-W and N-E direction. The Topmap of the plume in layer 17 correlates highly with the depth map in the same layer, see Figure 6.7. Some gas is accumulating where it meets the fault going N-E, while some migrates to the west of the fault and further up. The plume seems to be close to fully segregated by the end of simulation in 2020. The gas accumulated at the top of T1, T2_1 and T3. We are most likely seeing a geology effect - the tilting of the layers towards higher elevation guiding the migration path - and less so a relative permeability effect.

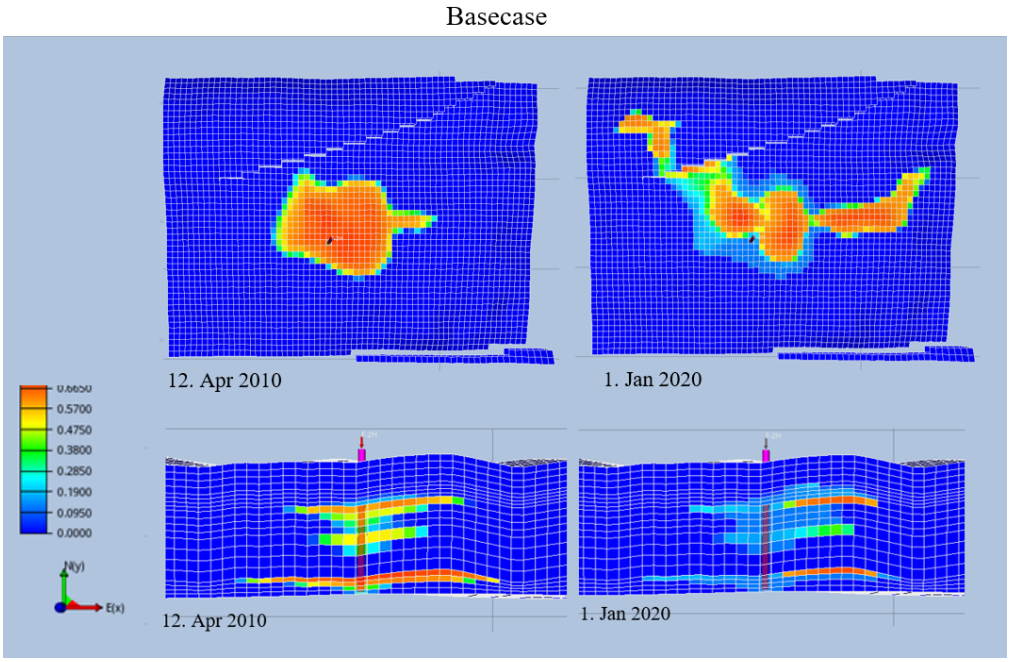

Figure 6.5: Model 0: Basecase. Topmap of the gas distribution in layer 17 (top of zone T1) and cross-section W-E through the well. Left hand shows the situation at end of injection, April 12, 2010, and right hand side shows the situation at end of simulation, January 1, 2020.

6.1.3 Model 1-4: Flaser and Wavy Bedding

The objective with model 1-4 is to establish whether or not there is a noticeable difference on the plume development when using relative permeability curves from upscaling in Viscous Limit versus in Capillary Equilibrium. Upscaled relative permeability tables were generated for each zone of Tubåen, T1-T5, applying both the Capillary Equilibrium and the

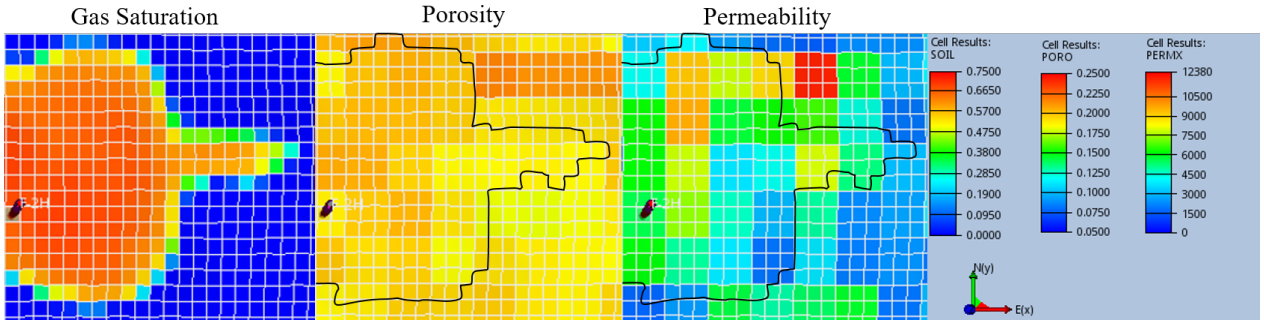

Figure 6.6: Model 0: Basecase. At end of injection, April 12, 2010, a small pier to east has formed.

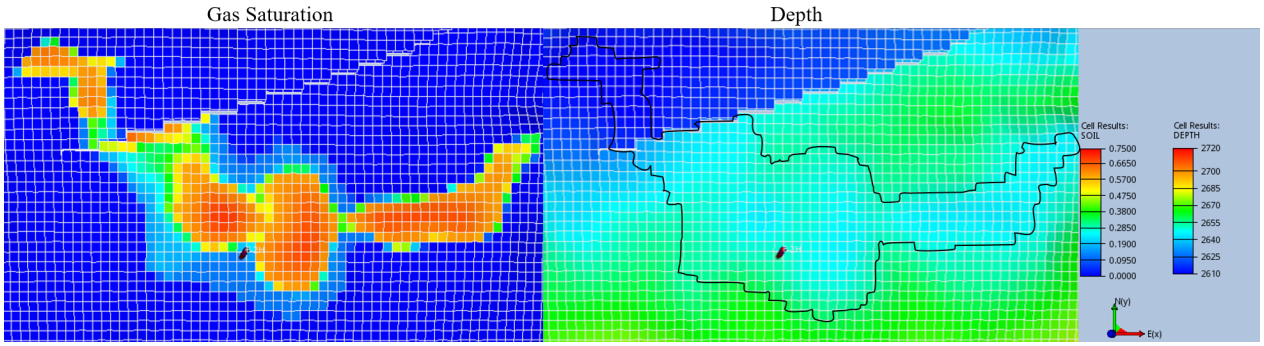

Figure 6.7: Model 0: Basecase. At end of simulation, January 1, 2020, the gas plume from topmap of layer 17 coincides well with the depth map of the same layer.

Viscous Limit option (see Appendix C). The two bedding types Wavy and Flaser were used as framework for the upscaling.

The upscaled relative permeability curves for T3, the uppermost perforated zone, are plotted and discussed in Section 4.6.1, but repeated here for a refresher. The relative permeability curves in z-direction from upscaling in Wavy bedding differ greatly from the input curve. The upscaled gas relative permeability curve has a broad saturation range in which it has zero relative permeability to water. The curvature means that vertical flow of CO_2 is limited to the when the drainage process has reduced the water saturation to almost connate water saturation. The upscaled relative permeability curves are a result of how the CE option requires capillary equilibrium between the layers within the bedding, and water is drawn towards the lower permeable layers. The effect of the CE option is greatest in Wavy bedding, explained by the bedding having continuous horizontal layers of *Mud*. The upscaled curves in Flaser bedding does not show the same limited vertical relative permeability, which can be explained by the model having *dis*continuous mud layers. Using the upscaled curves from CE in Wavy bedding as input in the full scale model should result in less segregation of the gas plume and rather a more unified and extensive plume - which is what we can see

in Figure 6.8.

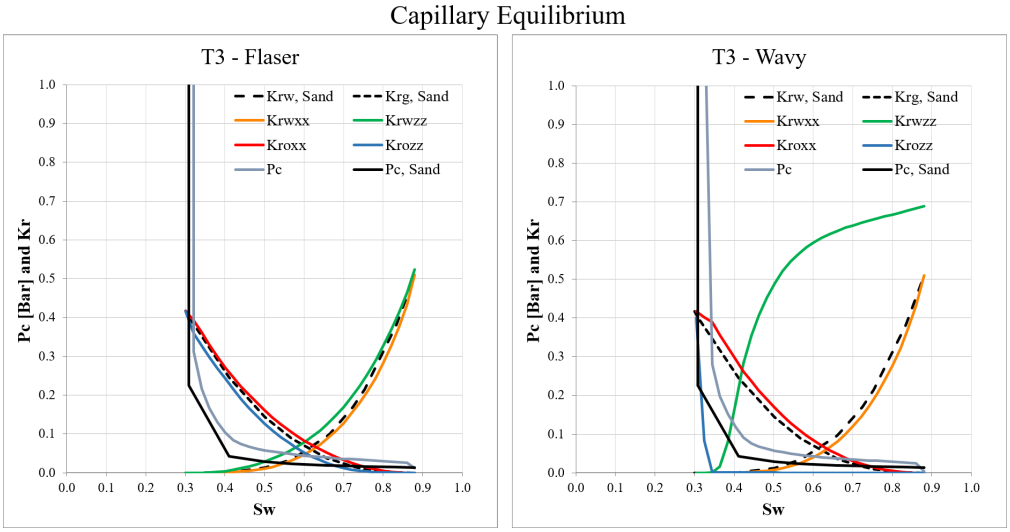

Figure 6.8: Input Releative permeability and capillary pressure curves for zone T3 after upscaling in the geological models Wavy and Flaser using the Capillary Limit option.

The result of using the Capillary Equilibrium option was twelve upscaled relative permeability and capillary pressure curves - six from using Wavy bedding and six from using Flaser bedding as framework. The same for using the Viscous Limit option. The six upscaled curves in each bedding corresponds to the six zones with different properties defined in Tubåen. The full Tables of the upscaled curves used as input in the full scale models are found in Appendix C.

To investigate the effect of upscaling with the CE option versus the VL option, the Basecase was first altered with input relative permeability curves created in Flaser bedding using the CE option, and then the curves from applying the VL option. The same was done with upscaled curves created in Wavy bedding. This way, it might be possible to distinguish between geological effects from the choice of bedding and the effect of Balance of Forces induced by the choice of using either the CE or the VL option.

Model 1 and 2, Flaser Bedding

The choice of upscaling in Capillary Equilibrium state versus in Viscous Limit did not seem to greatly affect the distribution of CO_2 in Tubåen with Flaser bedding. The mud layers in Flaser bedding are not continuous, and are therefore not expected to affect the vertical flow in any great manner. From Figure 6.9 and 6.10 it is possible to see that the CE method results in a plume with a smoother distribution of gas compared to the model upscaled with VL where the gas plume has a more defined boundary caused by the capillary pressure being

assumed to be zero and the saturations being greatly affected by the distribution of absolute permeability in the domain.

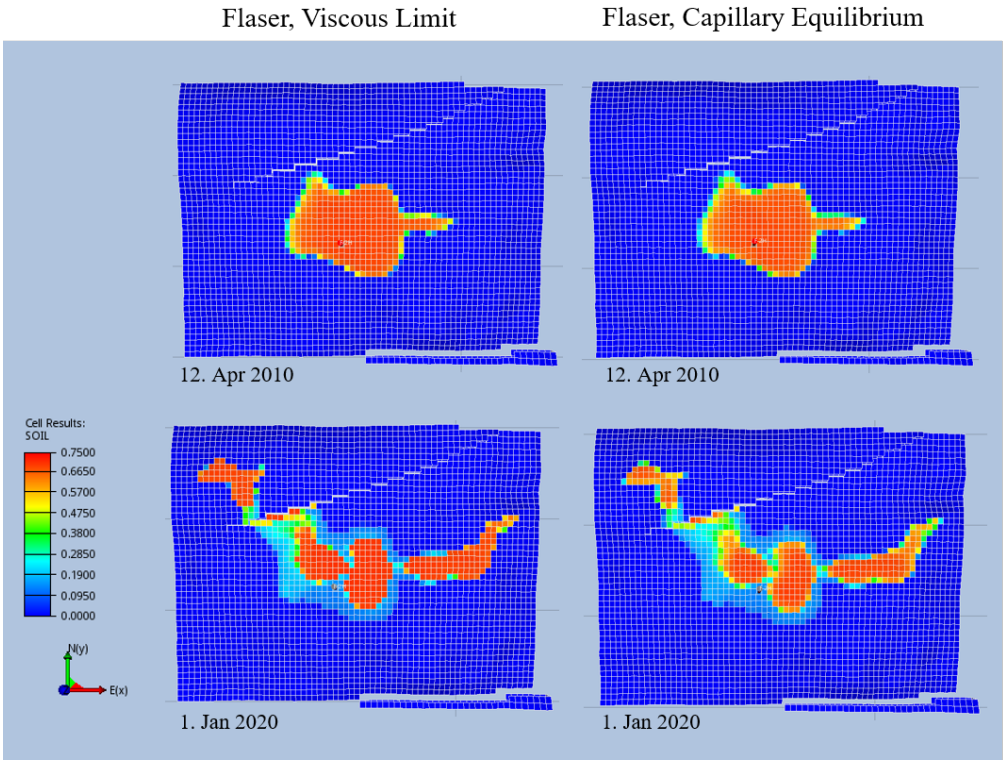

Figure 6.9: Model 1 and 2. Topmap and W-E cross-section with results from using Relative Permeability curves upscaled in Flaser bedding with Viscous Limit and Capillary Equilibrium conditions.

At the end of the injection period, April 12, 2010, a "pier" to the east as seen in the Basecase has formed. As previously discussed, it is likely this pier is due to the tilting of the layer, not relative permeability, as it is equally developed in both CE and VL. The difference between capillary equilibrium and viscous limit is noticeable in the vertical direction. At the end of simulation, the plume in VL is more segregated than the plume in CE. It is likely that the segregation in CE will reach the same level as in VL, but that it will take more time due to the mud layers creating alternating zones of high and low relative permeability of CO_2 (as discussed in Section 4.6.1).

Model 3 and 4, Wavy Bedding

The topmaps of Tubåen with Wavy bedding are very similar to the topmaps of Flaser bedding, where CE creates a smoother saturation gradient in the plume than VL which creates a more distinct plume boundary.

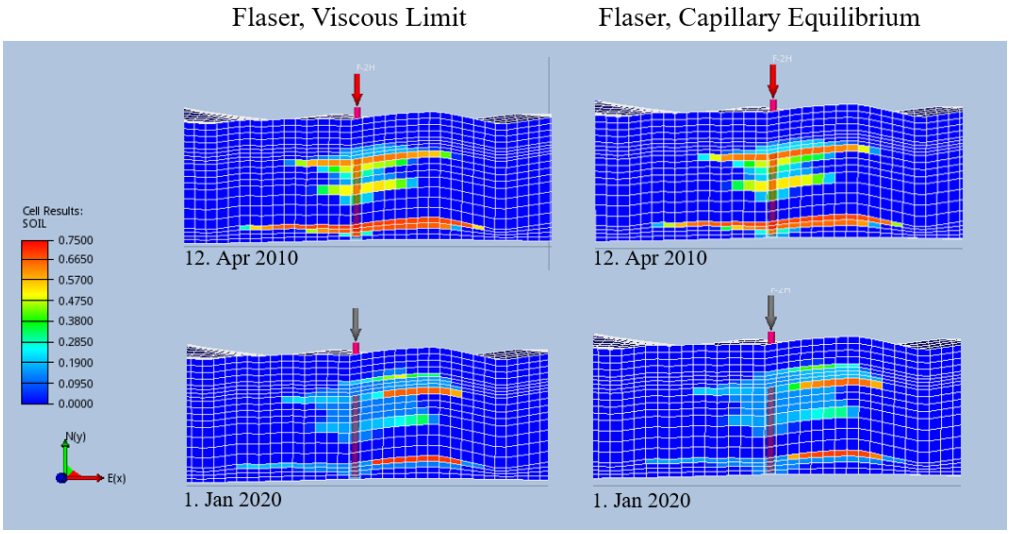

Figure 6.10: Model 1 and 2. W-E cross-section with results from using Relative Permeability curves upscaled in Flaser bedding with Viscous Limit and Capillary Equilibrium conditions.

The cross-sections of the models show a great difference between upscaling relative permeability curves in Wavy bedding versus Flaser bedding, as was expected from the plot of the upscaled curves, described in Section 4.6. At the end of the injection period, the saturation of the plume - and the plume itself - is more unified compared to Model 1 and 2 with upscaling in Flaser bedding. The lower degree of segregation can be explained by the higher content of mud distributed in continuous horizontal layers in Wavy bedding. The effects of the mud with CE and VL are previously discussed, but in short; vertical flow is much more affected by the mud in the CE option than in the VL option, but the vertical relative permeability of CO_2 is reduced in both cases.

The cross-sections from end of injections April 12, 2010 show how the plume is less segregated with the CE option than with the VL option. Both plumes are affected by gravitational forces, but the segregation happens much slower and has not yet reached the point where the gas is accumulating in specific areas. An interesting and somewhat unexpected result, is the greatly reduced segregation in the lowermost T1 zone where the permeability and porosity is very high. The reduced segregation is noticeable in both beddings, but clearly more defined in Wavy bedding.

After the gravitational dominated period, the difference between the VL option and the CE option is even clearer. With the VL option, the plume is clearly segregated, while in the CE limit, the segregation is far from complete, but the gas has moved in a more unified manner east towards higher elevation, permeability and porosity.

The effect of CE versus VL is more evident with input curves from upscaling in Wavy bedding than in Flaser bedding. Especially after the gravitational dominated period, the

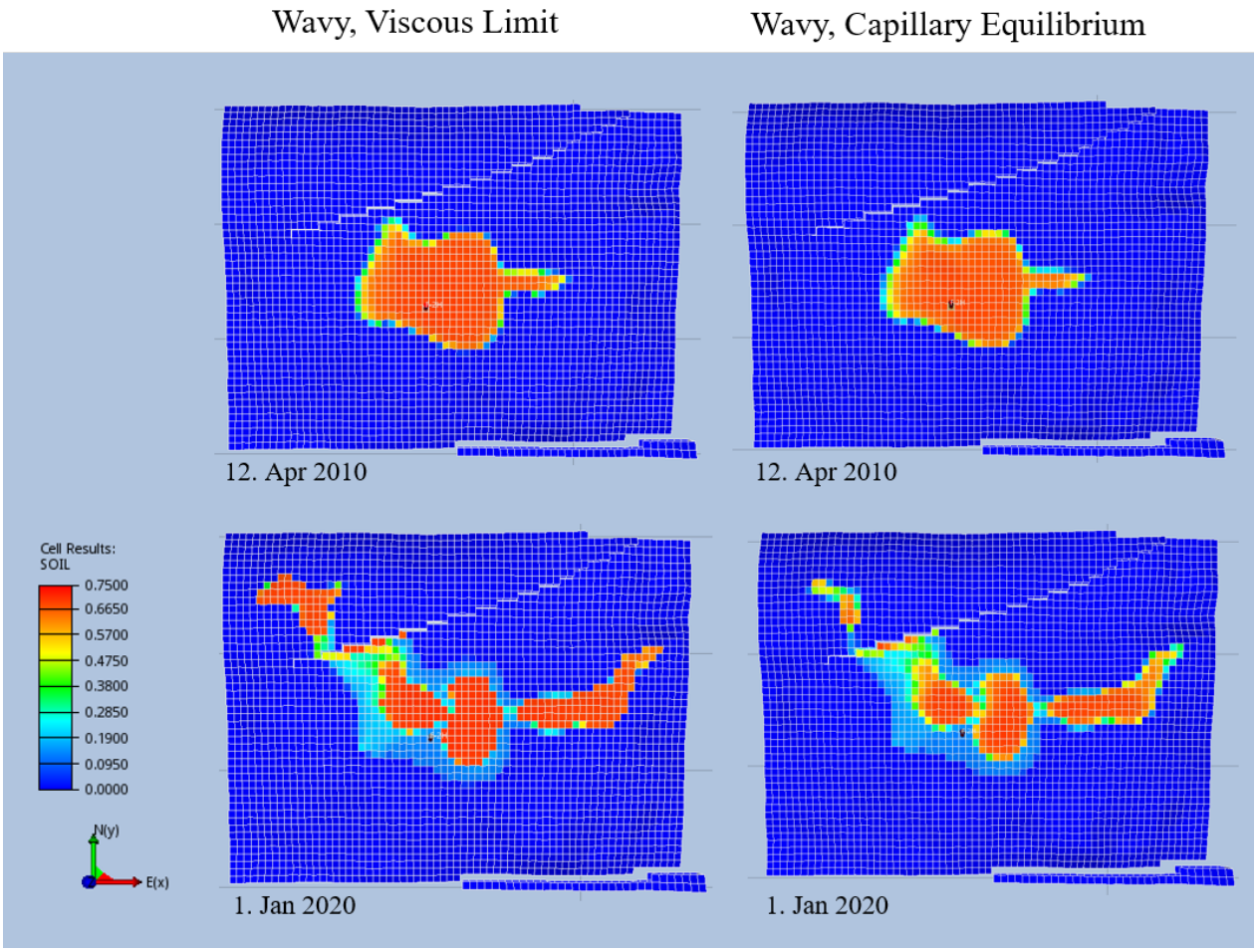

Figure 6.11: Model 3 and 4. Topmap with results from using Relative Permeability curves upscaled in Wavy bedding with Viscous Limit and Capillary Equilibrium conditions.

plume with CE migrates to the east (area with higher permeability, see the Topmap of layer 17) and stays quite uniform with a clearly increasing saturation gradient towards the top perforated zone T3 - likely to be predominately a gravitational effect due to the density difference between gas and water suppressed by the limited vertical flow of CO_2. In VL the plume becomes less uniform during the gravitational dominated period. The density difference drives the gas upwards towards top of zone T3. The spreading in VL correlates well with the cross-sectional view of the permeability distribution in the formation, Figure 6.2.

The migration pattern is therefore assumed to be influenced by both geological reasons and the upscaled relative permeability.

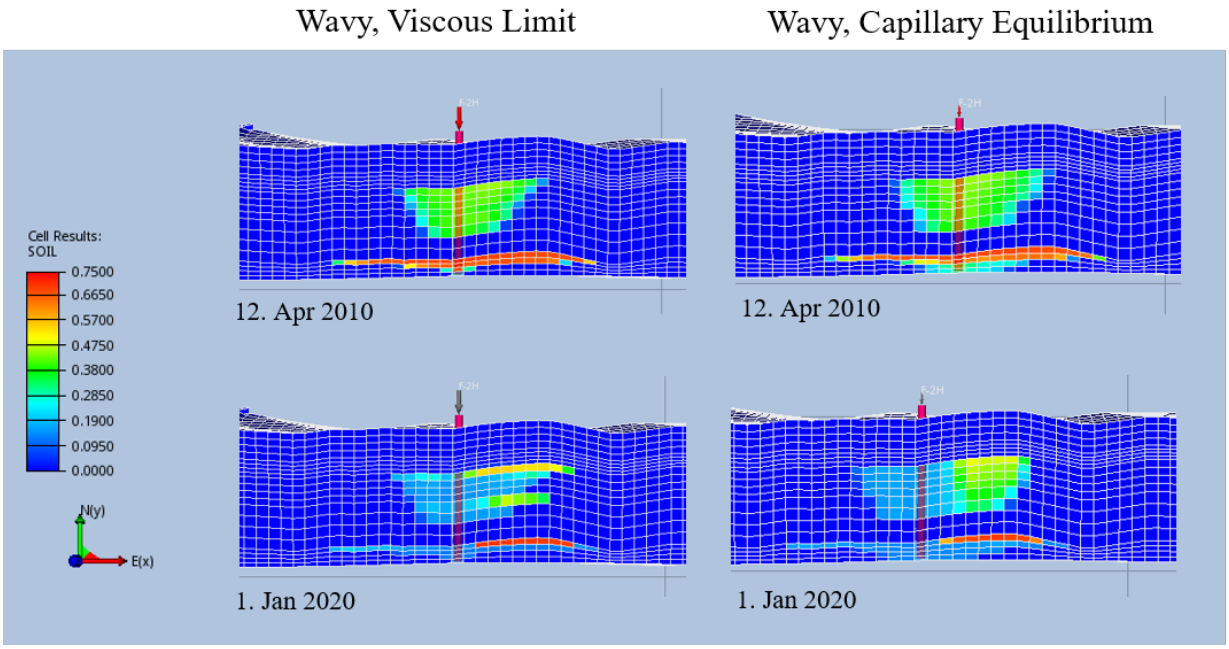

Figure 6.12: Model 3 and 4. W-E cross-section with results from using Relative Permeability curves upscaled in Wavy bedding with Viscous Limit and Capillary Equilibrium conditions.

6.1.4 Model 5 and 6: Mixed Bedding Using Permeability Cut-Off

The last 2 models have relative permeability tables distributed in the grid based on a set of permeability cut-off values. Every grid cell is characterized as either *Well Sorted Sand*, *Flaser bedding*, *Wavy bedding* or *Mud*. The cut-off values are determined based on the histogram of the permeability values (x-direction) in LGR4, see Figure 5.2. Both *Well Sorted Sand* and *Mud* are assigned unscaled relative permeability tables, see Table 5.4.

The idea behind using cut-off values is that the two bedding types, Wavy and Flaser, are typically found in different zones of a reservoir. As commented in Chapter 4 and seen from Table 4.2, does Wavy bedding contain more mud than Flaser bedding and it is therefore natural to assign Wavy to the lower permeability areas in the model. The result of using permeability cut-offs, is that we end up having areas with permeability upscaled in Flaser bedding, in Wavy bedding, and areas where the relative permeability curves are unscaled. Using cut-offs should yield a more realistic plume development in the full scale model.

Almost the entire zone T1 is gets characterized as *Well Sorted Sand*, which then assigns the cells unscaled relative permeability and capillary pressure curves - as in the Basecase. The gas distribution in T1 is therefore expected to be very similar in Model 0, 5 and 6. The tight layer T2_2 right above T1 is blocking most, if not all, the flow from T1 and upwards. A full overview of the SATNUM numbers is shown in Table 5.3, but satnum-numbers 5 and 6 are the unscaled curves for *Well Sorted Sand* and *Mud* respectively. All other odd numbers

are upscaled curves in Flaser bedding, while all other even numbers are upscaled curves in Wavy bedding.

The result from running the full scale model with relative permeability and capillary pressure curves assigned from the defined cut-off values, is shown with topmaps of zone T1 and a cross-section W-E through the well. At the end of the injection period the most prominent difference between CE and VL is that the gas saturation seen from the topmaps is less with CE than with VL due to reduced segregation.

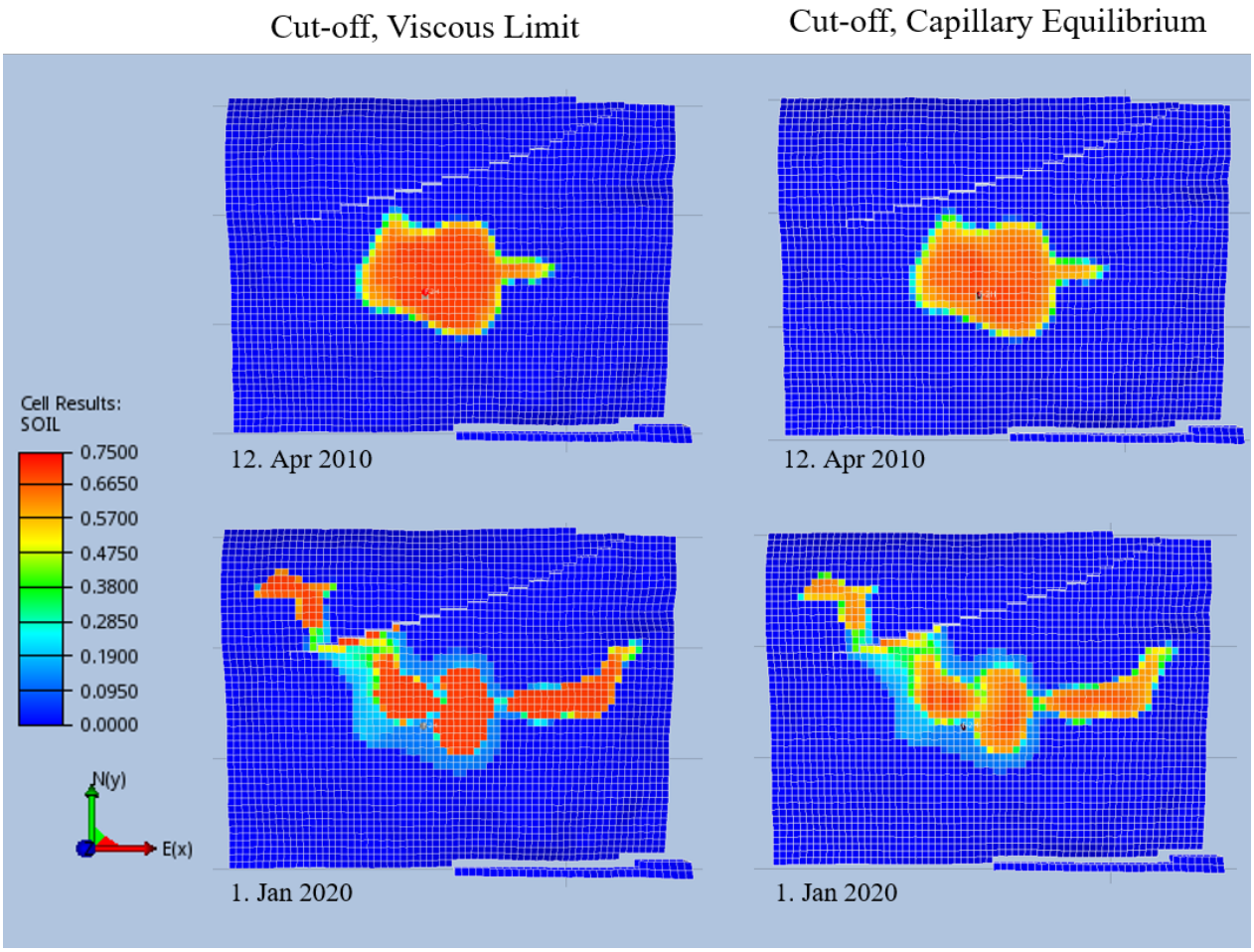

Figure 6.13: Model 5 and 6. Topmap of layer 17 with results from using a mix of upscaled and unscaled Relative Permeability curves with Viscous Limit and Capillary Equilibrium conditions.

The cross-sections of the models show how the VL option again results in more/faster segregation than the CE option. The result is quite similar to the models with Flaser bedding assigned to every zone.

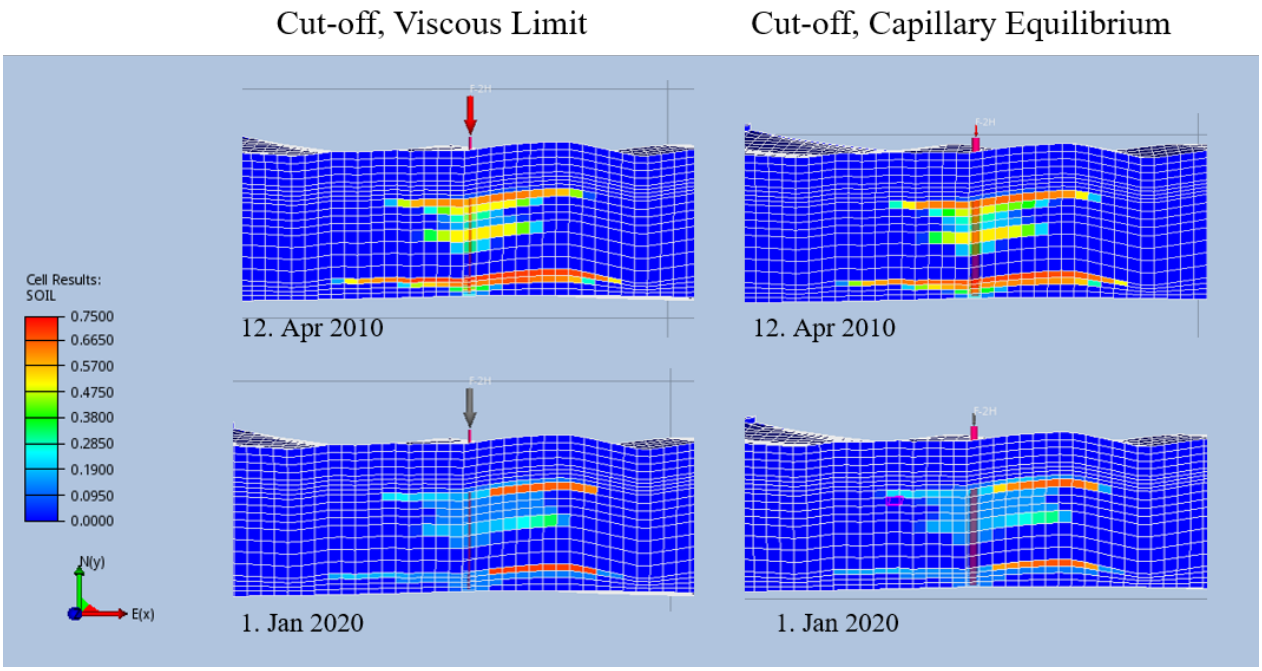

Figure 6.14: Model 5 and 6. W-E cross-section with results from using a mix of upscaled and unscaled Relative Permeability curves with Viscous Limit and Capillary Equilibrium conditions.

6.2 Comparison: Effect of Small Scale Heterogeneities

In order to better identify the effects of small scale heterogeneity on the plume development, the different models are compared to the Basecase.

Comparison: Basecase and Flaser Bedding

The plume development is similar in the Basecase and the models with Flaser bedding, but the effect of small scale hetereogeneities are visible. The Flaser model with the CE option has a less segregated plume than the Basecase at the end of the gravitational dominated period. This is due to the restricted vertical flow of gas - a result of the upscaled relative permeability curves. The discontinuous mud layers in Flaser bedding (where the model used has dimensions $0.5 \times 0.5 \times 0.5$m, are reducing the vertical relative permeability of the gas making it less mobile and thus limit/slow down the segregation. This effect is not seen in the Basecase where only the gravitational forces and the difference in *block* reservoir properties at dimensions $\sim 50 \times 54 \times 4$m affect the migration - dimensions far too coarse to see the effects of the small scale heteregeneities in the lithofacies.

The Flaser model with the VL option shows better segregation with close to residual gas saturation between the injection layers T2_1 and T3 as the vertical flow is not limited in

the same manner as the capillary equilibrium requirement leads to. The gas distribution is more affected by the absolute permeability, and is seen to accumulate in areas with good reservoir properties with sharper, more defined boundaries than with the CE option. The better vertical relative permeability of CO_2 with VL compared to CE substantiates that the plume is affected by the small scale heterogeneities.

The segregation with the VL option is more similar to the Basecase than with the CE option, but the horizontal distribution of the plume is more similar to the model with the CE option where there is a smoother saturation gradient towards the plume boundary.

Comparison: Basecase and Wavy Bedding

The plume development is very different in the Wavy model compared to the Basecase. The cross-sections from end of injections April 12, 2010 show how the gas is plume is much more unified in the models with Wavy bedding than in the Basecase. The effect of upscaling method is also clearly visible with less segregation using the CE option than with the VL option. Both plumes are clearly affected by the density difference between water and the injected CO_2, but the segregation happens much slower with the CE option and has not yet reached the point where the gas is accumulating in the areas with greatest reservoir properties. The low degree of segregation can be explained by the higher content of mud distributed in continuous horizontal layers in Wavy bedding. The vertical flow is much more affected by the mud in the CE option than in the VL option, but the vertical relative permeability of CO_2 is reduced in both cases.

After the gravitational dominated period, the plume in Wavy bedding with the VL option is starting to resemble the plume in the Basecase, but is still far from showing the same segregation. The plume development does however demonstrate the effect of using the VL option compared to the CE option. With the VL option, the plume is clearly segregated, while the with the CE option the segregation is far from complete, and gas has rather moved in a more unified manner east following the tilting of the layers towards higher elevation, permeability and porosity. The cross-plot demonstrates that the effect of using the CE option versus the VL option is greatest in the gravitational dominated period.

The small scale heterogeneities of Wavy bedding captured in the upscaled relative permeability curves greatly affect the plume development. Continuous horizontal mud layers in Wavy both reduce the k_v/k_h relationship and limit the saturation range of two-phase flow with both the VL and the CE option. The migration pattern is therefore influenced by both the geology and the upscaled relative permeability.

Comparison: Basecase and Cut-Off Models

The plume development of the cut-off model with the CE option shows a similar plume development as the Flaser models. The similarity is expected as the cut-off models contain predominantly Flaser bedding which has been shown to effect the vertical relative permeability of CO_2 less than Wavy bedding. The comparison between the Basecase and the cut-off models is therefore very similar to the comparison to the Flaser models.

A notable difference between the Basecase and the cut-off models, is the uppermost part of the plume development. The plume stops in the uppermost layer of T3 (or a little into the lowermost layer of T4) in the cut-off models, while it clearly continues up in the T4 zone in the Basecase. This observations is can be explained with the T4 being characterized as Wavy bedding in the cut-off models due to the low permeability of the zone. Wavy bedding has shown to greatly inhibit the gravitational segregation caused by the relative permeability of CO_2 being very low. The effect of these small scale heterogeneities are not accounted for in the Basecase, and is the most likely reason for the gas to migrate further up in the Basecase compared to the cut-off models.

Chapter 7

Conclusion and Recommendations for Further Work

Conclusion

- Small scale geological heterogeneities, demonstrated by Wavy bedding and Flaser bedding, are found to greatly affect the development of the plume.
- Models in both Wavy bedding and Flaser bedding picture a plume segregating less than in the Basecase.
- Upscaling relative permeability curves in Wavy bedding affects the plume development more than in Flaser bedding. The result is found to be due to Wavy having more continuous horizontal layers of mud.
- The effect of force balance on the small scale heterogeneities, demonstrated by the two end-member cases capillary equilibrium and Viscous limit, are found to be of great importance for the plume development - especially in the gravitational dominated period.
- The Capillary Equilibrium option has a greater impact on the relative permeability curves than the Viscous Limit option. The relative permeability of CO_2 is highly reduced under capillary dominated regime.

Recommendations for Further Work

Capillary number: Validity of the upscaling techniques
Two capillary numbers defined for the transition between viscous dominated flow and capillary dominated flow are described in the thesis, but not used to check the validity of the two upscaling techniques in the lithofacies models. This is a clear objective for further work.

The Hysteresis Effect
Only drainage relative permeability curves are used in this thesis, but it would be interesting to look at how the plume development is affected if the hysteresis effect is accounted for. Due to the injection history, it can be assumed that the accuracy of the simulation model would increase by adding imbibition curves.

Comparing Upscaled Models with Plume Data
A strong recommendation for further work is to compare the upscaled relative permeability curves in this thesis with seismic plume data. This was originally meant to be done in this thesis, but the data was unfortunately not supplied before the deadline.

Appendix A

OPM

Open Porous Media (OPM) is an open-source software containing, among others, a module that can be used as a toolbox for upscaling rock and fluid parameters.

> *OPM coordinates collaborative software development, maintains and distributes open-source software and open data sets, and seeks to ensure that these are available under a free license in a long-term perspective.*
>
> — *opm-project.org*

The software is available under the terms of the GNU General Public License (GPL) version 3.

A.1 The Upscaling Module

The Upscaling module contains programs that can do flow-based permeability upscaling as well as upscaling of relative permeability and capillary curves, using a steady-state approach.

The Upscaling module is designed for one or two-phase flow and lithofacies models described by Eclipse corner point grids. As previously mentioned; petrophysical properties of a reservoir/field are often in need of being transferred to a larger scale due to the computational cost. The Upscaling module of the OPM software can be used to compare end-member based upscaling techniques (CE and VL) on models with different lithofacies geometry.

A.2 Steps in the Code

1. Process command line options
2. Read Eclipse file

3. Read relperm- and J-function for each stone type
4. Tesselate the grid (Sintef code)
5. If gravity is included, compute gravity pressure contributions in each cell:
   (a) Compute height of model by averaging z-values of top layer corners
   (b) Calculate density difference between phases in SI-units
   (c) Go through each cell and find the z-values of the eight corners of the cell. Set height of cell equal to average of z-values of the corners minus half of model height to get the cell height relative to model centre. Set pressure difference for the cell equal to density difference times gravity constant times cell height times factor 10^-7 to obtain bars (same as P_c)
6. Find minimum and maximum capillary pressure from the J-functions in each cell
7. Upscale water saturation as a function of capillary pressure
8. Upscale single phase permeability
9. Upscale phase permeability for capillary pressures that corresponds to a uniform saturation grid, and compute relative permeability.
   (a) Find capillary pressure point to compute for
   (b) Find saturation and phase permeability in each cell
   (c) Upscale phase permeability for given capillary pressure
10. Print output to screen and optionally to file

Appendix B

Original and Scaled Reservoir Properties in the Lithofacies Models

Original and scaled layering averages of permeability and porosity in the 2 lithofacies beddings Wavy and Flaser.

- Flaser in T5 and T3 stand out as two models which could have been scaled with greater care. The permeability ratio between the two sands has been greatly altered giving a higher permeability difference. The new permeability ratio is assumed to affect the upscaling result.
- Zone T1 highly permeable, and has been made close to homogeneous.

Table B.1: Original and scaled layer averages of permeability and porosity in T5.

TUBÅEN 5						
Flaser						
Layer	Original k	Scaling factor k	Scaled k	Original ϕ	Scaling factor ϕ	Scaled ϕ
Sand1	100D	2.37	237mD	25%	0.4	10%
Sand2	150mD	4	600mD	30%	0.57	17%
Mud	0.01mD	10	0.1mD	5%	1	5%
		Average:	340mD			11.9%
Wavy						
Layer	Original k	Scaling factor k	Scaled k	Original ϕ	Scaling factor ϕ	Scaled ϕ
Sand1	100D	4.2	420mD	25%	0.6	15%
Sand2	150mD	4.53	680mD	30%	0.6	18%
Mud	0.01mD	10	0.1mD	5%	1	5%
		Average:	236mD			12%

Table B.2: Original and scaled layer averages of permeability and porosity in T4.

TUBÅEN 4						
Flaser						
Layer	Original k	Scaling factor k	Scaled k	Original ϕ	Scaling factor ϕ	Scaled ϕ
Sand1	100D	0.24	24mD	25%	0.24	6%
Sand2	150mD	0.33	50mD	30%	0.33	9%
Mud	0.01mD	10	0.1mD	5%	1	5%
		Average:	30.1mD			7%
Wavy						
Layer	Original k	Scaling factor k	Scaled k	Original ϕ	Scaling factor ϕ	Scaled ϕ
Sand1	100D	0.38	38mD	25%	0.28	7%
Sand2	150mD	0.4	60mD	30%	0.33	10%
Mud	0.01mD	10	0.1mD	5%	1	5%
		Average:	30mD			7.1%

Table B.3: Original and scaled layer averages of permeability and porosity in T3.

TUBÅEN 3						
Flaser						
Layer	Original k	Scaling factor k	Scaled k	Original ϕ	Scaling factor ϕ	Scaled ϕ
Sand1	100D	2.45	245mD	25%	0.48	12%
Sand2	150mD	4	600mD	30%	0.67	20.1%
Mud	0.01mD	10	0.1mD	5%	1	5%
		Average:	243mD			141%
Wavy						
Layer	Original k	Scaling factor k	Scaled k	Original ϕ	Scaling factor ϕ	Scaled ϕ
Sand1	100D	4.7	470mD	25%	0.64	16%
Sand2	150mD	4.3	650mD	30%	0.73	22%
Mud	0.01mD	10	0.1mD	5%	1	5%
		Average:	343mD			13.6%

Table B.4: Original and scaled layer averages of permeability and porosity in T2_1.

TUBÅEN 2_1						
Flaser						
Layer	Original k	Scaling factor k	Scaled k	Original ϕ	Scaling factor ϕ	Scaled ϕ
Sand1	100D	2.3	230mD	25%	0.4	10%
Sand2	150mD	2.27	340mD	30%	0.5	15%
Mud	0.01mD	1	0.01mD	5%	1	5%
		Average:	233mD			11.1%
Wavy						
Layer	Original k	Scaling factor k	Scaled k	Original ϕ	Scaling factor ϕ	Scaled ϕ
Sand1	100D	3.08	308mD	25%	0.5	12.5%
Sand2	150mD	3	450mD	30%	0.55	16.5%
Mud	0.01mD	10	0.1mD	5%	1	5%
		Average:	3232mD			11%

Table B.5: Original and scaled layer averages of permeability and porosity in T2_2.

TUBÅEN 2_2						
Flaser						
Layer	Original k	Scaling factor k	Scaled k	Original ϕ	Scaling factor ϕ	Scaled ϕ
Sand1	100D	0.001	0.1mD	25%	0.2004	5.01%
Sand2	150mD	0.001	0.15mD	30%	0.1670	5.01%
Mud	0.01mD	1	0.01mD	5%	1	5.01%
		Average:	0.1mD			5%
Wavy						
Layer	Original k	Scaling factor k	Scaled k	Original ϕ	Scaling factor ϕ	Scaled ϕ
Sand1	100D	0.0015	0.15mD	25%	0.2	5%
Sand2	150mD	0.0011	0.17mD	30%	0.167	5%
Mud	0.01mD	1	0.01mD	5%	1	5%
		Average:	0.1mD			5%

Table B.6: Original and scaled layer averages of permeability and porosity in T1.

TUBÅEN 1

Flaser

Layer	Original k	Scaling factor k	Scaled k	Original ϕ	Scaling factor ϕ	Scaled ϕ
Sand1	100D	30	2998mD	25%	0.74	18.5%
Sand2	150mD	40	5997mD	30%	0.77	23.1%
Mud	0.01mD	200000	2000mD	5%	3.19	16%
		Average:	4024mD			19.9%

Wavy

Layer	Original k	Scaling factor k	Scaled k	Original ϕ	Scaling factor ϕ	Scaled ϕ
Sand1	100D	35.5	3553mD	25%	0.76	19%
Sand2	150mD	46.7	7003mD	30%	0.77	23.1%
Mud	0.01mD	200000	200mD	5%	3.6	18%
		Average:	3997mD			19.9%

Appendix C

Relative Permeability Tables for the Full Scale Model

In the tables to follow are k_{rwxx} and k_{rgxx} the x-directional relative permeability of water and gas, respectively (representing the horizontal relative permeability). k_{rwzz} and k_{rgzz} are the z-directional relative permeability of water and gas, respectively. S_w and S_g are the water and gas saturations, respectively, and P_c is the capillary pressure.

C.1 Relative Permeability Tables for Water and CO2 in Viscous Limit

Table C.1: SATNUM 5, unscaled input for SandRock in VL

S_w	k_{rwxx}	P_c	k_{rwzz}	P_c	S_g	k_{rgxx}	P_c	k_{rgzz}	P_c
fraction	*mD*	*Bar*	*mD*	*Bar*	*fraction*	*mD*	*Bar*	*mD*	*Bar*
0.300	0.000E+00	0	0.000E+00	0	0	0.000E+00	0	0.000E+00	0
0.309	2.374E-07	0	2.374E-07	0	0.12	0.000E+00	0	0.000E+00	0
0.411	1.564E-03	0	1.564E-03	0	0.166	7.396E-04	0	7.396E-04	0
0.502	1.271E-02	0	1.271E-02	0	0.247	9.367E-03	0	9.367E-03	0
0.569	3.465E-02	0	3.465E-02	0	0.276	1.566E-02	0	1.566E-02	0
0.659	9.515E-02	0	9.515E-02	0	0.335	3.493E-02	0	3.493E-02	0
0.665	1.008E-01	0	1.008E-01	0	0.341	3.742E-02	0	3.742E-02	0
0.724	1.704E-01	0	1.704E-01	0	0.431	8.790E-02	0	8.790E-02	0
0.753	2.147E-01	0	2.147E-01	0	0.498	1.432E-01	0	1.432E-01	0
0.834	3.819E-01	0	3.819E-01	0	0.589	2.455E-01	0	2.455E-01	0
0.880	5.100E-01	0	5.100E-01	0	0.691	4.015E-01	0	4.015E-01	0
1.000	1.000E+00	0	1.000E+00	0	0.7	4.175E-01	0	4.175E-01	0

Table C.2: SATNUM 6, unscaled input for MudRock in VL

S_w	k_{rwxx}	P_c	k_{rwzz}	P_c	S_g	k_{rgxx}	P_c	k_{rgzz}	P_c
fraction	*mD*	*Bar*	*mD*	*Bar*	*fraction*	*mD*	*Bar*	*mD*	*Bar*
0.400	0.000E+00	0	0.000E+00	0	0	0.000E+00	0	0.000E+00	0
0.407	3.258E-07	0	3.258E-07	0	0.12	0.000E+00	0	0.000E+00	0
0.492	2.146E-03	0	2.146E-03	0	0.158068966	7.090E-04	0	7.090E-04	0
0.567	1.745E-02	0	1.745E-02	0	0.225103448	8.970E-03	0	8.970E-03	0
0.623	4.756E-02	0	4.756E-02	0	0.249103448	1.500E-02	0	1.500E-02	0
0.697	1.306E-01	0	1.306E-01	0	0.297931034	3.350E-02	0	3.350E-02	0
0.702	1.384E-01	0	1.384E-01	0	0.302896552	3.580E-02	0	3.580E-02	0
0.751	2.338E-01	0	2.338E-01	0	0.37737931	8.420E-02	0	8.420E-02	0
0.775	2.947E-01	0	2.947E-01	0	0.432827586	1.370E-01	0	1.370E-01	0
0.842	5.242E-01	0	5.242E-01	0	0.508137931	2.350E-01	0	2.350E-01	0
0.880	7.000E-01	0	7.000E-01	0	0.592551724	3.850E-01	0	3.850E-01	0
1.000	1.000E+00	0	1.000E+00	0	0.6	4.000E-01	0	4.000E-01	0

C.2 Relative Permeability Tables for Water and CO2 in Capillary Equilibrium

Table C.3: SATNUM 7, upscaled input Flaser T5 in VL

S_w	k_{rwxx}	P_c	k_{rwzz}	P_c	S_g	k_{rgxx}	P_c	k_{rgzz}	P_c
fraction	*mD*	*Bar*	*mD*	*Bar*	*fraction*	*mD*	*Bar*	*mD*	*Bar*
0.301	1.041E-14	0	4.550E-14	0	0	0.000E+00	0	0.000E+00	0
0.321	2.669E-06	0	2.660E-06	0	0.12	7.617E-13	0	1.225E-12	0
0.341	4.505E-05	0	4.500E-05	0	0.139964	1.464E-04	0	1.498E-04	0
0.361	1.969E-04	0	1.967E-04	0	0.159928	5.003E-04	0	5.123E-04	0
0.381	5.294E-04	0	5.291E-04	0	0.179892	1.542E-03	0	1.577E-03	0
0.401	1.114E-03	0	1.114E-03	0	0.199856	3.209E-03	0	3.274E-03	0
0.421	2.030E-03	0	2.032E-03	0	0.21982	5.455E-03	0	5.554E-03	0
0.441	3.451E-03	0	3.456E-03	0	0.239784	8.247E-03	0	8.382E-03	0
0.461	5.535E-03	0	5.547E-03	0	0.259748	1.177E-02	0	1.197E-02	0
0.481	8.434E-03	0	8.459E-03	0	0.279712	1.673E-02	0	1.699E-02	0
0.501	1.230E-02	0	1.235E-02	0	0.299676	2.274E-02	0	2.305E-02	0
0.521	1.705E-02	0	1.713E-02	0	0.31964	2.946E-02	0	2.980E-02	0
0.541	2.287E-02	0	2.300E-02	0	0.339604	3.688E-02	0	3.736E-02	0
0.561	3.050E-02	0	3.068E-02	0	0.359568	4.671E-02	0	4.722E-02	0
0.581	4.050E-02	0	4.077E-02	0	0.379532	5.703E-02	0	5.755E-02	0
0.601	5.232E-02	0	5.273E-02	0	0.399496	6.816E-02	0	6.868E-02	0
0.620	6.567E-02	0	6.626E-02	0	0.41946	8.043E-02	0	8.097E-02	0
0.640	8.033E-02	0	8.119E-02	0	0.439424	9.417E-02	0	9.475E-02	0
0.660	9.612E-02	0	9.736E-02	0	0.459388	1.094E-01	0	1.100E-01	0
0.680	1.172E-01	0	1.186E-01	0	0.479352	1.263E-01	0	1.269E-01	0
0.700	1.401E-01	0	1.420E-01	0	0.499316	1.450E-01	0	1.456E-01	0
0.720	1.652E-01	0	1.677E-01	0	0.51928	1.651E-01	0	1.656E-01	0
0.740	1.934E-01	0	1.966E-01	0	0.539244	1.863E-01	0	1.867E-01	0
0.760	2.277E-01	0	2.314E-01	0	0.559208	2.091E-01	0	2.094E-01	0
0.780	2.653E-01	0	2.702E-01	0	0.579172	2.336E-01	0	2.339E-01	0
0.800	3.056E-01	0	3.118E-01	0	0.599136	2.603E-01	0	2.604E-01	0
0.820	3.492E-01	0	3.570E-01	0	0.6191	2.889E-01	0	2.888E-01	0
0.840	3.971E-01	0	4.066E-01	0	0.639064	3.192E-01	0	3.188E-01	0
0.860	4.527E-01	0	4.633E-01	0	0.659028	3.508E-01	0	3.501E-01	0
0.880	5.100E-01	0	5.238E-01	0	0.678992	3.833E-01	0	3.823E-01	0
1.000	1.000E+00	0	1.000E+00	0	0.698956	4.175E-01	0	4.162E-01	0

Table C.4: SATNUM 8, upscaled input Wavy T5 in VL

S_w	k_{rwxx}	P_c	k_{rwzz}	P_c	S_g	k_{rgxx}	P_c	k_{rgzz}	P_c
fraction	*md*	*Bar*	*mD*	*Bar*	*fraction*	*mD*	*Bar*	*mD*	*Bar*
0.305	1.074E-14	0	3.290E-12	0	0	0.000E+00	0	0.000E+00	0
0.325	2.703E-06	0	2.610E-06	0	0.12	7.622E-13	0	8.723E-12	0
0.345	4.560E-05	0	4.440E-05	0	0.139811	1.447E-04	0	1.887E-04	0
0.365	1.992E-04	0	1.961E-04	0	0.159622	4.942E-04	0	6.477E-04	0
0.385	5.354E-04	0	5.324E-04	0	0.179433	1.523E-03	0	1.965E-03	0
0.405	1.126E-03	0	1.131E-03	0	0.199244	3.172E-03	0	4.010E-03	0
0.424	2.053E-03	0	2.081E-03	0	0.219055	5.397E-03	0	6.681E-03	0
0.444	3.488E-03	0	3.559E-03	0	0.238866	8.169E-03	0	9.911E-03	0
0.464	5.593E-03	0	5.752E-03	0	0.258678	1.166E-02	0	1.419E-02	0
0.484	8.519E-03	0	8.845E-03	0	0.278489	1.658E-02	0	1.994E-02	0
0.504	1.242E-02	0	1.304E-02	0	0.2983	2.255E-02	0	2.658E-02	0
0.523	1.720E-02	0	1.832E-02	0	0.318111	2.924E-02	0	3.366E-02	0
0.543	2.307E-02	0	2.480E-02	0	0.337922	3.660E-02	0	4.277E-02	0
0.563	3.076E-02	0	3.322E-02	0	0.357733	4.638E-02	0	5.290E-02	0
0.583	4.083E-02	0	4.434E-02	0	0.377544	5.668E-02	0	6.335E-02	0
0.603	5.273E-02	0	5.799E-02	0	0.397355	6.779E-02	0	7.455E-02	0
0.622	6.614E-02	0	7.392E-02	0	0.417166	8.004E-02	0	8.692E-02	0
0.642	8.084E-02	0	9.219E-02	0	0.436977	9.374E-02	0	1.012E-01	0
0.662	9.668E-02	0	1.130E-01	0	0.456788	1.089E-01	0	1.171E-01	0
0.682	1.179E-01	0	1.357E-01	0	0.476599	1.258E-01	0	1.340E-01	0
0.702	1.408E-01	0	1.660E-01	0	0.49641	1.445E-01	0	1.517E-01	0
0.722	1.659E-01	0	1.996E-01	0	0.516222	1.646E-01	0	1.709E-01	0
0.741	1.942E-01	0	2.364E-01	0	0.536033	1.858E-01	0	1.911E-01	0
0.761	2.286E-01	0	2.773E-01	0	0.555844	2.086E-01	0	2.128E-01	0
0.781	2.662E-01	0	3.295E-01	0	0.575655	2.331E-01	0	2.363E-01	0
0.801	3.064E-01	0	3.873E-01	0	0.595466	2.598E-01	0	2.610E-01	0
0.821	3.498E-01	0	4.512E-01	0	0.615277	2.885E-01	0	2.869E-01	0
0.840	3.976E-01	0	5.211E-01	0	0.635088	3.189E-01	0	3.139E-01	0
0.860	4.533E-01	0	5.909E-01	0	0.654899	3.506E-01	0	3.417E-01	0
0.880	5.100E-01	0	6.894E-01	0	0.67471	3.832E-01	0	3.703E-01	0
1.000	1.000E+00	0	1.000E+00	0	0.694521	4.175E-01	0		

Table C.5: SATNUM 9, upscaled input Flaser T4 in VL

S_w	k_{rwxx}	P_c	k_{rwzz}	P_c	S_g	k_{rgxx}	P_c	k_{rgzz}	P_c
fraction	*mD*	*Bar*	*mD*	*Bar*	*fraction*	*mD*	*Bar*	*mD*	*Bar*
0.302	2.774E-14	0	9.780E-14	0	0	0.000E+00	0	0.000E+00	0
0.322	2.675E-06	0	2.650E-06	0	0.12	7.630E-13	0	1.650E-12	0
0.342	4.515E-05	0	4.480E-05	0	0.139936	1.461E-04	0	1.587E-04	0
0.362	1.973E-04	0	1.964E-04	0	0.159871	4.993E-04	0	5.432E-04	0
0.382	5.305E-04	0	5.296E-04	0	0.179807	1.539E-03	0	1.666E-03	0
0.402	1.116E-03	0	1.117E-03	0	0.199742	3.203E-03	0	3.444E-03	0
0.421	2.035E-03	0	2.043E-03	0	0.219678	5.445E-03	0	5.816E-03	0
0.441	3.458E-03	0	3.479E-03	0	0.239614	8.233E-03	0	8.740E-03	0
0.461	5.546E-03	0	5.593E-03	0	0.259549	1.175E-02	0	1.249E-02	0
0.481	8.450E-03	0	8.547E-03	0	0.279485	1.671E-02	0	1.768E-02	0
0.501	1.232E-02	0	1.250E-02	0	0.29942	2.270E-02	0	2.388E-02	0
0.521	1.708E-02	0	1.741E-02	0	0.319356	2.942E-02	0	3.072E-02	0
0.541	2.290E-02	0	2.341E-02	0	0.339292	3.683E-02	0	3.864E-02	0
0.561	3.055E-02	0	3.127E-02	0	0.359227	4.666E-02	0	4.857E-02	0
0.581	4.056E-02	0	4.159E-02	0	0.379163	5.697E-02	0	5.894E-02	0
0.601	5.240E-02	0	5.394E-02	0	0.399099	6.809E-02	0	7.009E-02	0
0.621	6.576E-02	0	6.803E-02	0	0.419034	8.036E-02	0	8.241E-02	0
0.641	8.043E-02	0	8.372E-02	0	0.43897	9.410E-02	0	9.633E-02	0
0.661	9.622E-02	0	1.010E-01	0	0.458905	1.093E-01	0	1.118E-01	0
0.681	1.173E-01	0	1.225E-01	0	0.478841	1.262E-01	0	1.286E-01	0
0.701	1.402E-01	0	1.475E-01	0	0.498777	1.449E-01	0	1.471E-01	0
0.721	1.653E-01	0	1.750E-01	0	0.518712	1.650E-01	0	1.669E-01	0
0.740	1.936E-01	0	2.057E-01	0	0.538648	1.862E-01	0	1.878E-01	0
0.760	2.279E-01	0	2.419E-01	0	0.558583	2.090E-01	0	2.103E-01	0
0.780	2.655E-01	0	2.836E-01	0	0.578519	2.336E-01	0	2.345E-01	0
0.800	3.058E-01	0	3.289E-01	0	0.598455	2.602E-01	0	2.606E-01	0
0.820	3.494E-01	0	3.781E-01	0	0.61839	2.889E-01	0	2.884E-01	0
0.840	3.972E-01	0	4.322E-01	0	0.638326	3.192E-01	0	3.176E-01	0
0.860	4.529E-01	0	4.919E-01	0	0.658261	3.508E-01	0	3.481E-01	0
0.880	5.101E-01	0	5.605E-01	0	0.678197	3.833E-01	0	3.794E-01	0
1.000	1.000E+00	0	1.000E+00	0	0.698133	4.175E-01	0	4.124E-01	0

Table C.6: SATNUM 10, upscaled input Wavy T4 in VL

S_w	k_{rwxx}	P_c	k_{rwzz}	P_c	S_g	k_{rgxx}	P_c	k_{rgzz}	P_c
fraction	*mD*	*Bar*	*mD*	*Bar*	*fraction*	*mD*	*Bar*	*mD*	*Bar*
0.310	2.500E-14	0	1.180E-12	0	0	0.000E+00	0	0.000E+00	0
0.330	2.740E-06	0	2.650E-06	0	0.12	7.674E-13	0	7.279E-12	0
0.349	4.620E-05	0	4.500E-05	0	0.139649	1.430E-04	0	1.853E-04	0
0.369	2.018E-04	0	1.987E-04	0	0.159299	4.879E-04	0	6.355E-04	0
0.389	5.420E-04	0	5.391E-04	0	0.178948	1.504E-03	0	1.929E-03	0
0.408	1.139E-03	0	1.145E-03	0	0.198598	3.134E-03	0	3.943E-03	0
0.428	2.077E-03	0	2.105E-03	0	0.218247	5.337E-03	0	6.579E-03	0
0.448	3.528E-03	0	3.599E-03	0	0.237897	8.087E-03	0	9.772E-03	0
0.467	5.655E-03	0	5.815E-03	0	0.257546	1.155E-02	0	1.400E-02	0
0.487	8.610E-03	0	8.936E-03	0	0.277196	1.641E-02	0	1.967E-02	0
0.507	1.254E-02	0	1.316E-02	0	0.296845	2.234E-02	0	2.627E-02	0
0.526	1.736E-02	0	1.848E-02	0	0.316495	2.900E-02	0	3.331E-02	0
0.546	2.329E-02	0	2.501E-02	0	0.336144	3.631E-02	0	4.230E-02	0
0.566	3.106E-02	0	3.349E-02	0	0.355794	4.603E-02	0	5.239E-02	0
0.585	4.120E-02	0	4.468E-02	0	0.375443	5.631E-02	0	6.283E-02	0
0.605	5.317E-02	0	5.839E-02	0	0.395092	6.740E-02	0	7.401E-02	0
0.625	6.664E-02	0	7.436E-02	0	0.414742	7.963E-02	0	8.636E-02	0
0.644	8.139E-02	0	9.264E-02	0	0.434391	9.327E-02	0	1.006E-01	0
0.664	9.732E-02	0	1.134E-01	0	0.454041	1.084E-01	0	1.164E-01	0
0.684	1.187E-01	0	1.363E-01	0	0.47369	1.252E-01	0	1.333E-01	0
0.703	1.416E-01	0	1.665E-01	0	0.49334	1.439E-01	0	1.510E-01	0
0.723	1.667E-01	0	1.999E-01	0	0.512989	1.640E-01	0	1.702E-01	0
0.742	1.951E-01	0	2.365E-01	0	0.532639	1.853E-01	0	1.905E-01	0
0.762	2.297E-01	0	2.775E-01	0	0.552288	2.081E-01	0	2.122E-01	0
0.782	2.672E-01	0	3.294E-01	0	0.571938	2.326E-01	0	2.358E-01	0
0.801	3.073E-01	0	3.866E-01	0	0.591587	2.593E-01	0	2.606E-01	0
0.821	3.506E-01	0	4.497E-01	0	0.611237	2.881E-01	0	2.866E-01	0
0.841	3.982E-01	0	5.187E-01	0	0.630886	3.186E-01	0	3.137E-01	0
0.860	4.542E-01	0	5.883E-01	0	0.650535	3.504E-01	0	3.417E-01	0
0.880	5.102E-01	0	6.848E-01	0	0.670185	3.831E-01	0	3.705E-01	0
1.000	1.000E+00	0	1.000E+00	0	0.689834	4.175E-01	0	4.011E-01	0

Table C.7: SATNUM 11, upscaled input Flaser T3 in VL

S_w	k_{rwxx}	P_c	k_{rwzz}	P_c	S_g	k_{rgxx}	P_c	k_{rgzz}	P_c
fraction	*mD*	*Bar*	*mD*	*Bar*	*fraction*	*mD*	*Bar*	*mD*	*Bar*
0.301	1.041E-14	0	4.560E-14	0	0	0.000E+00	0	0.000E+00	0
0.321	2.668E-06	0	2.660E-06	0	0.12	7.617E-13	0	1.222E-12	0
0.341	4.503E-05	0	4.490E-05	0	0.13997	1.464E-04	0	1.498E-04	0
0.361	1.968E-04	0	1.966E-04	0	0.159939	5.006E-04	0	5.124E-04	0
0.381	5.291E-04	0	5.289E-04	0	0.179909	1.543E-03	0	1.577E-03	0
0.401	1.113E-03	0	1.113E-03	0	0.199879	3.210E-03	0	3.275E-03	0
0.421	2.030E-03	0	2.032E-03	0	0.219848	5.457E-03	0	5.555E-03	0
0.441	3.449E-03	0	3.455E-03	0	0.239818	8.250E-03	0	8.384E-03	0
0.461	5.533E-03	0	5.545E-03	0	0.259788	1.177E-02	0	1.197E-02	0
0.481	8.431E-03	0	8.456E-03	0	0.279757	1.674E-02	0	1.700E-02	0
0.501	1.229E-02	0	1.234E-02	0	0.299727	2.275E-02	0	2.305E-02	0
0.521	1.704E-02	0	1.713E-02	0	0.319697	2.946E-02	0	2.980E-02	0
0.541	2.286E-02	0	2.299E-02	0	0.339666	3.689E-02	0	3.736E-02	0
0.560	3.049E-02	0	3.067E-02	0	0.359636	4.673E-02	0	4.722E-02	0
0.580	4.049E-02	0	4.075E-02	0	0.379606	5.705E-02	0	5.755E-02	0
0.600	5.231E-02	0	5.271E-02	0	0.399575	6.817E-02	0	6.869E-02	0
0.620	6.565E-02	0	6.624E-02	0	0.419545	8.045E-02	0	8.097E-02	0
0.640	8.031E-02	0	8.116E-02	0	0.439515	9.419E-02	0	9.476E-02	0
0.660	9.609E-02	0	9.733E-02	0	0.459484	1.094E-01	0	1.101E-01	0
0.680	1.172E-01	0	1.185E-01	0	0.479454	1.263E-01	0	1.269E-01	0
0.700	1.401E-01	0	1.420E-01	0	0.499424	1.450E-01	0	1.456E-01	0
0.720	1.651E-01	0	1.677E-01	0	0.519393	1.651E-01	0	1.656E-01	0
0.740	1.934E-01	0	1.966E-01	0	0.539363	1.863E-01	0	1.868E-01	0
0.760	2.276E-01	0	2.313E-01	0	0.559333	2.091E-01	0	2.094E-01	0
0.780	2.653E-01	0	2.701E-01	0	0.579302	2.337E-01	0	2.339E-01	0
0.800	3.056E-01	0	3.117E-01	0	0.599272	2.603E-01	0	2.604E-01	0
0.820	3.492E-01	0	3.568E-01	0	0.619242	2.890E-01	0	2.888E-01	0
0.840	3.971E-01	0	4.065E-01	0	0.639211	3.193E-01	0	3.189E-01	0
0.860	4.527E-01	0	4.631E-01	0	0.659181	3.508E-01	0	3.501E-01	0
0.880	5.100E-01	0	5.236E-01	0	0.67915	3.833E-01	0	3.824E-01	0
1.000	1.000E+00	0	1.000E+00	0	0.69912	4.175E-01	0	4.162E-01	0

Table C.8: SATNUM 12, upscaled input Wavy T3 in VL

S_w	k_{rwxx}	P_c	k_{rwzz}	P_c	S_g	k_{rgxx}	P_c	k_{rgzz}	P_c
fraction	*mD*	*Bar*	*mD*	*Bar*	*fraction*	*mD*	*Bar*	*mD*	*Bar*
0.305	1.073E-14	0	3.380E-12	0	0	0.000E+00	0	0.000E+00	0
0.325	2.698E-06	0	2.610E-06	0	0.12	7.621E-13	0	8.737E-12	0
0.344	4.552E-05	0	4.440E-05	0	0.139834	1.450E-04	0	1.890E-04	0
0.364	1.989E-04	0	1.957E-04	0	0.159668	4.951E-04	0	6.490E-04	0
0.384	5.345E-04	0	5.315E-04	0	0.179502	1.526E-03	0	1.968E-03	0
0.404	1.124E-03	0	1.129E-03	0	0.199336	3.178E-03	0	4.018E-03	0
0.424	2.049E-03	0	2.077E-03	0	0.21917	5.406E-03	0	6.692E-03	0
0.444	3.482E-03	0	3.553E-03	0	0.239004	8.181E-03	0	9.926E-03	0
0.463	5.584E-03	0	5.743E-03	0	0.258838	1.168E-02	0	1.421E-02	0
0.483	8.506E-03	0	8.832E-03	0	0.278672	1.660E-02	0	1.997E-02	0
0.503	1.240E-02	0	1.302E-02	0	0.298506	2.257E-02	0	2.661E-02	0
0.523	1.718E-02	0	1.830E-02	0	0.31834	2.927E-02	0	3.369E-02	0
0.543	2.304E-02	0	2.477E-02	0	0.338174	3.664E-02	0	4.282E-02	0
0.563	3.072E-02	0	3.318E-02	0	0.358008	4.643E-02	0	5.295E-02	0
0.582	4.078E-02	0	4.429E-02	0	0.377843	5.673E-02	0	6.341E-02	0
0.602	5.267E-02	0	5.792E-02	0	0.397677	6.784E-02	0	7.461E-02	0
0.622	6.607E-02	0	7.384E-02	0	0.417511	8.010E-02	0	8.699E-02	0
0.642	8.076E-02	0	9.210E-02	0	0.437345	9.380E-02	0	1.013E-01	0
0.662	9.659E-02	0	1.129E-01	0	0.457179	1.090E-01	0	1.172E-01	0
0.682	1.178E-01	0	1.356E-01	0	0.477013	1.258E-01	0	1.341E-01	0
0.701	1.407E-01	0	1.659E-01	0	0.496847	1.446E-01	0	1.518E-01	0
0.721	1.658E-01	0	1.994E-01	0	0.516681	1.646E-01	0	1.709E-01	0
0.741	1.941E-01	0	2.363E-01	0	0.536515	1.859E-01	0	1.912E-01	0
0.761	2.285E-01	0	2.772E-01	0	0.556349	2.087E-01	0	2.129E-01	0
0.781	2.661E-01	0	3.294E-01	0	0.576183	2.332E-01	0	2.364E-01	0
0.801	3.063E-01	0	3.872E-01	0	0.596017	2.599E-01	0	2.611E-01	0
0.820	3.497E-01	0	4.511E-01	0	0.615851	2.886E-01	0	2.870E-01	0
0.840	3.975E-01	0	5.210E-01	0	0.635685	3.190E-01	0	3.139E-01	0
0.860	4.532E-01	0	5.909E-01	0	0.655519	3.507E-01	0	3.417E-01	0
0.880	5.100E-01	0	6.895E-01	0	0.675353	3.833E-01	0	3.703E-01	0
1.000	1.000E+00	0	1.000E+00	0	0.695187	4.175E-01	0	4.008E-01	0

Table C.9: SATNUM 13, upscaled input Flaser T2_1 in VL

S_w	k_{rwxx}	P_c	k_{rwzz}	P_c	S_g	k_{rgxx}	P_c	k_{rgzz}	P_c
fraction	*mD*	*Bar*	*mD*	*Bar*	*fraction*	*mD*	*Bar*	*mD*	*Bar*
0.301	1.043E-14	0	5.280E-14	0	0	0.000E+00	0	0.000E+00	0
0.321	2.669E-06	0	2.670E-06	0	0.12	7.617E-13	0	1.464E-12	0
0.341	4.506E-05	0	4.500E-05	0	0.139961	1.463E-04	0	1.469E-04	0
0.361	1.970E-04	0	1.969E-04	0	0.159922	5.002E-04	0	5.022E-04	0
0.381	5.295E-04	0	5.294E-04	0	0.179883	1.542E-03	0	1.547E-03	0
0.401	1.114E-03	0	1.114E-03	0	0.199844	3.208E-03	0	3.219E-03	0
0.421	2.031E-03	0	2.031E-03	0	0.219805	5.454E-03	0	5.470E-03	0
0.441	3.451E-03	0	3.452E-03	0	0.239766	8.245E-03	0	8.267E-03	0
0.461	5.536E-03	0	5.538E-03	0	0.259728	1.177E-02	0	1.180E-02	0
0.481	8.436E-03	0	8.440E-03	0	0.279689	1.673E-02	0	1.677E-02	0
0.501	1.230E-02	0	1.231E-02	0	0.299649	2.273E-02	0	2.279E-02	0
0.521	1.705E-02	0	1.706E-02	0	0.319611	2.945E-02	0	2.951E-02	0
0.541	2.287E-02	0	2.289E-02	0	0.339572	3.687E-02	0	3.695E-02	0
0.561	3.050E-02	0	3.053E-02	0	0.359532	4.671E-02	0	4.679E-02	0
0.581	4.051E-02	0	4.055E-02	0	0.379494	5.703E-02	0	5.711E-02	0
0.601	5.233E-02	0	5.240E-02	0	0.399455	6.815E-02	0	6.823E-02	0
0.621	6.568E-02	0	6.578E-02	0	0.419416	8.043E-02	0	8.051E-02	0
0.640	8.034E-02	0	8.048E-02	0	0.439377	9.417E-02	0	9.426E-02	0
0.660	9.612E-02	0	9.633E-02	0	0.459338	1.094E-01	0	1.095E-01	0
0.680	1.172E-01	0	1.174E-01	0	0.479299	1.263E-01	0	1.264E-01	0
0.700	1.401E-01	0	1.404E-01	0	0.49926	1.450E-01	0	1.451E-01	0
0.720	1.652E-01	0	1.656E-01	0	0.519221	1.651E-01	0	1.651E-01	0
0.740	1.934E-01	0	1.939E-01	0	0.539183	1.863E-01	0	1.864E-01	0
0.760	2.277E-01	0	2.283E-01	0	0.559144	2.091E-01	0	2.091E-01	0
0.780	2.653E-01	0	2.661E-01	0	0.579105	2.336E-01	0	2.337E-01	0
0.800	3.056E-01	0	3.066E-01	0	0.599066	2.603E-01	0	2.603E-01	0
0.820	3.492E-01	0	3.505E-01	0	0.619027	2.889E-01	0	2.889E-01	0
0.840	3.971E-01	0	3.987E-01	0	0.638988	3.192E-01	0	3.192E-01	0
0.860	4.527E-01	0	4.544E-01	0	0.658949	3.508E-01	0	3.507E-01	0
0.880	5.100E-01	0	5.123E-01	0	0.67891	3.833E-01	0	3.832E-01	0
1.000	1.000E+00	0	1.000E+00	0	0.698871	4.175E-01	0	4.173E-01	0

Table C.10: SATNUM 14, upscaled input Wavy T2_1 in VL

S_w	k_{rwxx}	P_c	k_{rwzz}	P_c	S_g	k_{rgxx}	P_c	k_{rgzz}	P_c
fraction	*mD*	*Bar*	*mD*	*Bar*	*fraction*	*mD*	*Bar*	*mD*	*Bar*
0.306	1.091E-14	0	2.740E-12	0	0	0.000E+00	0	0.000E+00	0
0.326	2.708E-06	0	2.620E-06	0	0.12	7.625E-13	0	8.645E-12	0
0.346	4.569E-05	0	4.450E-05	0	0.139786	1.445E-04	0	1.883E-04	0
0.366	1.996E-04	0	1.965E-04	0	0.159572	4.932E-04	0	6.463E-04	0
0.385	5.364E-04	0	5.334E-04	0	0.179358	1.520E-03	0	1.960E-03	0
0.405	1.128E-03	0	1.133E-03	0	0.199144	3.166E-03	0	4.002E-03	0
0.425	2.056E-03	0	2.085E-03	0	0.21893	5.388E-03	0	6.669E-03	0
0.445	3.494E-03	0	3.565E-03	0	0.238716	8.156E-03	0	9.894E-03	0
0.464	5.602E-03	0	5.762E-03	0	0.258502	1.164E-02	0	1.417E-02	0
0.484	8.533E-03	0	8.860E-03	0	0.278288	1.655E-02	0	1.991E-02	0
0.504	1.243E-02	0	1.306E-02	0	0.298074	2.251E-02	0	2.654E-02	0
0.524	1.722E-02	0	1.835E-02	0	0.31786	2.920E-02	0	3.361E-02	0
0.544	2.310E-02	0	2.484E-02	0	0.337646	3.655E-02	0	4.271E-02	0
0.563	3.081E-02	0	3.327E-02	0	0.357432	4.633E-02	0	5.283E-02	0
0.583	4.089E-02	0	4.440E-02	0	0.377218	5.662E-02	0	6.329E-02	0
0.603	5.279E-02	0	5.806E-02	0	0.397004	6.773E-02	0	7.448E-02	0
0.623	6.621E-02	0	7.401E-02	0	0.41679	7.998E-02	0	8.685E-02	0
0.643	8.092E-02	0	9.229E-02	0	0.436576	9.366E-02	0	1.011E-01	0
0.662	9.678E-02	0	1.131E-01	0	0.456362	1.088E-01	0	1.170E-01	0
0.682	1.180E-01	0	1.359E-01	0	0.476148	1.257E-01	0	1.339E-01	0
0.702	1.409E-01	0	1.661E-01	0	0.495934	1.444E-01	0	1.516E-01	0
0.722	1.660E-01	0	1.997E-01	0	0.51572	1.645E-01	0	1.708E-01	0
0.741	1.943E-01	0	2.365E-01	0	0.535506	1.857E-01	0	1.910E-01	0
0.761	2.288E-01	0	2.775E-01	0	0.555292	2.085E-01	0	2.128E-01	0
0.781	2.664E-01	0	3.297E-01	0	0.575078	2.331E-01	0	2.363E-01	0
0.801	3.065E-01	0	3.875E-01	0	0.594864	2.598E-01	0	2.610E-01	0
0.821	3.499E-01	0	4.513E-01	0	0.61465	2.885E-01	0	2.869E-01	0
0.840	3.977E-01	0	5.211E-01	0	0.634436	3.189E-01	0	3.139E-01	0
0.860	4.535E-01	0	5.910E-01	0	0.654222	3.506E-01	0	3.417E-01	0
0.880	5.100E-01	0	6.893E-01	0	0.674008	3.832E-01	0	3.703E-01	0
1.000	1.000E+00	0	1.000E+00	0	0.693794	4.175E-01	0	4.008E-01	0

Table C.11: SATNUM 15, upscaled input Flaser T2_2 in VL

S_w	k_{rwxx}	P_c	k_{rwzz}	P_c	S_g	k_{rgxx}	P_c	k_{rgzz}	P_c
fraction	*mD*	*Bar*	*mD*	*Bar*	*fraction*	*mD*	*Bar*	*mD*	*Bar*
0.303	8.211E-12	0	1.050E-11	0	0	0.000E+00	0	0.000E+00	0
0.323	2.682E-06	0	2.660E-06	0	0.12	8.211E-12	0	1.054E-11	0
0.343	4.526E-05	0	4.500E-05	0	0.139904	1.458E-04	0	1.527E-04	0
0.363	1.978E-04	0	1.972E-04	0	0.159808	4.983E-04	0	5.221E-04	0
0.382	5.317E-04	0	5.311E-04	0	0.179711	1.536E-03	0	1.605E-03	0
0.402	1.118E-03	0	1.119E-03	0	0.199615	3.197E-03	0	3.330E-03	0
0.422	2.039E-03	0	2.044E-03	0	0.219519	5.436E-03	0	5.643E-03	0
0.442	3.465E-03	0	3.478E-03	0	0.239423	8.221E-03	0	8.506E-03	0
0.462	5.558E-03	0	5.587E-03	0	0.259327	1.173E-02	0	1.215E-02	0
0.482	8.468E-03	0	8.527E-03	0	0.27923	1.668E-02	0	1.723E-02	0
0.502	1.235E-02	0	1.246E-02	0	0.299134	2.267E-02	0	2.335E-02	0
0.522	1.711E-02	0	1.731E-02	0	0.319038	2.938E-02	0	3.013E-02	0
0.542	2.295E-02	0	2.325E-02	0	0.338942	3.678E-02	0	3.782E-02	0
0.562	3.061E-02	0	3.104E-02	0	0.358845	4.660E-02	0	4.771E-02	0
0.581	4.064E-02	0	4.125E-02	0	0.378749	5.691E-02	0	5.806E-02	0
0.601	5.250E-02	0	5.341E-02	0	0.398653	6.803E-02	0	6.921E-02	0
0.621	6.587E-02	0	6.721E-02	0	0.418557	8.030E-02	0	8.151E-02	0
0.641	8.056E-02	0	8.247E-02	0	0.438461	9.402E-02	0	9.535E-02	0
0.661	9.638E-02	0	9.909E-02	0	0.458365	1.092E-01	0	1.107E-01	0
0.681	1.175E-01	0	1.205E-01	0	0.478268	1.261E-01	0	1.276E-01	0
0.701	1.404E-01	0	1.446E-01	0	0.498172	1.448E-01	0	1.461E-01	0
0.721	1.656E-01	0	1.710E-01	0	0.518076	1.649E-01	0	1.660E-01	0
0.741	1.938E-01	0	2.007E-01	0	0.53798	1.861E-01	0	1.871E-01	0
0.761	2.282E-01	0	2.361E-01	0	0.557884	2.089E-01	0	2.097E-01	0
0.780	2.658E-01	0	2.760E-01	0	0.577787	2.335E-01	0	2.340E-01	0
0.800	3.061E-01	0	3.189E-01	0	0.597691	2.601E-01	0	2.603E-01	0
0.820	3.497E-01	0	3.655E-01	0	0.617595	2.888E-01	0	2.885E-01	0
0.840	3.976E-01	0	4.166E-01	0	0.637499	3.191E-01	0	3.182E-01	0
0.860	4.533E-01	0	4.745E-01	0	0.657403	3.507E-01	0	3.490E-01	0
0.880	5.105E-01	0	5.375E-01	0	0.677306	3.833E-01	0	3.808E-01	0
1.000	1.000E+00	0	1.000E+00	0	0.69721	4.175E-01	0	4.143E-01	0

Table C.12: SATNUM 16, upscaled input Wavy T2_2 in VL

S_w	k_{rwxx}	P_c	k_{rwzz}	P_c	S_g	k_{rgxx}	P_c	k_{rgzz}	P_c
fraction	*mD*	*Bar*	*mD*	*Bar*	*fraction*	*mD*	*Bar*	*mD*	*Bar*
0.316	7.556E-12	0	2.010E-11	0	0	0.000E+00	0	0.000E+00	0
0.335	2.786E-06	0	2.720E-06	0	0.12	7.556E-12	0	2.014E-11	0
0.355	4.695E-05	0	4.610E-05	0	0.13945	1.414E-04	0	1.691E-04	0
0.374	2.050E-04	0	2.027E-04	0	0.1589	4.819E-04	0	5.781E-04	0
0.394	5.504E-04	0	5.484E-04	0	0.17835	1.485E-03	0	1.764E-03	0
0.413	1.157E-03	0	1.161E-03	0	0.1978	3.097E-03	0	3.632E-03	0
0.433	2.108E-03	0	2.129E-03	0	0.21725	5.279E-03	0	6.107E-03	0
0.452	3.580E-03	0	3.632E-03	0	0.2367	8.005E-03	0	9.135E-03	0
0.472	5.737E-03	0	5.852E-03	0	0.25615	1.144E-02	0	1.307E-02	0
0.491	8.731E-03	0	8.967E-03	0	0.2756	1.625E-02	0	1.845E-02	0
0.510	1.271E-02	0	1.316E-02	0	0.29505	2.214E-02	0	2.481E-02	0
0.530	1.759E-02	0	1.839E-02	0	0.3145	2.877E-02	0	3.172E-02	0
0.549	2.359E-02	0	2.481E-02	0	0.33395	3.604E-02	0	4.010E-02	0
0.569	3.146E-02	0	3.319E-02	0	0.3534	4.567E-02	0	5.005E-02	0
0.588	4.170E-02	0	4.418E-02	0	0.37285	5.592E-02	0	6.044E-02	0
0.608	5.379E-02	0	5.749E-02	0	0.3923	6.699E-02	0	7.159E-02	0
0.627	6.738E-02	0	7.283E-02	0	0.41175	7.919E-02	0	8.389E-02	0
0.647	8.224E-02	0	9.012E-02	0	0.4312	9.278E-02	0	9.788E-02	0
0.666	9.835E-02	0	1.094E-01	0	0.45065	1.079E-01	0	1.134E-01	0
0.686	1.198E-01	0	1.322E-01	0	0.4701	1.246E-01	0	1.303E-01	0
0.705	1.429E-01	0	1.601E-01	0	0.48955	1.433E-01	0	1.483E-01	0
0.724	1.682E-01	0	1.909E-01	0	0.509	1.634E-01	0	1.678E-01	0
0.744	1.968E-01	0	2.250E-01	0	0.52845	1.847E-01	0	1.884E-01	0
0.763	2.316E-01	0	2.643E-01	0	0.5479	2.074E-01	0	2.104E-01	0
0.783	2.693E-01	0	3.115E-01	0	0.56735	2.320E-01	0	2.342E-01	0
0.802	3.094E-01	0	3.629E-01	0	0.5868	2.587E-01	0	2.596E-01	0
0.822	3.528E-01	0	4.191E-01	0	0.60625	2.875E-01	0	2.865E-01	0
0.841	4.005E-01	0	4.806E-01	0	0.6257	3.181E-01	0	3.146E-01	0
0.861	4.569E-01	0	5.461E-01	0	0.64515	3.500E-01	0	3.437E-01	0
0.880	5.126E-01	0	6.273E-01	0	0.6646	3.828E-01	0	3.737E-01	0
1.000	1.000E+00	0	1.000E+00	0	0.68405	4.173E-01	0	4.054E-01	0

Table C.13: SATNUM 17, upscaled input Flaser T1 in VL

S_w	k_{rwxx}	P_c	k_{rwzz}	P_c	S_g	k_{rgxx}	P_c	k_{rgzz}	P_c
fraction	*mD*	*Bar*	*mD*	*Bar*	*fraction*	*mD*	*Bar*	*mD*	*Bar*
0.300	1.031E-14	0	1.030E-14	0	0.000	0.000E+00	0	0.000E+00	0
0.320	2.660E-06	0	2.660E-06	0	0.120	7.612E-13	0	7.612E-13	0
0.340	4.493E-05	0	4.490E-05	0	0.140	1.467E-04	0	1.467E-04	0
0.360	1.964E-04	0	1.964E-04	0	0.160	5.018E-04	0	5.018E-04	0
0.380	5.280E-04	0	5.280E-04	0	0.180	1.547E-03	0	1.547E-03	0
0.400	1.111E-03	0	1.111E-03	0	0.200	3.218E-03	0	3.218E-03	0
0.420	2.025E-03	0	2.025E-03	0	0.220	5.468E-03	0	5.468E-03	0
0.440	3.442E-03	0	3.442E-03	0	0.240	8.265E-03	0	8.265E-03	0
0.460	5.522E-03	0	5.522E-03	0	0.260	1.180E-02	0	1.180E-02	0
0.480	8.415E-03	0	8.415E-03	0	0.280	1.677E-02	0	1.677E-02	0
0.500	1.227E-02	0	1.227E-02	0	0.300	2.278E-02	0	2.278E-02	0
0.520	1.701E-02	0	1.701E-02	0	0.320	2.951E-02	0	2.951E-02	0
0.540	2.282E-02	0	2.282E-02	0	0.340	3.695E-02	0	3.695E-02	0
0.560	3.043E-02	0	3.043E-02	0	0.360	4.679E-02	0	4.679E-02	0
0.580	4.042E-02	0	4.042E-02	0	0.380	5.711E-02	0	5.711E-02	0
0.600	5.223E-02	0	5.223E-02	0	0.400	6.824E-02	0	6.824E-02	0
0.620	6.556E-02	0	6.556E-02	0	0.420	8.053E-02	0	8.053E-02	0
0.640	8.021E-02	0	8.021E-02	0	0.440	9.428E-02	0	9.428E-02	0
0.660	9.598E-02	0	9.598E-02	0	0.460	1.095E-01	0	1.095E-01	0
0.680	1.170E-01	0	1.170E-01	0	0.480	1.264E-01	0	1.264E-01	0
0.700	1.399E-01	0	1.399E-01	0	0.500	1.451E-01	0	1.451E-01	0
0.720	1.650E-01	0	1.650E-01	0	0.520	1.652E-01	0	1.652E-01	0
0.740	1.932E-01	0	1.932E-01	0	0.540	1.864E-01	0	1.864E-01	0
0.760	2.274E-01	0	2.274E-01	0	0.560	2.092E-01	0	2.092E-01	0
0.780	2.651E-01	0	2.651E-01	0	0.580	2.338E-01	0	2.338E-01	0
0.800	3.054E-01	0	3.054E-01	0	0.600	2.604E-01	0	2.604E-01	0
0.820	3.490E-01	0	3.490E-01	0	0.620	2.890E-01	0	2.890E-01	0
0.840	3.970E-01	0	3.970E-01	0	0.640	3.193E-01	0	3.193E-01	0
0.860	4.525E-01	0	4.525E-01	0	0.660	3.509E-01	0	3.509E-01	0
0.880	5.100E-01	0	5.100E-01	0	0.680	3.834E-01	0	3.834E-01	0
1.000	1.000E+00	0	1.000E+00	0	0.700	4.175E-01	0	4.175E-01	0

Table C.14: SATNUM 18, upscaled input Wavy T1 in VL

S_w	k_{rwxx}	P_c	k_{rwzz}	P_c	S_g	k_{rgxx}	P_c	k_{rgzz}	P_c
fraction	*mD*	*Bar*	*mD*	*Bar*	*fraction*	*mD*	*Bar*	*mD*	*Bar*
0.300	1.031E-14	0	1.030E-14	0	0.000	0.000E+00	0	0.000E+00	0
0.320	2.660E-06	0	2.660E-06	0	0.120	7.612E-13	0	7.612E-13	0
0.340	4.493E-05	0	4.490E-05	0	0.140	1.467E-04	0	1.467E-04	0
0.360	1.964E-04	0	1.964E-04	0	0.160	5.018E-04	0	5.018E-04	0
0.380	5.280E-04	0	5.280E-04	0	0.180	1.547E-03	0	1.547E-03	0
0.400	1.111E-03	0	1.111E-03	0	0.200	3.218E-03	0	3.218E-03	0
0.420	2.025E-03	0	2.025E-03	0	0.220	5.468E-03	0	5.468E-03	0
0.440	3.442E-03	0	3.442E-03	0	0.240	8.265E-03	0	8.265E-03	0
0.460	5.522E-03	0	5.522E-03	0	0.260	1.180E-02	0	1.180E-02	0
0.480	8.415E-03	0	8.415E-03	0	0.280	1.677E-02	0	1.677E-02	0
0.500	1.227E-02	0	1.227E-02	0	0.300	2.278E-02	0	2.278E-02	0
0.520	1.701E-02	0	1.701E-02	0	0.320	2.951E-02	0	2.951E-02	0
0.540	2.282E-02	0	2.282E-02	0	0.340	3.695E-02	0	3.695E-02	0
0.560	3.043E-02	0	3.043E-02	0	0.360	4.679E-02	0	4.679E-02	0
0.580	4.042E-02	0	4.042E-02	0	0.380	5.711E-02	0	5.711E-02	0
0.600	5.223E-02	0	5.223E-02	0	0.400	6.824E-02	0	6.824E-02	0
0.620	6.556E-02	0	6.556E-02	0	0.420	8.053E-02	0	8.053E-02	0
0.640	8.021E-02	0	8.021E-02	0	0.440	9.428E-02	0	9.428E-02	0
0.660	9.598E-02	0	9.598E-02	0	0.460	1.095E-01	0	1.095E-01	0
0.680	1.170E-01	0	1.170E-01	0	0.480	1.264E-01	0	1.264E-01	0
0.700	1.399E-01	0	1.399E-01	0	0.500	1.451E-01	0	1.451E-01	0
0.720	1.650E-01	0	1.650E-01	0	0.520	1.652E-01	0	1.652E-01	0
0.740	1.932E-01	0	1.932E-01	0	0.540	1.864E-01	0	1.864E-01	0
0.760	2.274E-01	0	2.274E-01	0	0.560	2.092E-01	0	2.092E-01	0
0.780	2.651E-01	0	2.651E-01	0	0.580	2.338E-01	0	2.338E-01	0
0.800	3.054E-01	0	3.054E-01	0	0.600	2.604E-01	0	2.604E-01	0
0.820	3.490E-01	0	3.490E-01	0	0.620	2.890E-01	0	2.890E-01	0
0.840	3.970E-01	0	3.970E-01	0	0.640	3.193E-01	0	3.193E-01	0
0.860	4.525E-01	0	4.525E-01	0	0.660	3.509E-01	0	3.509E-01	0
0.880	5.100E-01	0	5.100E-01	0	0.680	3.834E-01	0	3.834E-01	0
1.000	1.000E+00	0	1.000E+00	0	0.700	4.175E-01	0	4.175E-01	0

Table C.15: SATNUM 5, unscaled input for SandRock in CE

S_w	k_{rwxx}	P_c	k_{rwzz}	P_c	S_g	k_{rgxx}	P_c	k_{rgzz}	P_c
fraction	*mD*	*Bar*	*mD*	*Bar*	*fraction*	*mD*	*Bar*	*mD*	*Bar*
0.300	0.000E+00	0.230	0.000E+00	0.230	0.000	0.000E+00	0	0.000E+00	0
0.309	2.374E-07	0.225	2.374E-07	0.225	0.120	0.000E+00	0	0.000E+00	0
0.411	1.564E-03	0.042	1.564E-03	0.042	0.166	7.400E-04	0	7.400E-04	0
0.502	1.271E-02	0.028	1.271E-02	0.028	0.247	9.370E-03	0	9.370E-03	0
0.569	3.465E-02	0.023	3.465E-02	0.023	0.276	1.570E-02	0	1.570E-02	0
0.659	9.515E-02	0.019	9.515E-02	0.019	0.335	3.490E-02	0	3.490E-02	0
0.665	1.008E-01	0.019	1.008E-01	0.019	0.341	3.740E-02	0	3.740E-02	0
0.724	1.704E-01	0.017	1.704E-01	0.017	0.431	8.790E-02	0	8.790E-02	0
0.753	2.147E-01	0.017	2.147E-01	0.017	0.498	1.430E-01	0	1.430E-01	0
0.834	3.819E-01	0.015	3.819E-01	0.015	0.589	2.460E-01	0	2.460E-01	0
0.880	5.100E-01	0.014	5.100E-01	0.014	0.691	4.020E-01	0	4.020E-01	0
1.000	1.000E+00	0.000	1.000E+00	0.000	0.700	4.180E-01	0	4.180E-01	0

Table C.16: SATNUM 6, unscaled input for MudRock in CE

S_w	k_{rwxx}	P_c	k_{rwzz}	P_c	S_g	k_{rgxx}	P_c	k_{rgzz}	P_c
fraction	*mD*	*Bar*	*mD*	*Bar*	*fraction*	*mD*	*Bar*	*mD*	*Bar*
0.400	0.000E+00	0.400	0.000E+00	0.400	0.000	0.000E+00	0	0.000E+00	0
0.407	3.258E-07	0.373	3.258E-07	0.373	0.120	0.000E+00	0	0.000E+00	0
0.492	2.146E-03	0.106	2.146E-03	0.106	0.158	7.090E-04	0	7.090E-04	0
0.567	1.745E-02	0.079	1.745E-02	0.079	0.225	8.970E-03	0	8.970E-03	0
0.623	4.756E-02	0.068	4.756E-02	0.068	0.249	1.500E-02	0	1.500E-02	0
0.697	1.306E-01	0.059	1.306E-01	0.059	0.298	3.350E-02	0	3.350E-02	0
0.702	1.384E-01	0.059	1.384E-01	0.059	0.303	3.580E-02	0	3.580E-02	0
0.751	2.338E-01	0.054	2.338E-01	0.054	0.377	8.420E-02	0	8.420E-02	0
0.775	2.947E-01	0.053	2.947E-01	0.053	0.433	1.370E-01	0	1.370E-01	0
0.842	5.242E-01	0.048	5.242E-01	0.048	0.508	2.350E-01	0	2.350E-01	0
0.880	7.000E-01	0.046	7.000E-01	0.046	0.593	3.850E-01	0	3.850E-01	0
1.000	1.000E+00	0.000	1.000E+00	0.000	0.600	4.000E-01	0	4.000E-01	0

Table C.17: SATNUM 7, upscaled input Flaser T5 in CE

S_w	k_{rwxx}	P_c	k_{rwzz}	P_c	S_g	k_{rgxx}	P_c	k_{rgzz}	P_c
fraction	*mD*	*Bar*	*mD*	*Bar*	*fraction*	*mD*	*Bar*	*mD*	*Bar*
0.301	0.000E+00	0.300	0.000E+00	0.300	0.000	0.000E+00	0	0.000E+00	0
0.321	3.930E-06	0.295	4.120E-06	0.295	0.120	0.000E+00	0	0.000E+00	0
0.341	3.220E-05	0.202	1.043E-04	0.202	0.140	6.320E-05	0	2.918E-06	0
0.361	1.427E-04	0.156	6.716E-04	0.156	0.160	7.840E-04	0	6.045E-05	0
0.381	4.068E-04	0.122	2.051E-03	0.122	0.180	2.540E-03	0	2.506E-04	0
0.401	8.989E-04	0.096	4.327E-03	0.096	0.200	5.360E-03	0	6.802E-04	0
0.421	1.710E-03	0.078	7.447E-03	0.078	0.220	9.190E-03	0	1.486E-03	0
0.441	2.984E-03	0.069	1.137E-02	0.069	0.240	1.400E-02	0	2.865E-03	0
0.461	4.837E-03	0.062	1.616E-02	0.062	0.260	1.970E-02	0	5.019E-03	0
0.481	7.397E-03	0.058	2.197E-02	0.058	0.280	2.620E-02	0	8.072E-03	0
0.501	1.082E-02	0.054	2.884E-02	0.054	0.300	3.360E-02	0	1.213E-02	0
0.521	1.526E-02	0.050	3.675E-02	0.050	0.320	4.180E-02	0	1.730E-02	0
0.541	2.088E-02	0.048	4.569E-02	0.048	0.340	5.090E-02	0	2.374E-02	0
0.561	2.783E-02	0.045	5.569E-02	0.045	0.360	6.080E-02	0	3.153E-02	0
0.581	3.629E-02	0.043	6.690E-02	0.043	0.380	7.170E-02	0	4.076E-02	0
0.601	4.644E-02	0.041	7.950E-02	0.041	0.400	8.370E-02	0	5.143E-02	0
0.621	5.847E-02	0.039	9.371E-02	0.039	0.420	9.680E-02	0	6.356E-02	0
0.640	7.252E-02	0.038	1.097E-01	0.038	0.439	1.110E-01	0	7.716E-02	0
0.660	8.874E-02	0.036	1.277E-01	0.036	0.459	1.270E-01	0	9.224E-02	0
0.680	1.073E-01	0.035	1.480E-01	0.035	0.479	1.440E-01	0	1.088E-01	0
0.700	1.284E-01	0.033	1.707E-01	0.033	0.499	1.620E-01	0	1.267E-01	0
0.720	1.522E-01	0.032	1.960E-01	0.032	0.519	1.820E-01	0	1.461E-01	0
0.740	1.791E-01	0.031	2.243E-01	0.031	0.539	2.020E-01	0	1.672E-01	0
0.760	2.093E-01	0.030	2.556E-01	0.030	0.559	2.240E-01	0	1.902E-01	0
0.780	2.433E-01	0.029	2.903E-01	0.029	0.579	2.460E-01	0	2.160E-01	0
0.800	2.816E-01	0.028	3.283E-01	0.028	0.599	2.710E-01	0	2.433E-01	0
0.820	3.250E-01	0.026	3.699E-01	0.026	0.619	3.000E-01	0	2.701E-01	0
0.840	3.748E-01	0.025	4.151E-01	0.025	0.639	3.310E-01	0	2.984E-01	0
0.860	4.332E-01	0.024	4.649E-01	0.024	0.659	3.630E-01	0	3.281E-01	0
0.880	5.100E-01	0.011	5.238E-01	0.011	0.679	3.940E-01	0	3.596E-01	0
1.000	1.000E+00	0.000	1	0	0.699	4.180E-01	0	4.162E-01	0

Table C.18: SATNUM 8, upscaled input Wavy T5 in CE

S_w	k_{rwxx}	P_c	k_{rwzz}	P_c	S_g	k_{rgxx}	P_c	k_{rgzz}	P_c
fraction	*mD*	*Bar*	*mD*	*Bar*	*fraction*	*mD*	*Bar*	*mD*	*Bar*
0.306	0.000E+00	1.350	0.000E+00	1.420	0.000	0.000E+00	0	0.000E+00	0
0.325	1.269E-06	1.320	1.480E-04	1.320	0.120	0.000E+00	0	0.000E+00	0
0.345	2.200E-05	0.294	3.811E-04	0.294	0.140	7.650E-05	0	4.855E-05	0
0.365	5.131E-05	0.196	1.072E-02	0.196	0.160	9.750E-04	0	8.656E-05	0
0.385	1.683E-04	0.150	6.613E-02	0.150	0.179	2.980E-03	0	1.129E-04	0
0.405	4.551E-04	0.116	1.669E-01	0.116	0.199	6.020E-03	0	1.300E-04	0
0.424	9.941E-04	0.090	2.680E-01	0.090	0.219	1.000E-02	0	1.436E-04	0
0.444	1.870E-03	0.074	3.426E-01	0.074	0.239	1.490E-02	0	1.549E-04	0
0.464	3.238E-03	0.065	3.987E-01	0.065	0.259	2.060E-02	0	1.632E-04	0
0.484	5.245E-03	0.059	4.454E-01	0.059	0.279	2.730E-02	0	1.705E-04	0
0.504	8.036E-03	0.055	4.844E-01	0.055	0.298	3.480E-02	0	1.760E-04	0
0.523	1.178E-02	0.051	5.162E-01	0.051	0.318	4.330E-02	0	1.865E-04	0
0.543	1.664E-02	0.048	5.418E-01	0.048	0.338	5.290E-02	0	1.956E-04	0
0.563	2.281E-02	0.045	5.624E-01	0.045	0.358	6.350E-02	0	2.031E-04	0
0.583	3.047E-02	0.043	5.792E-01	0.043	0.378	7.520E-02	0	2.181E-04	0
0.603	3.984E-02	0.041	5.931E-01	0.041	0.397	8.820E-02	0	2.336E-04	0
0.623	5.109E-02	0.039	6.048E-01	0.039	0.417	1.030E-01	0	2.491E-04	0
0.642	6.442E-02	0.037	6.149E-01	0.037	0.437	1.180E-01	0	2.633E-04	0
0.662	8.001E-02	0.036	6.236E-01	0.036	0.457	1.350E-01	0	2.738E-04	0
0.682	9.808E-02	0.034	6.313E-01	0.034	0.477	1.540E-01	0	2.807E-04	0
0.702	1.188E-01	0.033	6.382E-01	0.033	0.496	1.740E-01	0	2.887E-04	0
0.722	1.426E-01	0.032	6.445E-01	0.032	0.516	1.960E-01	0	2.981E-04	0
0.741	1.696E-01	0.030	6.504E-01	0.030	0.536	2.180E-01	0	3.099E-04	0
0.761	2.003E-01	0.029	6.560E-01	0.029	0.556	2.420E-01	0	3.270E-04	0
0.781	2.350E-01	0.028	6.613E-01	0.028	0.576	2.680E-01	0	3.554E-04	0
0.801	2.742E-01	0.027	6.665E-01	0.027	0.596	2.980E-01	0	3.918E-04	0
0.821	3.189E-01	0.026	6.717E-01	0.026	0.615	3.300E-01	0	4.235E-04	0
0.840	3.702E-01	0.025	6.770E-01	0.025	0.635	3.630E-01	0	4.445E-04	0
0.860	4.304E-01	0.023	6.824E-01	0.023	0.655	3.950E-01	0	4.533E-04	0
0.880	5.100E-01	0.004	6.894E-01	0.004	0.675	4.010E-01	0	1.072E-01	0
1.000	1.000E+00	0.000	1	0	0.695	4.180E-01	0	4.008E-01	0

Table C.19: SATNUM 9, upscaled input Flaser T4 in CE

S_w	k_{rwxx}	P_c	k_{rwzz}	P_c	S_g	k_{rgxx}	P_c	k_{rgzz}	P_c
fraction	*mD*	*Bar*	*mD*	*Bar*	*fraction*	*mD*	*Bar*	*mD*	*Bar*
0.302	0.000E+00	0.900	0.000E+00	0.930	0.000	0.000E+00	0	0.000E+00	0
0.322	1.032E-05	0.838	1.350E-06	0.838	0.120	0.000E+00	0	0.000E+00	0
0.342	5.231E-05	0.534	4.070E-05	0.534	0.140	8.350E-05	0	4.190E-06	0
0.362	1.562E-04	0.407	3.289E-04	0.407	0.160	8.920E-04	0	5.828E-05	0
0.382	3.954E-04	0.318	1.156E-03	0.318	0.180	2.760E-03	0	2.287E-04	0
0.402	8.511E-04	0.249	2.748E-03	0.249	0.200	5.620E-03	0	6.033E-04	0
0.422	1.606E-03	0.201	5.191E-03	0.201	0.220	9.410E-03	0	1.310E-03	0
0.441	2.802E-03	0.174	8.580E-03	0.174	0.240	1.410E-02	0	2.481E-03	0
0.461	4.570E-03	0.158	1.327E-02	0.158	0.260	1.970E-02	0	4.195E-03	0
0.481	7.039E-03	0.145	1.969E-02	0.145	0.280	2.600E-02	0	6.507E-03	0
0.501	1.036E-02	0.135	2.810E-02	0.135	0.299	3.330E-02	0	9.500E-03	0
0.521	1.470E-02	0.127	3.852E-02	0.127	0.319	4.140E-02	0	1.326E-02	0
0.541	2.020E-02	0.120	5.088E-02	0.120	0.339	5.040E-02	0	1.786E-02	0
0.561	2.705E-02	0.113	6.511E-02	0.113	0.359	6.040E-02	0	2.333E-02	0
0.581	3.542E-02	0.108	8.116E-02	0.108	0.379	7.140E-02	0	2.970E-02	0
0.601	4.550E-02	0.103	9.907E-02	0.103	0.399	8.350E-02	0	3.695E-02	0
0.621	5.746E-02	0.098	1.188E-01	0.098	0.419	9.670E-02	0	4.511E-02	0
0.641	7.144E-02	0.094	1.404E-01	0.094	0.439	1.110E-01	0	5.418E-02	0
0.661	8.761E-02	0.090	1.638E-01	0.090	0.459	1.270E-01	0	6.419E-02	0
0.681	1.061E-01	0.087	1.890E-01	0.087	0.479	1.440E-01	0	7.513E-02	0
0.701	1.272E-01	0.084	2.160E-01	0.084	0.499	1.630E-01	0	8.699E-02	0
0.721	1.512E-01	0.081	2.449E-01	0.081	0.519	1.830E-01	0	9.977E-02	0
0.741	1.782E-01	0.078	2.758E-01	0.078	0.539	2.040E-01	0	1.135E-01	0
0.760	2.086E-01	0.075	3.089E-01	0.075	0.559	2.260E-01	0	1.285E-01	0
0.780	2.428E-01	0.072	3.441E-01	0.072	0.579	2.490E-01	0	1.451E-01	0
0.800	2.814E-01	0.070	3.815E-01	0.070	0.599	2.750E-01	0	1.625E-01	0
0.820	3.250E-01	0.067	4.214E-01	0.067	0.618	3.050E-01	0	1.803E-01	0
0.840	3.749E-01	0.064	4.637E-01	0.064	0.638	3.360E-01	0	1.991E-01	0
0.860	4.333E-01	0.059	5.089E-01	0.059	0.658	3.680E-01	0	2.187E-01	0
0.880	5.101E-01	0.026	5.605E-01	0.026	0.678	3.980E-01	0	2.398E-01	0
1.000	1.000E+00	0.000	1.000E+00	0.000	0.698	4.180E-01	0	4.124E-01	0

Table C.20: SATNUM 10, upscaled input Wavy T4 in CE

S_w	k_{rwxx}	P_c	k_{rwzz}	P_c	S_g	k_{rgxx}	P_c	k_{rgzz}	P_c
fraction	*mD*	*Bar*	*mD*	*Bar*	*fraction*	*mD*	*Bar*	*mD*	*Bar*
0.310	0.000E+00	1.800	0.000E+00	1.900	0.000	0.000E+00		0.000E+00	0
0.330	1.646E-06	1.770	1.513E-05	1.770	0.120	0.000E+00	0	0.000E+00	0
0.350	3.918E-05	1.083	1.554E-05	1.083	0.140	6.660E-05	0	5.699E-06	0
0.369	2.002E-04	0.751	2.690E-05	0.751	0.159	8.920E-04	0	1.033E-05	0
0.389	2.689E-04	0.480	1.025E-03	0.480	0.179	2.780E-03	0	1.310E-05	0
0.408	4.063E-04	0.361	7.632E-03	0.361	0.199	5.630E-03	0	1.492E-05	0
0.428	7.151E-04	0.277	2.540E-02	0.277	0.218	9.390E-03	0	1.616E-05	0
0.448	1.299E-03	0.212	5.689E-02	0.212	0.238	1.410E-02	0	1.707E-05	0
0.467	2.257E-03	0.172	9.723E-02	0.172	0.258	1.980E-02	0	1.778E-05	0
0.487	3.770E-03	0.152	1.436E-01	0.152	0.277	2.660E-02	0	1.831E-05	0
0.507	6.021E-03	0.139	1.972E-01	0.139	0.297	3.440E-02	0	1.872E-05	0
0.526	9.178E-03	0.128	2.542E-01	0.128	0.317	4.350E-02	0	1.905E-05	0
0.546	1.342E-02	0.119	3.095E-01	0.119	0.336	5.370E-02	0	1.936E-05	0
0.566	1.893E-02	0.111	3.597E-01	0.111	0.356	6.530E-02	0	1.991E-05	0
0.585	2.597E-02	0.105	4.039E-01	0.105	0.375	7.820E-02	0	2.092E-05	0
0.605	3.477E-02	0.099	4.426E-01	0.099	0.395	9.250E-02	0	2.261E-05	0
0.625	4.555E-02	0.094	4.764E-01	0.094	0.415	1.080E-01	0	2.435E-05	0
0.644	5.847E-02	0.090	5.060E-01	0.090	0.434	1.260E-01	0	2.600E-05	0
0.664	7.371E-02	0.086	5.318E-01	0.086	0.454	1.450E-01	0	2.729E-05	0
0.684	9.150E-02	0.082	5.543E-01	0.082	0.474	1.660E-01	0	2.809E-05	0
0.703	1.121E-01	0.079	5.740E-01	0.079	0.493	1.880E-01	0	2.900E-05	0
0.723	1.359E-01	0.076	5.915E-01	0.076	0.513	2.120E-01	0	3.011E-05	0
0.743	1.631E-01	0.073	6.070E-01	0.073	0.533	2.370E-01	0	3.170E-05	0
0.762	1.942E-01	0.071	6.210E-01	0.071	0.552	2.650E-01	0	3.462E-05	0
0.782	2.295E-01	0.068	6.337E-01	0.068	0.572	2.960E-01	0	3.851E-05	0
0.801	2.697E-01	0.066	6.452E-01	0.066	0.592	3.300E-01	0	4.195E-05	0
0.821	3.155E-01	0.063	6.558E-01	0.063	0.611	3.640E-01	0	4.438E-05	0
0.841	3.680E-01	0.060	6.657E-01	0.060	0.631	3.970E-01	0	6.575E-05	0
0.860	4.295E-01	0.056	6.750E-01	0.056	0.651	4.010E-01	0	3.547E-02	0
0.880	5.102E-01	0.010	6.848E-01	0.010	0.670	4.010E-01	0	2.160E-01	0
1.000	1.000E+00	0.000	1.000E+00	0.000	0.690	4.180E-01	0	4.011E-01	0

Table C.21: SATNUM 11, upscaled input Flaser T3 in CE

S_w	k_{rwxx}	P_c	k_{rwzz}	P_c	S_g	k_{rgxx}	P_c	k_{rgzz}	P_c
fraction	*mD*	*Bar*	*mD*	*Bar*	*fraction*	*mD*	*Bar*	*mD*	*Bar*
0.301	0.000E+00	0.320	0.000E+00	0.400	0.000	0.000E+00	0	0.000E+00	0
0.321	4.243E-06	0.312	4.710E-06	0.312	0.120	0.000E+00	0	0.000E+00	0
0.341	3.426E-05	0.217	1.137E-04	0.217	0.140	6.700E-05	0	3.827E-06	0
0.361	1.491E-04	0.167	7.008E-04	0.167	0.160	7.960E-04	0	6.673E-05	0
0.381	4.202E-04	0.131	2.102E-03	0.131	0.180	2.560E-03	0	2.708E-04	0
0.401	9.215E-04	0.103	4.396E-03	0.103	0.200	5.360E-03	0	7.257E-04	0
0.421	1.744E-03	0.085	7.512E-03	0.085	0.220	9.140E-03	0	1.580E-03	0
0.441	3.030E-03	0.074	1.140E-02	0.074	0.240	1.390E-02	0	3.031E-03	0
0.461	4.896E-03	0.067	1.616E-02	0.067	0.260	1.950E-02	0	5.275E-03	0
0.481	7.474E-03	0.062	2.193E-02	0.062	0.280	2.590E-02	0	8.410E-03	0
0.501	1.092E-02	0.058	2.876E-02	0.058	0.300	3.320E-02	0	1.255E-02	0
0.521	1.538E-02	0.055	3.661E-02	0.055	0.320	4.130E-02	0	1.781E-02	0
0.541	2.101E-02	0.051	4.547E-02	0.051	0.340	5.030E-02	0	2.432E-02	0
0.561	2.799E-02	0.049	5.538E-02	0.049	0.360	6.020E-02	0	3.219E-02	0
0.581	3.647E-02	0.046	6.649E-02	0.046	0.380	7.110E-02	0	4.147E-02	0
0.600	4.666E-02	0.044	7.900E-02	0.044	0.400	8.300E-02	0	5.216E-02	0
0.620	5.871E-02	0.042	9.309E-02	0.042	0.420	9.600E-02	0	6.428E-02	0
0.640	7.278E-02	0.041	1.090E-01	0.041	0.440	1.100E-01	0	7.786E-02	0
0.660	8.902E-02	0.039	1.268E-01	0.039	0.460	1.260E-01	0	9.289E-02	0
0.680	1.076E-01	0.038	1.469E-01	0.038	0.480	1.430E-01	0	1.094E-01	0
0.700	1.287E-01	0.036	1.694E-01	0.036	0.499	1.610E-01	0	1.273E-01	0
0.720	1.526E-01	0.035	1.945E-01	0.035	0.519	1.810E-01	0	1.466E-01	0
0.740	1.795E-01	0.034	2.226E-01	0.034	0.539	2.010E-01	0	1.675E-01	0
0.760	2.097E-01	0.032	2.537E-01	0.032	0.559	2.230E-01	0	1.903E-01	0
0.780	2.437E-01	0.031	2.882E-01	0.031	0.579	2.450E-01	0	2.158E-01	0
0.800	2.821E-01	0.030	3.262E-01	0.030	0.599	2.700E-01	0	2.429E-01	0
0.820	3.255E-01	0.029	3.680E-01	0.029	0.619	2.990E-01	0	2.698E-01	0
0.840	3.752E-01	0.027	4.135E-01	0.027	0.639	3.300E-01	0	2.980E-01	0
0.860	4.335E-01	0.026	4.637E-01	0.026	0.659	3.620E-01	0	3.276E-01	0
0.880	5.100E-01	0.011	5.236E-01	0.011	0.679	3.920E-01	0	3.589E-01	0
1.000	1.000E+00	0.000	1.000E+00	0.000	0.699	4.180E-01	0	4.162E-01	0

Table C.22: SATNUM 12, upscaled input Wavy T3 in CE

S_w	k_{rwxx}	P_c	k_{rwzz}	P_c	S_g	k_{rgxx}	P_c	k_{rgzz}	P_c
fraction	*mD*	*Bar*	*mD*	*Bar*	*fraction*	*mD*	*Bar*	*mD*	*Bar*
0.305	0.000E+00	1.300	0.000E+00	1.400	0.000	0.000E+00	0	0.000E+00	0
0.325	1.786E-06	1.240	1.566E-04	1.240	0.120	0.000E+00	0	0.000E+00	0
0.345	2.311E-05	0.279	7.538E-04	0.279	0.140	5.570E-05	0	6.143E-05	0
0.364	6.038E-05	0.197	1.640E-02	0.197	0.160	7.820E-04	0	1.081E-04	0
0.384	1.990E-04	0.152	8.009E-02	0.152	0.180	2.470E-03	0	1.416E-04	0
0.404	5.215E-04	0.118	1.833E-01	0.118	0.199	5.030E-03	0	1.633E-04	0
0.424	1.109E-03	0.091	2.829E-01	0.091	0.219	8.400E-03	0	1.774E-04	0
0.444	2.034E-03	0.075	3.540E-01	0.075	0.239	1.260E-02	0	1.879E-04	0
0.464	3.459E-03	0.067	4.078E-01	0.067	0.259	1.770E-02	0	1.951E-04	0
0.483	5.550E-03	0.061	4.532E-01	0.061	0.279	2.370E-02	0	2.006E-04	0
0.503	8.452E-03	0.057	4.911E-01	0.057	0.299	3.060E-02	0	2.046E-04	0
0.523	1.231E-02	0.053	5.218E-01	0.053	0.318	3.870E-02	0	2.080E-04	0
0.543	1.729E-02	0.050	5.463E-01	0.050	0.338	4.790E-02	0	2.112E-04	0
0.563	2.361E-02	0.047	5.661E-01	0.047	0.358	5.820E-02	0	2.138E-04	0
0.583	3.148E-02	0.044	5.823E-01	0.044	0.378	6.970E-02	0	2.163E-04	0
0.602	4.109E-02	0.042	5.958E-01	0.042	0.398	8.250E-02	0	2.188E-04	0
0.622	5.259E-02	0.040	6.072E-01	0.040	0.418	9.660E-02	0	2.211E-04	0
0.642	6.613E-02	0.039	6.169E-01	0.039	0.437	1.120E-01	0	2.303E-04	0
0.662	8.188E-02	0.037	6.254E-01	0.037	0.457	1.290E-01	0	2.460E-04	0
0.682	1.001E-01	0.036	6.329E-01	0.036	0.477	1.480E-01	0	2.589E-04	0
0.702	1.210E-01	0.034	6.396E-01	0.034	0.497	1.680E-01	0	2.667E-04	0
0.721	1.448E-01	0.033	6.458E-01	0.033	0.517	1.890E-01	0	2.749E-04	0
0.741	1.720E-01	0.032	6.515E-01	0.032	0.537	2.120E-01	0	2.849E-04	0
0.761	2.028E-01	0.031	6.570E-01	0.031	0.556	2.360E-01	0	2.989E-04	0
0.781	2.377E-01	0.030	6.623E-01	0.030	0.576	2.620E-01	0	3.242E-04	0
0.801	2.772E-01	0.029	6.674E-01	0.029	0.596	2.920E-01	0	3.597E-04	0
0.821	3.218E-01	0.028	6.725E-01	0.028	0.616	3.240E-01	0	3.924E-04	0
0.840	3.727E-01	0.026	6.777E-01	0.026	0.636	3.560E-01	0	4.178E-04	0
0.860	4.322E-01	0.025	6.831E-01	0.025	0.656	3.890E-01	0	4.291E-04	0
0.880	5.100E-01	0.004	6.895E-01	0.004	0.675	4.010E-01	0	8.256E-02	0
1.000	1.000E+00	0.000	1.000E+00	0.000	0.695	4.180E-01	0	4.008E-01	0

Table C.23: SATNUM 13, upscaled input Flaser T2_1 in CE

S_w	k_{rwxx}	P_c	k_{rwzz}	P_c	S_g	k_{rgxx}	P_c	k_{rgzz}	P_c
fraction	*mD*	*Bar*	*mD*	*Bar*	*fraction*	*mD*	*Bar*	*mD*	*Bar*
0.300	0.000E+00	0.230	0.000E+00	0.230	0.000	0.000E+00	0	0.000E+00	0
0.309	2.374E-07	0.225	2.374E-07	0.225	0.120	0.000E+00	0	0.000E+00	0
0.411	1.564E-03	0.042	1.564E-03	0.042	0.166	7.400E-04	0	7.396E-04	0
0.502	1.271E-02	0.028	1.271E-02	0.028	0.247	9.370E-03	0	9.367E-03	0
0.569	3.465E-02	0.023	3.465E-02	0.023	0.276	1.570E-02	0	1.566E-02	0
0.659	9.515E-02	0.019	9.515E-02	0.019	0.335	3.490E-02	0	3.493E-02	0
0.665	1.008E-01	0.019	1.008E-01	0.019	0.341	3.740E-02	0	3.742E-02	0
0.724	1.704E-01	0.017	1.704E-01	0.017	0.431	8.790E-02	0	8.790E-02	0
0.753	2.147E-01	0.017	2.147E-01	0.017	0.498	1.430E-01	0	1.432E-01	0
0.834	3.819E-01	0.015	3.819E-01	0.015	0.589	2.460E-01	0	2.455E-01	0
0.880	5.100E-01	0.014	5.100E-01	0.014	0.691	4.020E-01	0	4.015E-01	0
1.000	1.000E+00	0.000	1.000E+00	0.000	0.700	4.180E-01	0	4.175E-01	0

Table C.24: SATNUM 14, upscaled input Wavy T2_1 in CE

S_w	k_{rwxx}	P_c	k_{rwzz}	P_c	S_g	k_{rgxx}	P_c	k_{rgzz}	P_c
fraction	*mD*	*Bar*	*mD*	*Bar*	*fraction*	*mD*	*Bar*	*mD*	*Bar*
0.306	0.000E+00	1.500	0.000E+00	1.500	0.000	0.000E+00	0	0.000E+00	0
0.326	1.212E-06	1.401	1.062E-04	1.401	0.120	0.000E+00	0	0.000E+00	0
0.346	2.929E-05	0.386	1.414E-04	0.386	0.140	5.720E-05	0	4.033E-05	0
0.366	5.231E-05	0.231	5.373E-03	0.231	0.160	8.080E-04	0	7.338E-05	0
0.385	1.521E-04	0.175	4.011E-02	0.175	0.179	2.560E-03	0	9.380E-05	0
0.405	4.129E-04	0.135	1.179E-01	0.135	0.199	5.220E-03	0	1.070E-04	0
0.425	9.210E-04	0.105	2.139E-01	0.105	0.219	8.730E-03	0	1.163E-04	0
0.445	1.753E-03	0.084	2.951E-01	0.084	0.239	1.310E-02	0	1.231E-04	0
0.465	3.049E-03	0.073	3.573E-01	0.073	0.259	1.840E-02	0	1.283E-04	0
0.484	4.984E-03	0.067	4.105E-01	0.067	0.278	2.470E-02	0	1.324E-04	0
0.504	7.711E-03	0.062	4.558E-01	0.062	0.298	3.190E-02	0	1.353E-04	0
0.524	1.139E-02	0.057	4.931E-01	0.057	0.318	4.030E-02	0	1.378E-04	0
0.544	1.617E-02	0.054	5.232E-01	0.054	0.338	4.980E-02	0	1.400E-04	0
0.563	2.227E-02	0.051	5.475E-01	0.051	0.357	6.040E-02	0	1.420E-04	0
0.583	2.991E-02	0.048	5.675E-01	0.048	0.377	7.230E-02	0	1.438E-04	0
0.603	3.930E-02	0.045	5.841E-01	0.045	0.397	8.540E-02	0	1.469E-04	0
0.623	5.060E-02	0.043	5.981E-01	0.043	0.417	1.000E-01	0	1.581E-04	0
0.643	6.398E-02	0.041	6.099E-01	0.041	0.437	1.160E-01	0	1.692E-04	0
0.662	7.960E-02	0.040	6.201E-01	0.040	0.456	1.330E-01	0	1.792E-04	0
0.682	9.770E-02	0.038	6.289E-01	0.038	0.476	1.530E-01	0	1.858E-04	0
0.702	1.185E-01	0.037	6.366E-01	0.037	0.496	1.730E-01	0	1.911E-04	0
0.722	1.424E-01	0.035	6.436E-01	0.035	0.516	1.960E-01	0	1.973E-04	0
0.742	1.695E-01	0.034	6.500E-01	0.034	0.536	2.190E-01	0	2.051E-04	0
0.761	2.004E-01	0.033	6.559E-01	0.033	0.555	2.430E-01	0	2.168E-04	0
0.781	2.354E-01	0.032	6.615E-01	0.032	0.575	2.710E-01	0	2.379E-04	0
0.801	2.751E-01	0.031	6.669E-01	0.031	0.595	3.010E-01	0	2.630E-04	0
0.821	3.200E-01	0.029	6.722E-01	0.029	0.615	3.340E-01	0	2.847E-04	0
0.840	3.714E-01	0.028	6.775E-01	0.028	0.634	3.670E-01	0	2.995E-04	0
0.860	4.315E-01	0.026	6.829E-01	0.026	0.654	4.000E-01	0	3.056E-04	0
0.880	5.100E-01	0.005	6.893E-01	0.005	0.674	4.010E-01	0	1.312E-01	0
1.000	1.000E+00	0.000	1.000E+00	0.000	0.694	4.180E-01	0	4.008E-01	0

Table C.25: SATNUM 15, upscaled input Flaser T2_2 in CE

S_w	k_{rwxx}	P_c	k_{rwzz}	P_c	S_g	k_{rgxx}	P_c	k_{rgzz}	P_c
fraction	*mD*	*Bar*	*mD*	*Bar*	*fraction*	*mD*	*Bar*	*mD*	*Bar*
0.303	0.000E+00	9.500	0.000E+00	10.000	0.000	0.000E+00	0	0.000E+00	0
0.323	3.076E-06	9.448	1.460E-06	9.448	0.120	0.000E+00	0	0.000E+00	0
0.343	4.032E-05	6.826	2.750E-05	6.826	0.140	1.250E-04	0	1.675E-06	0
0.363	1.690E-04	5.337	1.620E-04	5.337	0.160	1.210E-03	0	2.541E-05	0
0.382	4.652E-04	4.270	4.891E-04	4.270	0.180	3.550E-03	0	1.008E-04	0
0.402	1.065E-03	3.459	1.042E-03	3.459	0.200	7.030E-03	0	2.674E-04	0
0.422	2.172E-03	2.900	1.786E-03	2.900	0.220	1.150E-02	0	5.800E-04	0
0.442	3.680E-03	2.525	2.827E-03	2.525	0.239	1.680E-02	0	1.097E-03	0
0.462	5.511E-03	2.271	4.345E-03	2.271	0.259	2.290E-02	0	1.847E-03	0
0.482	7.928E-03	2.085	6.560E-03	2.085	0.279	2.980E-02	0	2.846E-03	0
0.502	1.114E-02	1.938	9.686E-03	1.938	0.299	3.740E-02	0	4.121E-03	0
0.522	1.531E-02	1.814	1.389E-02	1.814	0.319	4.590E-02	0	5.701E-03	0
0.542	2.064E-02	1.707	1.929E-02	1.707	0.339	5.510E-02	0	7.609E-03	0
0.562	2.727E-02	1.614	2.600E-02	1.614	0.359	6.530E-02	0	9.861E-03	0
0.581	3.539E-02	1.533	3.418E-02	1.533	0.379	7.650E-02	0	1.245E-02	0
0.601	4.518E-02	1.461	4.403E-02	1.461	0.399	8.870E-02	0	1.538E-02	0
0.621	5.682E-02	1.396	5.582E-02	1.396	0.419	1.020E-01	0	1.865E-02	0
0.641	7.049E-02	1.337	6.978E-02	1.337	0.439	1.170E-01	0	2.225E-02	0
0.661	8.637E-02	1.284	8.616E-02	1.284	0.458	1.330E-01	0	2.619E-02	0
0.681	1.046E-01	1.234	1.052E-01	1.234	0.478	1.500E-01	0	3.047E-02	0
0.701	1.255E-01	1.187	1.272E-01	1.187	0.498	1.690E-01	0	3.513E-02	0
0.721	1.491E-01	1.143	1.526E-01	1.143	0.518	1.890E-01	0	4.030E-02	0
0.741	1.758E-01	1.100	1.819E-01	1.100	0.538	2.100E-01	0	4.623E-02	0
0.761	2.059E-01	1.059	2.156E-01	1.059	0.558	2.310E-01	0	5.471E-02	0
0.781	2.398E-01	1.017	2.542E-01	1.017	0.578	2.520E-01	0	8.110E-02	0
0.800	2.781E-01	0.976	2.984E-01	0.976	0.598	2.740E-01	0	1.585E-01	0
0.820	3.217E-01	0.932	3.485E-01	0.932	0.618	3.000E-01	0	2.353E-01	0
0.840	3.719E-01	0.884	4.047E-01	0.884	0.638	3.280E-01	0	2.890E-01	0
0.860	4.312E-01	0.824	4.670E-01	0.824	0.657	3.580E-01	0	3.295E-01	0
0.880	5.105E-01	0.366	5.375E-01	0.366	0.677	3.880E-01	0	3.682E-01	0
1.000	1.000E+00	0.000	1.000E+00	0.000	0.697	4.180E-01	0	4.143E-01	0

Table C.26: SATNUM 16, upscaled input Wavy T2_2 in CE

S_w	k_{rwxx}	P_c	k_{rwzz}	P_c	S_g	k_{rgxx}	P_c	k_{rgzz}	P_c
fraction	*mD*	*Bar*	*mD*	*Bar*	*fraction*	*mD*	*Bar*	*mD*	*Bar*
0.316	0.000E+00	9.500	0.000E+00	10.000	0.000	0.000E+00	0	0.000E+00	0
0.335	3.235E-06	9.489	1.964E-06	9.489	0.120	0.000E+00	0	0.000E+00	0
0.355	3.167E-05	6.770	3.452E-05	6.770	0.140	9.100E-05	0	4.064E-07	0
0.374	1.294E-04	5.438	2.037E-04	5.438	0.159	1.090E-03	0	7.261E-07	0
0.394	3.713E-04	4.592	5.764E-04	4.592	0.178	3.280E-03	0	9.109E-07	0
0.413	8.718E-04	3.970	1.169E-03	3.970	0.198	6.510E-03	0	1.033E-06	0
0.433	1.823E-03	3.494	1.940E-03	3.494	0.217	1.080E-02	0	1.111E-06	0
0.452	3.511E-03	3.119	2.842E-03	3.119	0.237	1.610E-02	0	1.172E-06	0
0.472	6.317E-03	2.772	4.019E-03	2.772	0.256	2.240E-02	0	1.214E-06	0
0.491	9.242E-03	2.376	6.348E-03	2.376	0.276	3.000E-02	0	1.246E-06	0
0.510	1.129E-02	2.082	1.065E-02	2.082	0.295	3.880E-02	0	1.271E-06	0
0.530	1.380E-02	1.885	1.738E-02	1.885	0.315	4.890E-02	0	1.293E-06	0
0.549	1.722E-02	1.732	2.718E-02	1.732	0.334	6.040E-02	0	1.313E-06	0
0.569	2.181E-02	1.605	4.038E-02	1.605	0.353	7.340E-02	0	1.331E-06	0
0.588	2.783E-02	1.498	5.710E-02	1.498	0.373	8.790E-02	0	1.348E-06	0
0.608	3.555E-02	1.407	7.751E-02	1.407	0.392	1.040E-01	0	1.372E-06	0
0.627	4.527E-02	1.329	1.018E-01	1.329	0.412	1.220E-01	0	1.427E-06	0
0.647	5.722E-02	1.260	1.300E-01	1.260	0.431	1.420E-01	0	1.466E-06	0
0.666	7.159E-02	1.200	1.618E-01	1.200	0.451	1.630E-01	0	1.513E-06	0
0.686	8.861E-02	1.145	1.965E-01	1.145	0.470	1.870E-01	0	1.578E-06	0
0.705	1.086E-01	1.096	2.336E-01	1.096	0.490	2.110E-01	0	1.720E-06	0
0.724	1.318E-01	1.051	2.724E-01	1.051	0.509	2.370E-01	0	6.336E-06	0
0.744	1.587E-01	1.010	3.126E-01	1.010	0.529	2.570E-01	0	1.110E-03	0
0.763	1.897E-01	0.971	3.542E-01	0.971	0.548	2.700E-01	0	1.590E-02	0
0.783	2.252E-01	0.934	3.968E-01	0.934	0.567	2.840E-01	0	5.561E-02	0
0.802	2.658E-01	0.897	4.404E-01	0.897	0.587	3.010E-01	0	1.112E-01	0
0.822	3.123E-01	0.860	4.848E-01	0.860	0.606	3.200E-01	0	1.715E-01	0
0.841	3.659E-01	0.819	5.303E-01	0.819	0.626	3.420E-01	0	2.308E-01	0
0.861	4.290E-01	0.766	5.770E-01	0.766	0.645	3.670E-01	0	2.809E-01	0
0.880	5.126E-01	0.130	6.273E-01	0.130	0.665	3.940E-01	0	3.328E-01	0
1.000	1.000E+00	0.000	1.000E+00	0.000	0.684	4.170E-01	0	4.054E-01	0

Table C.27: SATNUM 17, upscaled input Flaser T1 in CE

S_w	k_{rwxx}	P_c	k_{rwzz}	P_c	S_g	k_{rgxx}	P_c	k_{rgzz}	P_c
fraction	*mD*	*Bar*	*mD*	*Bar*	*fraction*	*mD*	*Bar*	*mD*	*Bar*
0.300	0.000E+00	0.120	0.000E+00	0.200	0.000	0.000E+00	0	0.000E+00	0
0.320	3.329E-06	0.101	1.510E-06	0.101	0.120	0.000E+00	0	0.000E+00	0
0.340	4.312E-05	0.073	2.860E-05	0.073	0.140	8.290E-05	0	5.467E-07	0
0.360	1.776E-04	0.056	1.660E-04	0.056	0.160	9.930E-04	0	1.181E-05	0
0.380	4.753E-04	0.044	5.041E-04	0.044	0.180	3.130E-03	0	5.561E-05	0
0.400	1.007E-03	0.035	1.088E-03	0.035	0.200	6.510E-03	0	1.631E-04	0
0.420	1.874E-03	0.029	1.914E-03	0.029	0.220	1.100E-02	0	3.914E-04	0
0.440	3.230E-03	0.026	3.050E-03	0.026	0.240	1.650E-02	0	8.488E-04	0
0.460	5.176E-03	0.024	4.641E-03	0.024	0.260	2.280E-02	0	1.671E-03	0
0.480	7.834E-03	0.022	6.882E-03	0.022	0.280	2.980E-02	0	3.029E-03	0
0.500	1.136E-02	0.020	9.950E-03	0.020	0.300	3.760E-02	0	5.189E-03	0
0.520	1.590E-02	0.019	1.399E-02	0.019	0.320	4.610E-02	0	8.516E-03	0
0.540	2.160E-02	0.018	1.912E-02	0.018	0.340	5.530E-02	0	1.346E-02	0
0.560	2.863E-02	0.017	2.545E-02	0.017	0.360	6.530E-02	0	2.037E-02	0
0.580	3.713E-02	0.016	3.313E-02	0.016	0.380	7.620E-02	0	2.934E-02	0
0.600	4.728E-02	0.016	4.237E-02	0.016	0.400	8.800E-02	0	4.026E-02	0
0.620	5.928E-02	0.015	5.343E-02	0.015	0.420	1.010E-01	0	5.306E-02	0
0.640	7.328E-02	0.014	6.660E-02	0.014	0.440	1.150E-01	0	6.765E-02	0
0.660	8.944E-02	0.014	8.221E-02	0.014	0.460	1.300E-01	0	8.398E-02	0
0.680	1.079E-01	0.013	1.006E-01	0.013	0.480	1.460E-01	0	1.020E-01	0
0.700	1.288E-01	0.013	1.223E-01	0.013	0.500	1.640E-01	0	1.216E-01	0
0.720	1.524E-01	0.012	1.476E-01	0.012	0.520	1.830E-01	0	1.430E-01	0
0.740	1.788E-01	0.012	1.770E-01	0.012	0.540	2.030E-01	0	1.665E-01	0
0.760	2.086E-01	0.011	2.111E-01	0.011	0.560	2.230E-01	0	1.928E-01	0
0.780	2.420E-01	0.011	2.499E-01	0.011	0.580	2.440E-01	0	2.226E-01	0
0.800	2.797E-01	0.010	2.935E-01	0.010	0.600	2.680E-01	0	2.537E-01	0
0.820	3.227E-01	0.010	3.416E-01	0.010	0.620	2.960E-01	0	2.829E-01	0
0.840	3.724E-01	0.009	3.937E-01	0.009	0.640	3.260E-01	0	3.127E-01	0
0.860	4.313E-01	0.009	4.493E-01	0.009	0.660	3.570E-01	0	3.445E-01	0
0.880	5.100E-01	0.004	5.100E-01	0.004	0.680	3.870E-01	0	3.792E-01	0
1.000	1.000E+00	0.000	1.000E+00	0.000	0.700	4.180E-01	0	4.175E-01	0

Table C.28: SATNUM 18, upscaled input Wavy T1 in CE

S_w	k_{rwxx}	P_c	k_{rwzz}	P_c	S_g	k_{rgxx}	P_c	k_{rgzz}	P_c
fraction	*mD*	*Bar*	*mD*	*Bar*	*fraction*	*mD*	*Bar*	*mD*	*Bar*
0.300	0.000E+00	0.120	0.000E+00	0.200	0.000	0.000E+00	0	0.000E+00	0
0.320	3.808E-06	0.101	1.329E-06	0.101	0.120	0.000E+00	0	0.000E+00	0
0.340	4.382E-05	0.072	2.368E-05	0.072	0.140	1.180E-04	0	9.625E-08	0
0.360	1.724E-04	0.056	1.574E-04	0.056	0.160	1.360E-03	0	1.566E-07	0
0.380	4.558E-04	0.044	5.069E-04	0.044	0.180	4.120E-03	0	2.148E-07	0
0.400	9.609E-04	0.035	1.092E-03	0.035	0.200	8.330E-03	0	2.802E-07	0
0.420	1.810E-03	0.030	1.906E-03	0.030	0.220	1.380E-02	0	3.732E-07	0
0.440	3.142E-03	0.026	3.009E-03	0.026	0.240	2.020E-02	0	7.511E-07	0
0.460	5.079E-03	0.024	4.498E-03	0.024	0.260	2.750E-02	0	1.321E-06	0
0.480	7.743E-03	0.022	6.544E-03	0.022	0.280	3.560E-02	0	2.913E-06	0
0.500	1.124E-02	0.020	9.349E-03	0.020	0.300	4.440E-02	0	2.712E-05	0
0.520	1.569E-02	0.019	1.308E-02	0.019	0.320	5.380E-02	0	2.284E-04	0
0.540	2.126E-02	0.018	1.787E-02	0.018	0.340	6.380E-02	0	1.023E-03	0
0.560	2.813E-02	0.017	2.383E-02	0.017	0.360	7.450E-02	0	3.267E-03	0
0.580	3.648E-02	0.016	3.107E-02	0.016	0.380	8.580E-02	0	8.131E-03	0
0.600	4.646E-02	0.016	3.979E-02	0.016	0.400	9.780E-02	0	1.653E-02	0
0.620	5.825E-02	0.015	5.029E-02	0.015	0.420	1.110E-01	0	2.856E-02	0
0.640	7.196E-02	0.014	6.304E-02	0.014	0.440	1.250E-01	0	4.367E-02	0
0.660	8.765E-02	0.014	7.862E-02	0.014	0.460	1.400E-01	0	6.120E-02	0
0.680	1.054E-01	0.013	9.762E-02	0.013	0.480	1.560E-01	0	8.073E-02	0
0.700	1.254E-01	0.013	1.205E-01	0.013	0.500	1.730E-01	0	1.021E-01	0
0.720	1.479E-01	0.012	1.477E-01	0.012	0.520	1.910E-01	0	1.255E-01	0
0.740	1.734E-01	0.012	1.795E-01	0.012	0.540	2.100E-01	0	1.515E-01	0
0.760	2.022E-01	0.011	2.162E-01	0.011	0.560	2.290E-01	0	1.809E-01	0
0.780	2.349E-01	0.011	2.578E-01	0.011	0.580	2.490E-01	0	2.134E-01	0
0.800	2.723E-01	0.010	3.041E-01	0.010	0.600	2.710E-01	0	2.474E-01	0
0.820	3.153E-01	0.010	3.541E-01	0.010	0.620	2.990E-01	0	2.782E-01	0
0.840	3.657E-01	0.009	4.060E-01	0.009	0.640	3.290E-01	0	3.076E-01	0
0.860	4.267E-01	0.008	4.579E-01	0.008	0.660	3.600E-01	0	3.396E-01	0
0.880	5.100E-01	0.002	5.100E-01	0.002	0.680	3.890E-01	0	3.761E-01	0
1.000	1.000E+00	0.000	1.000E+00	0.000	0.700	4.180E-01	0	4.175E-01	0

Appendix D

Matlab scripts

D.1 Reading Lithofacies Models

The script is used to find the initial distribution of layering types, permeability and porosity in Wavy bedding. Similar script for Flaser.

```
clear
% 1 = TBED Flood Sand1
% 2 = TBED Flood Sand2
% 3 = TBED Flood Mud
% 4 = TBED Ebb Sand1
% 5 = TBED Ebb Sand2
% 6 = TBED Ebb Mud

% Regroup to:
% Rock1 = (1)Flood Sand1 + (4)Ebb Sand1
% Rock2 = (2)Flood Sand2 + (5)Ebb Sand2
% Rock3 = (3)Flood Mud + (6)Ebb Mud

% ====================================

NumBlocks = 50*50*113;

% ====================================

SATNUM_input = dlmread('wavySATNUM.DATA');
s = numel(SATNUM_input);
SATNUM_trans = SATNUM_input';
SATNUM = zeros(s,1); % Make SATNUM a vector
for i = 1:s
```

```
    SATNUM(i) = SATNUM_trans(i);
end
SATNUM = SATNUM(1:s-(s-NumBlocks));



PERMX_input = dlmread('wavyPERMX.DATA');
pe = numel(PERMX_input);
PERMX_trans = PERMX_input';
PERMX= zeros(pe,1);
for i = 1:pe
    PERMX(i) = PERMX_trans(i);
end
PERMX = PERMX(1:pe-(pe-NumBlocks));



ACTNUM_input = dlmread('wavyACTNUM.DATA');
a = numel(ACTNUM_input);
ACTNUM_trans = ACTNUM_input';
ACTNUM= zeros(a,1);
for i = 1:a
    ACTNUM(i) = ACTNUM_trans(i);
end

ACTNUM = ACTNUM(1:a-(a-NumBlocks));
ActiveCells = nnz(ACTNUM);


PORO_input = dlmread('wavyPORO.DATA');
po = numel(PORO_input);
PORO_trans = PORO_input';
PORO= zeros(po,1);

% Need to eliminate the empty spaces in the first column of the PORO
% matrix. These 4 empty spaces are made into zero by the PORO= zeros(po,1),
% and need to be skipped when values from PORO_trans are allocated to PORO.
for i = 1:4
    PORO(i) = PORO_trans(i);
end

for i = 5:(po-4)
    PORO(i) = PORO_trans(i+4);
end
```

```
ZCORN_input = dlmread('wavyZCORN.DATA');
z = numel(ZCORN_input);
ZCORN_trans = ZCORN_input';
ZCORN= zeros(z,1);
% Changing the ZCORN; adding 0.5 to make positive values
for i = 1:z
    ZCORN(i) = ZCORN_trans(i)+0.5; %0.5 is the value I increase ZCORN with
    %to get positive values
end



COORD_input = dlmread('wavyCOORD.DATA');
c = numel(COORD_input);
COORD = zeros(c,1);
% Need to change negative z-values. Increase these with 0.5 as in ZCORN.
% Adding 0.5 to all z-values (every 3rd) make positive values. We only have
% negative z-values.
COORD_trans = COORD_input';
for i = 1:c
    COORD(i) = COORD_trans(i);
    if COORD(i) < 0
       COORD(i) = COORD_trans(i) + 0.5; % increase wiht 0.5 if neg value
    else
       COORD(i) = COORD(i);
    end
end


% ====================================
% SATNUM
% Grouping of rock types
% ====================================

Layer_original(1)= sum((SATNUM.*ACTNUM)==1);
Layer_original(2)= sum((SATNUM.*ACTNUM)==2);
Layer_original(3)= sum((SATNUM.*ACTNUM)==3);
Layer_original(4)= sum((SATNUM.*ACTNUM)==4);
Layer_original(5)= sum((SATNUM.*ACTNUM)==5);
Layer_original(6)= sum((SATNUM.*ACTNUM)==6);

PercLayer_original = Layer_original./ActiveCells;

% Making an empty column vector
```

```
SATNUM_new = zeros(NumBlocks,1);

% Re-organizing the rock types
for i = 1:NumBlocks;
    if SATNUM(i) == 1
        SATNUM_new(i) = 1;
    elseif SATNUM(i) == 2
        SATNUM_new(i) = 2;
    elseif SATNUM(i) == 3
        SATNUM_new(i) = 3;
    elseif SATNUM(i) == 4
        SATNUM_new(i) = 1;
    elseif SATNUM(i) == 5
        SATNUM_new(i) = 2;
    elseif SATNUM(i) == 6
        SATNUM_new(i) = 3;
    end
end


SATNUM_active = SATNUM_new.*ACTNUM;



% ====================================
% PERMX
% Checking average permeability in each rock type
% ====================================


RockSumPerm = [0,0,0]; % will be used to sum up the permeability values
% within each rock type

PERMX_new = zeros(NumBlocks,1);
num_rock = [0,0,0];

for i = 1:NumBlocks;
    if SATNUM_new(i) == 1
        PERMX_new(i) = PERMX(i);
        RockSumPerm(1) = RockSumPerm(1) + PERMX_new(i)*ACTNUM(i);
        num_rock(1) = num_rock(1) + 1;
    elseif SATNUM_new(i) == 2
        PERMX_new(i) = PERMX(i);
        RockSumPerm(2) = RockSumPerm(2) + PERMX_new(i)*ACTNUM(i);
        num_rock(2) = num_rock(2) + 1;
```

```
    elseif SATNUM_new(i) == 3
        PERMX_new(i) = PERMX(i);
        RockSumPerm(3) = RockSumPerm(3) + PERMX_new(i)*ACTNUM(i);
        num_rock(3) = num_rock(3) + 1;
    end
end

% Making an vector of the active permeability values
PERMX_active = PERMX.*ACTNUM;

% NumLayer: how many active blocks/cells in each layer.
ActiveCellsRock_new(1) = sum(SATNUM_active==1);
ActiveCellsRock_new(2) = sum(SATNUM_active==2);
ActiveCellsRock_new(3) = sum(SATNUM_active==3);


TotAvgPerm = sum(RockSumPerm)/ActiveCells;

% PercLayer: how the layers are distributed in percentage.
PercLayer = ActiveCellsRock_new./ActiveCells;

% Making the new average permeability vector for the three layer types:
AvgPerm_new(1)= RockSumPerm(1)/ActiveCellsRock_new(1);
AvgPerm_new(2)= RockSumPerm(2)/ActiveCellsRock_new(2);
AvgPerm_new(3)= RockSumPerm(3)/ActiveCellsRock_new(3);


PERMX_hist=PERMX_active(PERMX_active~=0);
hist_flaser=histogram(PERMX_active);


% ====================================
% PORO
% checking average porosity in each rock type
% making a new file with the avg poro after combining rocktypes
% ====================================

% Making an empty column vector
PORO_new = zeros(NumBlocks,1);

RockSumPoro = [0,0,0]; % will be used to sum up the permeability values

% Calculating the avg porosity for each rock type
for i = 1:NumBlocks;
    if SATNUM_new(i) == 1
```

```
        PORO_new(i) = PORO(i);
        RockSumPoro(1) = RockSumPoro(1) + PORO_new(i)*ACTNUM(i);
    elseif SATNUM_new(i) == 2
        PORO_new(i) = PORO(i);
        RockSumPoro(2) = RockSumPoro(2) + PORO_new(i)*ACTNUM(i);
    elseif SATNUM_new(i) == 3
        PORO_new(i) = PORO(i);
        RockSumPoro(3) = RockSumPoro(3) + PORO_new(i)*ACTNUM(i);
    end
end

% Making an vector of the active porosity values
PORO_active = PORO_new.*ACTNUM;

TotAvgPoro = sum(RockSumPoro)/ActiveCells;

% Making the new average porosity vector for the three layer types:
AvgPoro_new(1)= RockSumPoro(1)/ActiveCellsRock_new(1);
AvgPoro_new(2)= RockSumPoro(2)/ActiveCellsRock_new(2);
AvgPoro_new(3)= RockSumPoro(3)/ActiveCellsRock_new(3);
```

D.2 Altering Lithofacies Models

Script demonstrates altering Wavy bedding for T1. Flaser bedding has similar script.

```
clear
% 1 = TBED Flood Sand1
% 2 = TBED Flood Sand2
% 3 = TBED Flood Mud
% 4 = TBED Ebb Sand1
% 5 = TBED Ebb Sand2
% 6 = TBED Ebb Mud

% Regroup to:
% Rock1 = (1)Flood Sand1 + (4)Ebb Sand1
% Rock2 = (2)Flood Sand2 + (5)Ebb Sand2
% Rock3 = (3)Flood Mud + (6)Ebb Mud

% avgPERMX is supposed to be around 4D (Raport, Statoil)
% ====================================

NumBlocks = 50*50*113;
H = 10;

% ====================================

SATNUM_input = dlmread('wavySATNUM.DATA');
s = numel(SATNUM_input);
SATNUM_trans = SATNUM_input';
SATNUM = zeros(s,1); % Make SATNUM a vector
for i = 1:s
    SATNUM(i) = SATNUM_trans(i);
end
% Remove difference between number of grid blocks and the number of values
% in the data (extra values there to fill up matrix))
SATNUM = SATNUM(1:s-(s-NumBlocks));



PERMX_input = dlmread('wavyPERMX.DATA');
pe = numel(PERMX_input);
PERMX_trans = PERMX_input';
PERMX= zeros(pe,1);
for i = 1:pe
    PERMX(i) = PERMX_trans(i);
```

```
end
PERMX = PERMX(1:pe-(pe-NumBlocks));



ACTNUM_input = dlmread('wavyACTNUM.DATA');
a = numel(ACTNUM_input);
ACTNUM_trans = ACTNUM_input';
ACTNUM= zeros(a,1);
for i = 1:a
    ACTNUM(i) = ACTNUM_trans(i);
end

ACTNUM = ACTNUM(1:a-(a-NumBlocks));
ActiveCells = nnz(ACTNUM);


PORO_input = dlmread('wavyPORO.DATA');
po = numel(PORO_input);
PORO_trans = PORO_input';
PORO= zeros(po,1);

% Need to eliminate the empty spaces in the first column of the PORO
% matrix. These 4 empty spaces are made into zero by the PORO= zeros(po,1),
% and need to be skipped when values from PORO_trans are allocated to PORO.
for i = 1:4
    PORO(i) = PORO_trans(i);
end

for i = 5:(po-4)
    PORO(i) = PORO_trans(i+4);
end


ZCORN_input = dlmread('wavyZCORN.DATA');
z = numel(ZCORN_input);
ZCORN_trans = ZCORN_input';
ZCORN= zeros(z,1);
% Changing the ZCORN; adding 0.5 to make positive values
for i = 1:z
    ZCORN(i) = ZCORN_trans(i)+0.5; %0.5 is the value I increase ZCORN with
    % to get positive values
end
```

```
COORD_input = dlmread('wavyCOORD.DATA');
c = numel(COORD_input);
COORD = zeros(c,1);
% Need to change negative z-values. Increase these with 0.5 as in ZCORN.
% Adding 0.5 to all z-values (every 3rd) make positive values. We only have
% negative z-values.
COORD_trans = COORD_input';
for i = 1:c
    COORD(i) = COORD_trans(i);
    if COORD(i) < 0
       COORD(i) = COORD_trans(i) + 0.5; % increase wiht 0.5 if neg value
    else
       COORD(i) = COORD(i);
    end
end


% ====================================
% SATNUM
% Grouping of rock types
% ====================================

% Making an empty column vector
SATNUM_new = zeros(NumBlocks,1);

% Re-organizing the rock types
for i = 1:NumBlocks;
    if SATNUM(i) == 1
        SATNUM_new(i) = 1;
    elseif SATNUM(i) == 2
        SATNUM_new(i) = 2;
    elseif SATNUM(i) == 3
        SATNUM_new(i) = 3;
    elseif SATNUM(i) == 4
        SATNUM_new(i) = 1;
    elseif SATNUM(i) == 5
        SATNUM_new(i) = 2;
    elseif SATNUM(i) == 6
        SATNUM_new(i) = 3;
    end
end


SATNUM_active = SATNUM_new.*ACTNUM;
```

```
% ====================================
% PERMX
% Checking average permeability in each rock type
% ====================================

% Making an vector of the active permeability values
PERMX_active = PERMX.*ACTNUM;

RockSumPerm = [0,0,0]; % will be used to sum up the permeability values
% within each rock type

PERMX_new = zeros(NumBlocks,1);

for i = 1:NumBlocks;
    if SATNUM_new(i) == 1
        PERMX_new(i) = PERMX(i)*35.5; %Sand 1,initially 100md, want 3550md
        RockSumPerm(1) = RockSumPerm(1) + PERMX_new(i)*ACTNUM(i);
    elseif SATNUM_new(i) == 2
        PERMX_new(i) = PERMX(i)*46.7; % Sand2, initially 150, want 7000md
        RockSumPerm(2) = RockSumPerm(2) + PERMX_new(i)*ACTNUM(i);
    elseif SATNUM_new(i) == 3
        PERMX_new(i) = PERMX(i)*200000; % Mud, initially 0.01md, want2000md
        RockSumPerm(3) = RockSumPerm(3) + PERMX_new(i)*ACTNUM(i);
    end
end

% ActivePerm=PERMX_new.*ACTNUM;

% NumLayer: how many active blocks/cells in each layer.
ActiveCellsRock_new(1) = sum(SATNUM_active==1);
ActiveCellsRock_new(2) = sum(SATNUM_active==2);
ActiveCellsRock_new(3) = sum(SATNUM_active==3);


TotAvgPerm = sum(RockSumPerm)/ActiveCells;

% PercLayer: how the layers are distributed in percentage.
PercLayer = ActiveCellsRock_new./ActiveCells;

% Making the new average permeability vector for the three layer types:
AvgPerm_new(1)= RockSumPerm(1)/ActiveCellsRock_new(1);
AvgPerm_new(2)= RockSumPerm(2)/ActiveCellsRock_new(2);
AvgPerm_new(3)= RockSumPerm(3)/ActiveCellsRock_new(3);
```

```
kH = TotAvgPerm*H;

% PERMX_hist=PERMX_active(PERMX_active~=0);
% hist_flaser=histogram(PERMX_active);



% ====================================
% PORO
% checking average porosity in each rock type
% making a new file with the avg poro after combining rocktypes
% ====================================

% Making an empty column vector
PORO_new = zeros(NumBlocks,1);

RockSumPoro = [0,0,0]; % will be used to sum up the permeability values

% Calculating the avg porosity for each rock type
for i = 1:NumBlocks;
    if SATNUM_new(i) == 1
        PORO_new(i) = PORO(i)*0.76; %Sand1 initially 25%, want 19%
        RockSumPoro(1) = RockSumPoro(1) + PORO_new(i)*ACTNUM(i);
    elseif SATNUM_new(i) == 2
        PORO_new(i) = PORO(i)*0.77; %Sand2 initially 30%, want 23%
        RockSumPoro(2) = RockSumPoro(2) + PORO_new(i)*ACTNUM(i);
    elseif SATNUM_new(i) == 3
        PORO_new(i) = PORO(i)*3.6 ;%Mud initially 5.01%, want 18%
        RockSumPoro(3) = RockSumPoro(3) + PORO_new(i)*ACTNUM(i);
    end
end

% Making an vector of the active, scaled, permeability values
PORO_active = PORO_new.*ACTNUM;

TotAvgPoro = sum(RockSumPoro)/ActiveCells;

% Making the new average porosity vector for the three layer types:
AvgPoro_new(1)= RockSumPoro(1)/ActiveCellsRock_new(1);
AvgPoro_new(2)= RockSumPoro(2)/ActiveCellsRock_new(2);
AvgPoro_new(3)= RockSumPoro(3)/ActiveCellsRock_new(3);
```

D.3 Extracting Res. Prop. from LGR4 in the E300 Model

```
% The PERMX and PORO datapoints for LGR4. These tables are defined
% within the LGR and therefore need to be at the right dimensions of
% 99x30x20.

% Take in the LGR4 PERMX and PORO data file from e300 model. This data only
% consist of the elements for the LGR.
PERMXe300 = textscan(fopen('tubaenPERMX.DATA'), '%f'); %loading one value
% at the time, avoiding the "empty holes"
PERMXe300=PERMXe300{1};
pe_xe300 = numel(PERMXe300);

POROe300 = textscan(fopen('tubaenPORO.DATA'), '%f'); %loading one value at
% the time, avoiding the "empty holes"
POROe300=POROe300{1}; % The data is organized correctly; the values are
% read row by row.
poe300 = numel(POROe300);


% ========================================================================
% LGR4 area in the E300 model:
% ========================================================================

NXe300LGR4=99;
NYe300LGR4=30;
NZe300LGR4=20;

PERMX_mat = vec2mat(PERMXe300,NXe300LGR4);
PORO_mat = vec2mat(POROe300,NXe300LGR4);

% "s" = "start"
% "e" = "end"

i_s= 1;
i_e= 99;
j_s = zeros(1,20);
j_e = zeros(1,20);

% Working through the 20 layers. Making a matrix of the LGR elements, with
% the right dimensions. NXe100 number of columns, and 30*20 number of rows.
% The first 30*99 is then the first layer, k=1.
```

```
for i = 1:20
    j_s(i)= 1+NYe300LGR4*(i-1);
    j_e(i)= NYe300LGR4+NYe300LGR4*(i-1);
end

% ========================================================================
% Looking at PERMEABILITY e300

LGR4_perm_k1= PERMX_mat(j_s(1):j_e(1), i_s:i_e);
LGR4_perm_k2= PERMX_mat(j_s(2):j_e(2), i_s:i_e);
LGR4_perm_k3= PERMX_mat(j_s(3):j_e(3), i_s:i_e);
LGR4_perm_k4= PERMX_mat(j_s(4):j_e(4), i_s:i_e);
LGR4_perm_k5= PERMX_mat(j_s(5):j_e(5), i_s:i_e);
LGR4_perm_k6= PERMX_mat(j_s(6):j_e(6), i_s:i_e);
LGR4_perm_k7= PERMX_mat(j_s(7):j_e(7), i_s:i_e);
LGR4_perm_k8= PERMX_mat(j_s(8):j_e(8), i_s:i_e);
LGR4_perm_k9= PERMX_mat(j_s(9):j_e(9), i_s:i_e);
LGR4_perm_k10= PERMX_mat(j_s(10):j_e(10), i_s:i_e);
LGR4_perm_k11= PERMX_mat(j_s(11):j_e(11), i_s:i_e);
LGR4_perm_k12= PERMX_mat(j_s(12):j_e(12), i_s:i_e);
LGR4_perm_k13= PERMX_mat(j_s(13):j_e(13), i_s:i_e);
LGR4_perm_k14= PERMX_mat(j_s(14):j_e(14), i_s:i_e);
LGR4_perm_k15= PERMX_mat(j_s(15):j_e(15), i_s:i_e);
LGR4_perm_k16= PERMX_mat(j_s(16):j_e(16), i_s:i_e);
LGR4_perm_k17= PERMX_mat(j_s(17):j_e(17), i_s:i_e);
LGR4_perm_k18= PERMX_mat(j_s(18):j_e(18), i_s:i_e);
LGR4_perm_k19= PERMX_mat(j_s(19):j_e(19), i_s:i_e);
LGR4_perm_k20= PERMX_mat(j_s(20):j_e(20), i_s:i_e);

% The full matrix of LGR4:
LGR4_permE300= [LGR4_perm_k1;LGR4_perm_k2;LGR4_perm_k3;LGR4_perm_k4;
    LGR4_perm_k5;LGR4_perm_k6;LGR4_perm_k7;LGR4_perm_k8;LGR4_perm_k9;
    LGR4_perm_k10;LGR4_perm_k11;LGR4_perm_k12;LGR4_perm_k13;LGR4_perm_k14;
    LGR4_perm_k15;LGR4_perm_k16;LGR4_perm_k17;LGR4_perm_k18;LGR4_perm_k19;
    LGR4_perm_k20];

% Making the matrix into an array. Copies the matrix created above into a
% .DATA file, before loading it in again as an array.
LGR4_permE300Array = textscan(fopen('LGR4_permE300.DATA'), '%f'); %loading
%one value at the time, avoiding the "empty holes"
LGR4_permE300Array=LGR4_permE300Array{1};

% ========================================================================
% Looking at POROSITY e300
```

```
LGR4_poro_k1= PORO_mat(j_s(1):j_e(1), i_s:i_e);
LGR4_poro_k2= PORO_mat(j_s(2):j_e(2), i_s:i_e);
LGR4_poro_k3= PORO_mat(j_s(3):j_e(3), i_s:i_e);
LGR4_poro_k4= PORO_mat(j_s(4):j_e(4), i_s:i_e);
LGR4_poro_k5= PORO_mat(j_s(5):j_e(5), i_s:i_e);
LGR4_poro_k6= PORO_mat(j_s(6):j_e(6), i_s:i_e);
LGR4_poro_k7= PORO_mat(j_s(7):j_e(7), i_s:i_e);
LGR4_poro_k8= PORO_mat(j_s(8):j_e(8), i_s:i_e);
LGR4_poro_k9= PORO_mat(j_s(9):j_e(9), i_s:i_e);
LGR4_poro_k10= PORO_mat(j_s(10):j_e(10), i_s:i_e);
LGR4_poro_k11= PORO_mat(j_s(11):j_e(11), i_s:i_e);
LGR4_poro_k12= PORO_mat(j_s(12):j_e(12), i_s:i_e);
LGR4_poro_k13= PORO_mat(j_s(13):j_e(13), i_s:i_e);
LGR4_poro_k14= PORO_mat(j_s(14):j_e(14), i_s:i_e);
LGR4_poro_k15= PORO_mat(j_s(15):j_e(15), i_s:i_e);
LGR4_poro_k16= PORO_mat(j_s(16):j_e(16), i_s:i_e);
LGR4_poro_k17= PORO_mat(j_s(17):j_e(17), i_s:i_e);
LGR4_poro_k18= PORO_mat(j_s(18):j_e(18), i_s:i_e);
LGR4_poro_k19= PORO_mat(j_s(19):j_e(19), i_s:i_e);
LGR4_poro_k20= PORO_mat(j_s(20):j_e(20), i_s:i_e);

% The full matrix of LGR4:
LGR4_poroE300=[LGR4_poro_k1;LGR4_poro_k2;LGR4_poro_k3;LGR4_poro_k4;
    LGR4_poro_k5;LGR4_poro_k6;LGR4_poro_k7;LGR4_poro_k8;LGR4_poro_k9;
    LGR4_poro_k10;LGR4_poro_k11;LGR4_poro_k12;LGR4_poro_k13;LGR4_poro_k14;
    LGR4_poro_k15;LGR4_poro_k16;LGR4_poro_k17;LGR4_poro_k18;LGR4_poro_k19;
    LGR4_poro_k20];

% Making the matrix into an array. Copies the matrix created above into a
% .DATA file, before loading it in again as an array.
LGR4_poroE300Array = textscan(fopen('LGR4_poroE300.DATA'), '%f');
LGR4_poroE300Array=LGR4_poroE300Array{1};
```

D.4 Replacing Grid Values in E100, Basecase

User specify which property, here demonstrated with "EQLNUM". LGR4 and LGR4_2 in E100 are assigned the properties from LGR4 in E300.

```
% Making Eclipse-tables for E100 model with transferred properties from the
% E300 LGR4.

% OBS: Need to run the "e100_LGR_usingE300" for the PERMX and PORO data

EQLNUMe100 = textscan(fopen('e100_EQLNUM.DATA'), '%f'); %loading one value
% at the time, avoiding the "empty holes"
EQLNUMe100=EQLNUMe100{1}; % The data is organized correctly; the values are
% read row by row.

EQLNUMe300 = textscan(fopen('e300_EQLNUM.DATA'), '%f'); %loading one value
% at the time, avoiding the "empty holes"
EQLNUMe300=EQLNUMe300{1}; % The data is organized correctly; the values are
% read row by row.


% i E100:
% LGR4   241 339   57 86    1 5
% LGR4_2 241 339   27 56    1 5

NXe100=520;
NYe100=145;

% "s" = "start"
% "e" = "end"

i_s_E100LGR4 = 241;
i_e_E100LGR4 = 339;
j_s_E100LGR4 = 57;
j_e_E100LGR4 = 86;

for i = 1:5
    j_s_E100LGR4_i(i)= j_s_E100LGR4+NYe100*(i-1);
    j_e_E100LGR4_i(i)= j_e_E100LGR4+NYe100*(i-1);
end

i_s_E100LGR4_2 = 241;
i_e_E100LGR4_2 = 339;
j_s_E100LGR4_2 = 27;
```

```
j_e_E100LGR4_2 = 56;

for i = 1:5
    j_s_E100LGR4_2_i(i)= j_s_E100LGR4_2+NYe100*(i-1);
    j_e_E100LGR4_2_i(i)= j_e_E100LGR4_2+NYe100*(i-1);
end

% We are transferring data from the LGR4 area in the E300 model to the E100
% model. LGR4 in E300 is replacing an 33x10x1 part of the main grid, and
% the refinement is 3 times in the x- and y-direction, and 20 times in the
% z-direction. I E100, on the other hand, the grid is originally more
% refined, so that additional refinement is only necessary in the
% z-direction. The area making up the new LGR in E100 is therefore
% 99x30x5, while it is 33x10x1 in E300. We therefore need to expand the
% 33x10x1 by repeating each element in the horizontal plane 3 times, before
% repeating the layer 5 times to expand to 99x30x5.

% LGR4 from E300
% 101 133   141 150    15 15
NXe300FULL=194;
NYe300FULL=176;

EQLNUM_matE100 = vec2mat(EQLNUMe100,NXe100);
EQLNUM_matE300 = vec2mat(EQLNUMe300,NXe300FULL);

i_s_E300FULL = 101;
i_e_E300FULL = 133;
j_s_E300FULL = 141;
j_e_E300FULL = 150;

j_s_E300_k15 = j_s_E300FULL + NYe300FULL*14; %multiply by K15-1 for being
% in the 15th layer.
j_e_E300_k15 = j_e_E300FULL + NYe300FULL*14;

EQLNUM_E300_k15 = ...
EQLNUM_matE300(j_s_E300_k15:j_e_E300_k15, i_s_E300FULL:i_e_E300FULL);

% Next: repeating every element in the horizontal plane 3 times, to expand
% from 33x10 to 99x30, which is the horizontal area for the new LGR in
% E100.
EQLNUM_E300_k15_exp = zeros(30,99);


% Next: making a matrix of layer 15.
EQLNUM_E300_k15_exp(1:30,1:99) = [EQLNUM_E300_k15_exp(1,1:99);
```

```
                                    EQLNUM_E300_k15_exp(1,1:99);
                                    EQLNUM_E300_k15_exp(1,1:99);
                                    EQLNUM_E300_k15_exp(2,1:99);
                                    EQLNUM_E300_k15_exp(2,1:99);
                                    EQLNUM_E300_k15_exp(2,1:99);
                                    EQLNUM_E300_k15_exp(3,1:99);
                                    EQLNUM_E300_k15_exp(3,1:99);
                                    EQLNUM_E300_k15_exp(3,1:99);
                                    EQLNUM_E300_k15_exp(4,1:99);
                                    EQLNUM_E300_k15_exp(4,1:99);
                                    EQLNUM_E300_k15_exp(4,1:99);
                                    EQLNUM_E300_k15_exp(5,1:99);
                                    EQLNUM_E300_k15_exp(5,1:99);
                                    EQLNUM_E300_k15_exp(5,1:99);
                                    EQLNUM_E300_k15_exp(6,1:99);
                                    EQLNUM_E300_k15_exp(6,1:99);
                                    EQLNUM_E300_k15_exp(6,1:99);
                                    EQLNUM_E300_k15_exp(7,1:99);
                                    EQLNUM_E300_k15_exp(7,1:99);
                                    EQLNUM_E300_k15_exp(7,1:99);
                                    EQLNUM_E300_k15_exp(8,1:99);
                                    EQLNUM_E300_k15_exp(8,1:99);
                                    EQLNUM_E300_k15_exp(8,1:99);
                                    EQLNUM_E300_k15_exp(9,1:99);
                                    EQLNUM_E300_k15_exp(9,1:99);
                                    EQLNUM_E300_k15_exp(9,1:99);
                                    EQLNUM_E300_k15_exp(10,1:99);
                                    EQLNUM_E300_k15_exp(10,1:99);
                                    EQLNUM_E300_k15_exp(10,1:99)];


% Next: expanding to make layer 15 into 5 layers.
EQLNUM_E300_k15_exp_5layers = [EQLNUM_E300_k15_exp;EQLNUM_E300_k15_exp;...
    EQLNUM_E300_k15_exp;EQLNUM_E300_k15_exp;EQLNUM_E300_k15_exp];

% Insert the LGR4 values from E300 into the E100 grid, making LGR4_e100 and
% LGR4_2_e100 (both LGR's with the same values).

EQLNUM_matE100_withE300 = EQLNUM_matE100;

for i = 0:4
EQLNUM_matE100_withE300((j_s_E100LGR4+NYe100*i):(j_e_E100LGR4+NYe100*i),...
i_s_E100LGR4:i_e_E100LGR4) = EQLNUM_E300_k15_exp;
EQLNUM_matE100_withE300((j_s_E100LGR4_2+NYe100*i):(j_e_E100LGR4_2+NYe100*i)...
,i_s_E100LGR4_2:i_e_E100LGR4_2) = EQLNUM_E300_k15_exp;
```

```
end

% Making the new matrix for E100, containing specifics from the E300 model,
% into an array. First: copies the matrix created above into a
% xxx_matE100_withE300.DATA file, before loading it in again as an array.

EQLNUMe100_withE300 = textscan(fopen('EQLNUM_matE100_withE300.DATA'),...
'%f');
%loading one value at the time, avoiding the "empty holes".
EQLNUMe100_withE300=EQLNUMe100_withE300{1};
% The data is organized correctly; the values are read row by row.

% Input tables under the REGIONS section had originally zero value for mnay
% gridblocks - not an option in Eclipse. Therefore, for the EQLNUM, SATNUM,
% FIPNUM and PVTNUM, the zeros were replaced by 1's (this does not affect
% the LGR areas, which are the only areas we are looking at).
for i = 1: length(EQLNUMe100_withE300)
    if EQLNUMe100_withE300(i)==0
        EQLNUMe100_withE300(i)=1;
    end
end
```

D.5 Replacing Grid Values in E100, Cut-Off Models

Using cut-off values to assign bedding (SATNUM) and correct kv/kh relationship for scaling of PERMZ.

```
clear
% Altering the reservoir properties using MULTIPLY

% LGR4
% Layer 15 (Tubaen) is subdivided into 20 new layers around the injection
% well.

% PERMX_input; From the LGR of E300
PERMX = textscan(fopen('tubaenPERMX.DATA'), '%f'); %loading one value at
% the time, avoiding the "empty holes"
PERMX=PERMX{1};% The data is organized correctly; the values are read row
% by row.
pe = numel(PERMX);

% PERMZ_input; From the full E300
PERMZe300 = textscan(fopen('e300_PERMZ.DATA'), '%f');
PERMZe300=PERMZe300{1};
pz3 = numel(PERMZe300);

% PERMZ_input; From E100
PERMZe100 = textscan(fopen('e100_PERMZ.DATA'), '%f');
PERMZe100=PERMZe100{1};
pz1 = numel(PERMZe100);

% PORO_input; From the LGR of E300
PORO = textscan(fopen('tubaenPORO.DATA'), '%f');
PORO=PORO{1};
po = numel(PORO);

% SATNUM_input; from E100
SATNUMe100 = textscan(fopen('e100_SATNUM.DATA'), '%f');
SATNUMe100=SATNUMe100{1};
sat = numel(SATNUMe100);


% Have checked that pe = po, and will from now on use "p" as the number of
% PERMX and PORO elements.

p = po;
```

```
% Number of layers in the new LGR4
NumberOfLayers = 20;

% Number of elements per layer:
ElementsPerLayer = p/NumberOfLayers;

PERMY = PERMX;
PERMZ = PERMX; % OBS! Instead of multiplying here, I multiply with the
% correct Kv/Kh for each individual layer and the facies type used.


% Cut off for Homogeneous (very high perm), Flaser (medium high perm) and
% Wavy (relatively low perm)

% Using the perm distribution to set cut-offs.

High = 1200; %mD, the limit where all higher
% values of permeability are not upscaled.

% Flaser is in between Low and High

Low = 110; %md, the upper limit for Wavy

Shale = 1; %mD, the upper limit for Shale


%%=================================================================
% Multiply all PERMX with the multiply value used in the original E300
% grid.
% Need to use the new perm and poro data (From tubaen_adjusted_full)
%%=================================================================

% The following scaling values are chosen to reach the defined average goal
% permeability value in each zone. The scaling is necessary as the input
% values are the original permeability tables in the E300 model.

ElementsT5 = ElementsPerLayer*4;

for i=1:ElementsT5
PERMX_LGR(i) = PERMX(i)*0.96338; %want to have about 340mD
PERMZ_LGR(i) = PERMZ(i);
end

% Making Group 2; T4 layer 5-8. 4 layers.
```

```
ElementsT4 = ElementsT5 + ElementsPerLayer*4;

for i=(ElementsT5+1):ElementsT4
PERMX_LGR(i) = PERMX(i)*0.08501;  %want to have about 30mD
PERMZ_LGR(i) = PERMZ(i);
end

% Making Group 3; Tubaen-3, layer 9-12. 4 layers.

ElementsT3 = ElementsT4 + ElementsPerLayer*4;

for i=(ElementsT4+1):ElementsT3
PERMX_LGR(i) = PERMX(i)*0.9719; %want to have about 343mD
PERMZ_LGR(i) = PERMZ(i);
end

% Making Group 4.1; The perforation interval, T2_1 layer 13-14. 2 layers.

ElementsT2_1 = ElementsT3 + ElementsPerLayer*2;

for i=(ElementsT3+1):ElementsT2_1
PERMX_LGR(i) = PERMX(i)*0.6574; %want to have about 232mD
PERMZ_LGR(i) = PERMZ(i);
end

% Making Group 4.2; Tubaen-2.2, mud. Layer 15-16. 2 layers.

ElementsT2_2 = ElementsT2_1 + ElementsPerLayer*2;

for i=(ElementsT2_1+1):ElementsT2_2
PERMX_LGR(i) = PERMX(i)*0.000284; %want to have about 0.10mD
PERMZ_LGR(i) = PERMZ(i);
end


%Making Group 5; Tubaen-1, layer 17-20. 4 layers.

ElementsT1 = ElementsT2_2 + ElementsPerLayer*4;

for i=(ElementsT2_2+1):ElementsT1
PERMX_LGR(i) = PERMX(i)*11.334; %want to have about 4000mD
PERMZ_LGR(i) = PERMZ(i);
end
```

```
%%=================================================================
% Creating new SATNUM file based on cut-offs.
% Need to make new SATNUM based on the new perm
%%=================================================================

PERMZ_LGR_new = zeros(p, 1);

for i=1:ElementsT5
     if PERMX_LGR(i)>= High
         PERMZ_LGR_new(i) = PERMZ_LGR(i)*0.1; %multiply by original kv/kh
         SAT_LGR(i) = 5; % have SATNUM 1-4 in the file already
         %(outside Tubaen)
     elseif PERMX_LGR(i)>Low % Flaser
         PERMZ_LGR_new(i) = PERMZ_LGR(i)*0.175672995; %kv/kh from upscaling
         % T5 in Flaser bedding.
         SAT_LGR(i) = 7;
     elseif PERMX_LGR(i)>Shale % Wavy
         PERMZ_LGR_new(i) = PERMZ_LGR(i)*0.002126819; %kv/kh from upscaling
         % T5 in Wavy bedding
         SAT_LGR(i) = 8;
     else%shale
         PERMZ_LGR_new(i) = PERMZ_LGR(i)*0.1; %Same kv/kh as original
         SAT_LGR(i) = 6;
     end
end


% Making Group 2; T4 layer 5-8. 4 layers. Counting from the top and down.
% Allocate the next 4*ElementsPerLayer this Group and MULTIPLY by correct
% value.

for i=(ElementsT5+1):ElementsT4
     if PERMX_LGR(i)>= High
         PERMZ_LGR_new(i) = PERMZ_LGR(i)*0.1;
         SAT_LGR(i) = 5;
     elseif PERMX_LGR(i)>Low % Flaser
         PERMZ_LGR_new(i) = PERMZ_LGR(i)*0.280743765;
         SAT_LGR(i) = 9;
      elseif PERMX_LGR(i)>Shale % Wavy
         PERMZ_LGR_new(i) = PERMZ_LGR(i)*0.02100357;
         SAT_LGR(i) = 10;
     else %shale;
         PERMZ_LGR_new(i) = PERMZ_LGR(i)*0.1;
         SAT_LGR(i) = 6;
     end
```

```
end


% Making Group 3; Tubaen-3, layer 9-12. 4 layers.

for i=(ElementsT4+1):ElementsT3
     if PERMX_LGR(i)>= High
         PERMZ_LGR_new(i) = PERMZ_LGR(i)*0.1;
         SAT_LGR(i) = 5;
     elseif PERMX_LGR(i)>Low % Flaser
         PERMZ_LGR_new(i) = PERMZ_LGR(i)*0.176871743;
         SAT_LGR(i) = 11;
     elseif PERMX_LGR(i)>Shale % Wavy
         PERMZ_LGR_new(i) = PERMZ_LGR(i)*0.002078058;
         SAT_LGR(i) = 12;
     else%shale
         PERMZ_LGR_new(i) = PERMZ_LGR(i)*0.1;
         SAT_LGR(i) = 6;
     end
end


% Making Group 4.1; The perforation interval, T2_1 layer 13-14. 2 layers.

for i=(ElementsT3+1):ElementsT2_1
     if PERMX_LGR(i)>= High
         PERMZ_LGR_new(i) = PERMZ_LGR(i)*0.1;
         SAT_LGR(i) = 5;
     elseif PERMX_LGR(i)>Low % Flaser
         % Was not upscaled in Cap limit, only in viscous
         PERMZ_LGR_new(i) = PERMZ_LGR(i)*0.18013833;
         SAT_LGR(i) = 13;
      elseif PERMX_LGR(i)>Shale % Wavy
         PERMZ_LGR_new(i) = PERMZ_LGR(i)*0.00301965;
         SAT_LGR(i) = 14;
     else%shale;
         PERMZ_LGR_new(i) = PERMZ_LGR(i)*0.1;
         SAT_LGR(i) = 6;
     end
end



% Making Group 4.2; Tubaen-2.2, mud. Layer 15-16. 2 layers.
for i=(ElementsT2_1+1):ElementsT2_2
```

```
    if PERMX_LGR(i)>= High
        PERMZ_LGR_new(i) = PERMZ_LGR(i)*0.1;
        SAT_LGR(i) = 5;
    elseif PERMX_LGR(i)>Low % Flaser
        PERMZ_LGR_new(i) = PERMZ_LGR(i)*0.770951916;
        SAT_LGR(i) = 15;
    elseif PERMX_LGR(i)>Shale % Wavy
        PERMZ_LGR_new(i) = PERMZ_LGR(i)*0.373526314;
        SAT_LGR(i) = 16;
    else%shale
        PERMZ_LGR_new(i) = PERMZ_LGR(i)*0.1;
        SAT_LGR(i) = 6;
    end
end


%Making Group 5; Tubaen-1, layer 17-20. 4 layers.
for i=(ElementsT2_2+1):ElementsT1
    if PERMX_LGR(i)>= High
        PERMZ_LGR_new(i) = PERMZ_LGR(i)*0.1;
        SAT_LGR(i) = 5;
    elseif PERMX_LGR(i)>Low % Flaser
        PERMZ_LGR_new(i) = PERMZ_LGR(i)*0.860800201;
        SAT_LGR(i) = 17;
    elseif PERMX_LGR(i)>Shale % Wavy
        PERMZ_LGR_new(i) = PERMZ_LGR(i)*0.811061107;
        SAT_LGR(i) = 18;
    else %shale
        PERMZ_LGR_new(i) = PERMZ_LGR(i)*0.1;
        SAT_LGR(i) = 6;
    end
end

% Printed PERMZ_LGR_new is the table to be used for the cut-off cases

% ========================================================================
% LGR data for E100 and E300
% ========================================================================

NXe100=520;
NYe100=145;

i_startE100LGR4 = 241;
i_endE100LGR4 = 339;
j_startE100LGR4 = 57;
```

```
j_endE100LGR4 = 86;

i_startE100LGR4_2 = 241;
i_endE100LGR4_2 = 339;
j_startE100LGR4_2 = 27;
j_endE100LGR4_2 = 56;

NXe300FULL=194;
NYe300FULL=176;

i_startE300FULL = 101;
i_endE300FULL = 133;
j_startE300FULL = 141;
j_endE300FULL = 150;

j_startE300_k15 = j_startE300FULL + NYe300FULL*14; %multiply by K15-1 for
% being in the 15th layer.
j_endE300_k15 = j_endE300FULL + NYe300FULL*14;


c = i_startE100LGR4;
d = i_endE100LGR4;
a = j_startE100LGR4;
b = j_endE100LGR4;
a_2 = j_startE100LGR4_2;
b_2 = j_endE100LGR4_2;



% ========================================================================
% Making E100 data with the cut-off-adjusted SATNUM values.
% ========================================================================

SATNUM_matE100_cutoff = vec2mat(SATNUMe100,NXe100);
SATNUM_matE100_withE300_cutoff = SATNUM_matE100_cutoff;

SAT_LGR_mat = vec2mat(SAT_LGR,(332-234+1));

%Allocate the LGR values for SATNUM to the right place in the E100 grid.
%Place every 4th 30*99 value from SAT_LGR_mat. Because 4 and 4 layers are
%alike in the E300 LGR, as we have 5 groups (each divided into 4).

SATNUM_matE100_withE300_cutoff(a:b, c:d) = SAT_LGR_mat(1:30,1:99);
SATNUM_matE100_withE300_cutoff(a_2:b_2,c:d) = SAT_LGR_mat(1:30,1:99);
```

```
SATNUM_matE100_withE300_cutoff((a+NYe100):(b+NYe100), c:d)= ...
    SAT_LGR_mat((1+4*30):(5*30),1:99);
SATNUM_matE100_withE300_cutoff((a_2+NYe100):(b_2+NYe100), c:d)= ...
    SAT_LGR_mat((1+4*30):(5*30),1:99);

SATNUM_matE100_withE300_cutoff((a+2*NYe100):(b+2*NYe100), c:d)= ...
    SAT_LGR_mat((1+8*30):(9*30),1:99);
SATNUM_matE100_withE300_cutoff((a_2+2*NYe100):(b_2+2*NYe100), c:d)= ...
    SAT_LGR_mat((1+8*30):(9*30),1:99);

SATNUM_matE100_withE300_cutoff((a+3*NYe100):(b+3*NYe100), c:d)= ...
    SAT_LGR_mat((1+12*30):(13*30),1:99);
SATNUM_matE100_withE300_cutoff((a_2+3*NYe100):(b_2+3*NYe100), c:d)= ...
    SAT_LGR_mat((1+12*30):(13*30),1:99);

SATNUM_matE100_withE300_cutoff((a+4*NYe100):(b+4*NYe100), c:d)= ...
    SAT_LGR_mat((1+16*30):(17*30),1:99);
SATNUM_matE100_withE300_cutoff((a_2+4*NYe100):(b_2+4*NYe100), c:d)= ...
    SAT_LGR_mat((1+16*30):(17*30),1:99);


SATNUMe100_withE300_cutoff = ...
    textscan(fopen('SATNUM_matE100_withE300_cutoff.DATA'), '%f'); %loading
% one value at the time, avoiding the "empty holes"
SATNUMe100_withE300_cutoff=SATNUMe100_withE300_cutoff{1}; % The data is
%organized correctly; the values are read row by row.

for i = 1:(length(SATNUMe100_withE300_cutoff))
    if SATNUMe100_withE300_cutoff(i)==0
        SATNUMe100_withE300_cutoff(i)=1;
    end
end

SATNUMe100_withE300_cutoff_Krzz = SATNUMe100_withE300_cutoff+18;

% ========================================================================
% Making E100 data with the cut-off-adjusted PERMZ values.
% ========================================================================

PERMZ_matE100_cutoff = vec2mat(PERMZe100,NXe100);
PERMZ_matE100_withE300_cutoff = PERMZ_matE100_cutoff;
PERMZ_LGR_mat = vec2mat(PERMZ_LGR,(332-234+1));

%Allocate the LGR values for PERMZ to the right place in the E100 grid.
%Place every 4th 30*99 value from PERMZ_LGR_mat. Because 4 and 4 layers are
```

```
%alike in the E300 LGR, as we have 5 groups (each divided into 4).

PERMZ_matE100_withE300_cutoff(a:b, c:d) = PERMZ_LGR_mat(1:30,1:99);
PERMZ_matE100_withE300_cutoff(a_2:b_2,c:d) = PERMZ_LGR_mat(1:30,1:99);

PERMZ_matE100_withE300_cutoff((a+NYe100):(b+NYe100), c:d)= ...
    PERMZ_LGR_mat((1+4*30):(5*30),1:99);
PERMZ_matE100_withE300_cutoff((a_2+NYe100):(b_2+NYe100), c:d)= ...
    PERMZ_LGR_mat((1+4*30):(5*30),1:99);

PERMZ_matE100_withE300_cutoff((a+2*NYe100):(b+2*NYe100), c:d)= ...
    PERMZ_LGR_mat((1+8*30):(9*30),1:99);
PERMZ_matE100_withE300_cutoff((a_2+2*NYe100):(b_2+2*NYe100), c:d)= ...
    PERMZ_LGR_mat((1+8*30):(9*30),1:99);

PERMZ_matE100_withE300_cutoff((a+3*NYe100):(b+3*NYe100), c:d)= ...
    PERMZ_LGR_mat((1+12*30):(13*30),1:99);
PERMZ_matE100_withE300_cutoff((a_2+3*NYe100):(b_2+3*NYe100), c:d)= ...
    PERMZ_LGR_mat((1+12*30):(13*30),1:99);

PERMZ_matE100_withE300_cutoff((a+4*NYe100):(b+4*NYe100), c:d)= ...
    PERMZ_LGR_mat((1+16*30):(17*30),1:99);
PERMZ_matE100_withE300_cutoff((a_2+4*NYe100):(b_2+4*NYe100), c:d)= ...
    PERMZ_LGR_mat((1+16*30):(17*30),1:99);


PERMZe100_withE300_cutoff = ...
    textscan(fopen('PERMZ_matE100_withE300_cutoff.DATA'), '%f'); %loading
% one value at the time, avoiding the "empty holes"
PERMZe100_withE300_cutoff=PERMZe100_withE300_cutoff{1}; % The data is
% organized correctly; the values are read row by row.
```

D.6 Replacing Grid Values in E100, Flaser Models

Assigns bedding (SATNUM) and correct kv/kh relationship for scaling of PERMZ in Flaser models.

```
clear
% Changed the MULTIPLY values

% LGR4
% Layer 15 (Tubaen) is subdivided into 20 new layers around the injection
% well.

% PERMX_input; From the LGR of E300
PERMX = textscan(fopen('tubaenPERMX.DATA'), '%f'); %loading one value at
% the time, avoiding the "empty holes"
PERMX=PERMX{1};
pe = numel(PERMX);

% PERMZ_input; From the full E300
PERMZe300 = textscan(fopen('e300_PERMZ.DATA'), '%f'); %loading one value at
% the time, avoiding the "empty holes"
PERMZe300=PERMZe300{1};
pz3 = numel(PERMZe300);

% PERMZ_input; From E100
PERMZe100 = textscan(fopen('e100_PERMZ.DATA'), '%f'); %loading one value at
% the time, avoiding the "empty holes"
PERMZe100=PERMZe100{1};
pz1 = numel(PERMZe100);

% PORO_input; From the LGR of E300
PORO = textscan(fopen('tubaenPORO.DATA'), '%f'); %loading one value at the
% time, avoiding the "empty holes"
PORO=PORO{1}; % The data is organized correctly; the values are read row by
% row.
po = numel(PORO);

% SATNUM_input; from E100
SATNUMe100 = textscan(fopen('e100_SATNUM.DATA'), '%f'); %loading one value
% at the time, avoiding the "empty holes"
SATNUMe100=SATNUMe100{1};
sat = numel(SATNUMe100);
```

```
% Have checked that pe = po, and will from now on use "p" as the number of
% PERMX and PORO elements.

p = po;

% Number of layers in the new LGR4
NumberOfLayers = 20;

% Number of elements per layer:
ElementsPerLayer = p/NumberOfLayers;

PERMY = PERMX;
PERMZ = PERMX; % OBS! Instead of multiplying here, I multiply with the
% correct Kv/Kh for each individual layer and the facies type used.


% Cut off for Homogeneous (very high perm), Flaser (medium high perm) and
% Wavy (relatively low perm)


% Using the perm distribution to set cut offs.

High = 1200; %mD, the limit where all higher
% values of permeability are not upscaled.

Low = 110; %md, the upper limit for Wavy

Shale = 1; %mD, the upper limit for Shale

% Flaser is in between Low and High



%%================================================================
% Multiply all PERMX with the multiply value used in the original E300
% grid.
% Need to use the new perm and poro data (From tubaen_adjusted_full)
%%================================================================

ElementsT5 = ElementsPerLayer*4;

for i=1:ElementsT5
PERMX_LGR(i) = PERMX(i)*0.96338; %want to have about 340mD
PERMZ_LGR(i) = PERMZ(i);
end
```

```
% Making Group 2; T4 layer 5-8. 4 layers.

ElementsT4 = ElementsT5 + ElementsPerLayer*4;

for i=(ElementsT5+1):ElementsT4
PERMX_LGR(i) = PERMX(i)*0.08501;  %want to have about 30mD
PERMZ_LGR(i) = PERMZ(i);
end

% Making Group 3; Tubaen-3, layer 9-12. 4 layers.

ElementsT3 = ElementsT4 + ElementsPerLayer*4;

for i=(ElementsT4+1):ElementsT3
PERMX_LGR(i) = PERMX(i)*0.9719; %want to have about 343mD
PERMZ_LGR(i) = PERMZ(i);
end

% Making Group 4.1; The perforation interval, T2_1 layer 13-14. 2 layers.

ElementsT2_1 = ElementsT3 + ElementsPerLayer*2;

for i=(ElementsT3+1):ElementsT2_1
PERMX_LGR(i) = PERMX(i)*0.6574; %want to have about 232mD
PERMZ_LGR(i) = PERMZ(i);
end

% Making Group 4.2; Tubaen-2.2, mud. Layer 15-16. 2 layers.

ElementsT2_2 = ElementsT2_1 + ElementsPerLayer*2;

for i=(ElementsT2_1+1):ElementsT2_2
PERMX_LGR(i) = PERMX(i)*0.000284; %want to have about 0.10mD
PERMZ_LGR(i) = PERMZ(i);
end


%Making Group 5; Tubaen-1, layer 17-20. 4 layers.

ElementsT1 = ElementsT2_2 + ElementsPerLayer*4;

for i=(ElementsT2_2+1):ElementsT1
PERMX_LGR(i) = PERMX(i)*11.334; %want to have about 4000mD
PERMZ_LGR(i) = PERMZ(i);
```

```
end



%%=================================================================
% Creating new SATNUM file based on cutoffs.
% Need to make new SATNUM based on the new perm
%%=================================================================

PERMZ_LGR_new = zeros(p, 1);

for i=1:ElementsT5 % Flaser
         PERMZ_LGR_new(i) = PERMZ_LGR(i)*0.175672995;
         SAT_LGR(i) = 7;
end


% Making Group 2; T4 layer 5-8. 4 layers. Counting from the top and down.
% Allocate the next 4*ElementsPerLayer this Group and MULTIPLY by correct value.

for i=(ElementsT5+1):ElementsT4 % Flaser
         PERMZ_LGR_new(i) = PERMZ_LGR(i)*0.280743765;
         SAT_LGR(i) = 9;
end


% Making Group 3; Tubaen-3, layer 9-12. 4 layers.

for i=(ElementsT4+1):ElementsT3 % Flaser
         PERMZ_LGR_new(i) = PERMZ_LGR(i)*0.176871743;
         SAT_LGR(i) = 11;
end


% Making Group 4.1; The perforation interval, T2_1 layer 13-14. 2 layers.

for i=(ElementsT3+1):ElementsT2_1 % Flaser
         % Was not upscaled in Cap limit, only in viscous
         PERMZ_LGR_new(i) = PERMZ_LGR(i)*0.18013833;
         SAT_LGR(i) = 13;
end
```

```
% Making Group 4.2; Tubaen-2.2, mud. Layer 15-16. 2 layers.

for i=(ElementsT2_1+1):ElementsT2_2 % Flaser
         PERMZ_LGR_new(i) = PERMZ_LGR(i)*0.770951916;
         SAT_LGR(i) = 15;
end


%Making Group 5; Tubaen-1, layer 17-20. 4 layers.

for i=(ElementsT2_2+1):ElementsT1 % Flaser
         PERMZ_LGR_new(i) = PERMZ_LGR(i)*0.860800201;
         SAT_LGR(i) = 17;
end

%PERMZ_LGR_new is the table to be used for the cutoff cases

% ========================================================================
% LGR data for E100 and E300
% ========================================================================

NXe100=520;
NYe100=145;

i_startE100LGR4 = 241;
i_endE100LGR4 = 339;
j_startE100LGR4 = 57;
j_endE100LGR4 = 86;

i_startE100LGR4_2 = 241;
i_endE100LGR4_2 = 339;
j_startE100LGR4_2 = 27;
j_endE100LGR4_2 = 56;

NXe300FULL=194;
NYe300FULL=176;

i_startE300FULL = 101;
i_endE300FULL = 133;
j_startE300FULL = 141;
j_endE300FULL = 150;

j_startE300_k15 = j_startE300FULL + NYe300FULL*14; %multiply by K15-1 for
% being in the 15th layer.
j_endE300_k15 = j_endE300FULL + NYe300FULL*14;
```

```
c = i_startE100LGR4;
d = i_endE100LGR4;
a = j_startE100LGR4;
b = j_endE100LGR4;
a_2 = j_startE100LGR4_2;
b_2 = j_endE100LGR4_2;



% ========================================================================
% Making E100 data with the cut-off-adjusted SATNUM values.
% ========================================================================

SATNUM_matE100_cutoff = vec2mat(SATNUMe100,NXe100);
SATNUM_matE100_withE300_cutoff = SATNUM_matE100_cutoff;

SAT_LGR_mat = vec2mat(SAT_LGR,(339-241+1));

%Allocate the LGR values for SATNUM to the right place in the E100 grid.
%Place every 4th 30*99 value from SAT_LGR_mat. Because 4 and 4 layers are
%alike in the E300 LGR, as we have 5 groups (each divided into 4).

SATNUM_matE100_withE300_cutoff(a:b, c:d) = SAT_LGR_mat(1:30,1:99);
SATNUM_matE100_withE300_cutoff(a_2:b_2,c:d) = SAT_LGR_mat(1:30,1:99);

SATNUM_matE100_withE300_cutoff((a+NYe100):(b+NYe100), c:d)= ...
    SAT_LGR_mat((1+4*30):(5*30),1:99);
SATNUM_matE100_withE300_cutoff((a_2+NYe100):(b_2+NYe100), c:d)= ...
    SAT_LGR_mat((1+4*30):(5*30),1:99);

SATNUM_matE100_withE300_cutoff((a+2*NYe100):(b+2*NYe100), c:d)= ...
    SAT_LGR_mat((1+8*30):(9*30),1:99);
SATNUM_matE100_withE300_cutoff((a_2+2*NYe100):(b_2+2*NYe100), c:d)= ...
    SAT_LGR_mat((1+8*30):(9*30),1:99);

SATNUM_matE100_withE300_cutoff((a+3*NYe100):(b+3*NYe100), c:d)= ...
    SAT_LGR_mat((1+12*30):(13*30),1:99);
SATNUM_matE100_withE300_cutoff((a_2+3*NYe100):(b_2+3*NYe100), c:d)= ...
    SAT_LGR_mat((1+12*30):(13*30),1:99);

SATNUM_matE100_withE300_cutoff((a+4*NYe100):(b+4*NYe100), c:d)= ...
    SAT_LGR_mat((1+16*30):(17*30),1:99);
SATNUM_matE100_withE300_cutoff((a_2+4*NYe100):(b_2+4*NYe100), c:d)= ...
```

```
    SAT_LGR_mat((1+16*30):(17*30),1:99);


SATNUMe100_withE300_cutoff = ...
    textscan(fopen('SATNUM_matE100_withE300_cutoff.DATA'), '%f'); %loading
% one value at the time, avoiding the "empty holes"
SATNUMe100_withE300_cutoff=SATNUMe100_withE300_cutoff{1}; % The data is
% organized correctly; the values are read row by row.

for i = 1:(length(SATNUMe100_withE300_cutoff))
    if SATNUMe100_withE300_cutoff(i)==0
        SATNUMe100_withE300_cutoff(i)=1;
    end
end

SATNUMe100_withE300_cutoff_Krzz = SATNUMe100_withE300_cutoff+18;

% ========================================================================
% Making E100 data with the cut-off-adjusted PERMZ values.
% ========================================================================

PERMZ_matE100_cutoff = vec2mat(PERMZe100,NXe100);
PERMZ_matE100_withE300_cutoff = PERMZ_matE100_cutoff;
PERMZ_LGR_mat = vec2mat(PERMZ_LGR,(339-241+1));

%Allocate the LGR values for PERMZ to the right place in the E100 grid.
%Place every 4th 30*99 value from PERMZ_LGR_mat. Because 4 and 4 layers are
%alike in the E300 LGR, as we have 5 groups (each divided into 4).

PERMZ_matE100_withE300_cutoff(a:b, c:d) = PERMZ_LGR_mat(1:30,1:99);
PERMZ_matE100_withE300_cutoff(a_2:b_2,c:d) = PERMZ_LGR_mat(1:30,1:99);

PERMZ_matE100_withE300_cutoff((a+NYe100):(b+NYe100), c:d)= ...
    PERMZ_LGR_mat((1+4*30):(5*30),1:99);
PERMZ_matE100_withE300_cutoff((a_2+1+NYe100):(b_2+1+NYe100), c:d)= ...
    PERMZ_LGR_mat((1+4*30):(5*30),1:99);

PERMZ_matE100_withE300_cutoff((a+2*NYe100):(b+2*NYe100), c:d)= ...
    PERMZ_LGR_mat((1+8*30):(9*30),1:99);
PERMZ_matE100_withE300_cutoff((a_2+1+2*NYe100):(b_2+1+2*NYe100), c:d)= ...
    PERMZ_LGR_mat((1+8*30):(9*30),1:99);

PERMZ_matE100_withE300_cutoff((a+3*NYe100):(b+3*NYe100), c:d)= ...
    PERMZ_LGR_mat((1+12*30):(13*30),1:99);
PERMZ_matE100_withE300_cutoff((a_2+3*NYe100):(b_2+3*NYe100), c:d)= ...
```

```
    PERMZ_LGR_mat((1+12*30):(13*30),1:99);

PERMZ_matE100_withE300_cutoff((a+4*NYe100):(b+4*NYe100), c:d)= ...
    PERMZ_LGR_mat((1+16*30):(17*30),1:99);
PERMZ_matE100_withE300_cutoff((a_2+4*NYe100):(b_2+4*NYe100), c:d)= ...
    PERMZ_LGR_mat((1+16*30):(17*30),1:99);


PERMZe100_withE300_cutoff = ...
    textscan(fopen('PERMZ_matE100_withE300_cutoff.DATA'), '%f'); %loading
% one value at the time, avoiding the "empty holes"
PERMZe100_withE300_cutoff=PERMZe100_withE300_cutoff{1}; % The data is
% organized correctly; the values are read row by row.
```

D.7 Replacing Grid Values in E100, Wavy Models

Assigns bedding (SATNUM) and correct kv/kh relationship for scaling of PERMZ in Wavy models.

```
clear
% Changed the MULTIPLY values

% LGR4
% Layer 15 (Tubaen) is subdivided into 20 new layers around the injection
% well.

% PERMX_input; From the LGR of E300
PERMX = textscan(fopen('tubaenPERMX.DATA'), '%f'); %loading one value at
% the time, avoiding the "empty holes"
PERMX=PERMX{1}; % The data is organized correctly
pe = numel(PERMX);

% PERMZ_input; From the full E300
PERMZe300 = textscan(fopen('e300_PERMZ.DATA'), '%f');
PERMZe300=PERMZe300{1};
pz3 = numel(PERMZe300);

% PERMZ_input; From E100
PERMZe100 = textscan(fopen('e100_PERMZ.DATA'), '%f');
PERMZe100=PERMZe100{1};
pz1 = numel(PERMZe100);

% PORO_input; From the LGR of E300
PORO = textscan(fopen('tubaenPORO.DATA'), '%f');
PORO=PORO{1};
po = numel(PORO);

% SATNUM_input; from E100
SATNUMe100 = textscan(fopen('e100_SATNUM.DATA'), '%f');
SATNUMe100=SATNUMe100{1};
sat = numel(SATNUMe100);


% Have checked that pe = po, and will from now on use "p" as the number of
% PERMX and PORO elements.

p = po;
```

```
% Number of layers in the new LGR4
NumberOfLayers = 20;

% Number of elements per layer:
ElementsPerLayer = p/NumberOfLayers;

PERMY = PERMX;
PERMZ = PERMX; % OBS! Instead of multiplying here, I multiply with the
% correct Kv/Kh for each individual layer and the facies type used.


% Cut off for Homogeneous (very high perm), Flaser (medium high perm) and
% Wavy (relatively low perm)

% Using the perm distribution to set cut offs.

High = 1200; %mD, the limit where all higher
% values of permeability are not upscaled.

Low = 110; %md, the upper limit for Wavy

Shale = 1; %mD, the upper limit for Shale

% Flaser is in between Low and High




%%=================================================================
% Multiply all PERMX with the multiply value used in the original E300
% grid.
% Need to use the new perm and poro data (From tubaen_adjusted_full)
%%=================================================================

ElementsT5 = ElementsPerLayer*4;

for i=1:ElementsT5
PERMX_LGR(i) = PERMX(i)*0.96338; %want to have about 340mD
PERMZ_LGR(i) = PERMZ(i);
end

% Making Group 2; T4 layer 5-8. 4 layers.

ElementsT4 = ElementsT5 + ElementsPerLayer*4;
```

```
for i=(ElementsT5+1):ElementsT4
PERMX_LGR(i) = PERMX(i)*0.08501;  %want to have about 30mD
PERMZ_LGR(i) = PERMZ(i);
end

% Making Group 3; Tubaen-3, layer 9-12. 4 layers.

ElementsT3 = ElementsT4 + ElementsPerLayer*4;

for i=(ElementsT4+1):ElementsT3
PERMX_LGR(i) = PERMX(i)*0.9719; %want to have about 343mD
PERMZ_LGR(i) = PERMZ(i);
end

% Making Group 4.1; The perforation interval, T2_1 layer 13-14. 2 layers.

ElementsT2_1 = ElementsT3 + ElementsPerLayer*2;

for i=(ElementsT3+1):ElementsT2_1
PERMX_LGR(i) = PERMX(i)*0.6574; %want to have about 232mD
PERMZ_LGR(i) = PERMZ(i);
end

% Making Group 4.2; Tubaen-2.2, mud. Layer 15-16. 2 layers.

ElementsT2_2 = ElementsT2_1 + ElementsPerLayer*2;

for i=(ElementsT2_1+1):ElementsT2_2
PERMX_LGR(i) = PERMX(i)*0.000284; %want to have about 0.10mD
PERMZ_LGR(i) = PERMZ(i);
end


%Making Group 5; Tubaen-1, layer 17-20. 4 layers.

ElementsT1 = ElementsT2_2 + ElementsPerLayer*4;

for i=(ElementsT2_2+1):ElementsT1
PERMX_LGR(i) = PERMX(i)*11.334; %want to have about 4000mD
PERMZ_LGR(i) = PERMZ(i);
end
```

```
%%=================================================================
% Creating new SATNUM file based on cutoffs.
% Need to make new SATNUM based on the new perm
%%=================================================================

PERMZ_LGR_new = zeros(p, 1);

for i=1:ElementsT5 % Wavy
         PERMZ_LGR_new(i) = PERMZ_LGR(i)*0.002126819;
         SAT_LGR(i) = 8;
end

% Making Group 2; T4 layer 5-8. 4 layers. Counting from the top and down.
% Allocate the next 4*ElementsPerLayer this Group and MULTIPLY by correct
% value.

for i=(ElementsT5+1):ElementsT4 % Wavy
         PERMZ_LGR_new(i) = PERMZ_LGR(i)*0.02100357;
         SAT_LGR(i) = 10;
end

% Making Group 3; Tubaen-3, layer 9-12. 4 layers.

for i=(ElementsT4+1):ElementsT3 % Wavy
         PERMZ_LGR_new(i) = PERMZ_LGR(i)*0.002078058;
         SAT_LGR(i) = 12;
end

% Making Group 4.1; The perforation interval, T2_1 layer 13-14. 2 layers.

for i=(ElementsT3+1):ElementsT2_1 % Wavy
         PERMZ_LGR_new(i) = PERMZ_LGR(i)*0.00301965;
         SAT_LGR(i) = 14;
end

% Making Group 4.2; Tubaen-2.2, mud. Layer 15-16. 2 layers.

for i=(ElementsT2_1+1):ElementsT2_2 % Wavy
         PERMZ_LGR_new(i) = PERMZ_LGR(i)*0.373526314;
         SAT_LGR(i) = 16;
end


%Making Group 5; Tubaen-1, layer 17-20. 4 layers.
```

```
for i=(ElementsT2_2+1):ElementsT1 %Wavy
        PERMZ_LGR_new(i) = PERMZ_LGR(i)*0.811061107;
        SAT_LGR(i) = 18;
end

%PERMZ_LGR_new is the table to be used for the cutoff cases

% ========================================================================
% LGR data for E100 and E300
% ========================================================================

NXe100=520;
NYe100=145;

i_startE100LGR4 = 241;
i_endE100LGR4 = 339;
j_startE100LGR4 = 57;
j_endE100LGR4 = 86;

i_startE100LGR4_2 = 241;
i_endE100LGR4_2 = 339;
j_startE100LGR4_2 = 27;
j_endE100LGR4_2 = 56;

NXe300FULL=194;
NYe300FULL=176;

i_startE300FULL = 101;
i_endE300FULL = 133;
j_startE300FULL = 141;
j_endE300FULL = 150;

j_startE300_k15 = j_startE300FULL + NYe300FULL*14; %multiply by K15-1 for
% being in the 15th layer.
j_endE300_k15 = j_endE300FULL + NYe300FULL*14;


c = i_startE100LGR4;
d = i_endE100LGR4;
a = j_startE100LGR4;
b = j_endE100LGR4;
a_2 = j_startE100LGR4_2;
b_2 = j_endE100LGR4_2;
```

```
% ========================================================================
% Making E100 data with the cut-off-adjusted SATNUM values.
% ========================================================================

SATNUM_matE100_cutoff = vec2mat(SATNUMe100,NXe100);
SATNUM_matE100_withE300_cutoff = SATNUM_matE100_cutoff;

SAT_LGR_mat = vec2mat(SAT_LGR,(339-241+1));

%Allocate the LGR values for SATNUM to the right place in the E100 grid.
%Place every 4th 30*99 value from SAT_LGR_mat. Because 4 and 4 layers are
%alike in the E300 LGR, as we have 5 groups (each divided into 4).

SATNUM_matE100_withE300_cutoff(a:b, c:d) = SAT_LGR_mat(1:30,1:99);
SATNUM_matE100_withE300_cutoff(a_2:b_2,c:d) = SAT_LGR_mat(1:30,1:99);

SATNUM_matE100_withE300_cutoff((a+NYe100):(b+NYe100), c:d)= ...
    SAT_LGR_mat((1+4*30):(5*30),1:99);
SATNUM_matE100_withE300_cutoff((a_2+NYe100):(b_2+NYe100), c:d)= ...
    SAT_LGR_mat((1+4*30):(5*30),1:99);

SATNUM_matE100_withE300_cutoff((a+2*NYe100):(b+2*NYe100), c:d)= ...
    SAT_LGR_mat((1+8*30):(9*30),1:99);
SATNUM_matE100_withE300_cutoff((a_2+2*NYe100):(b_2+2*NYe100), c:d)= ...
    SAT_LGR_mat((1+8*30):(9*30),1:99);

SATNUM_matE100_withE300_cutoff((a+3*NYe100):(b+3*NYe100), c:d)= ...
    SAT_LGR_mat((1+12*30):(13*30),1:99);
SATNUM_matE100_withE300_cutoff((a_2+3*NYe100):(b_2+3*NYe100), c:d)= ...
SAT_LGR_mat((1+12*30):(13*30),1:99);

SATNUM_matE100_withE300_cutoff((a+4*NYe100):(b+4*NYe100), c:d)= ...
    SAT_LGR_mat((1+16*30):(17*30),1:99);
SATNUM_matE100_withE300_cutoff((a_2+4*NYe100):(b_2+4*NYe100), c:d)= ...
    SAT_LGR_mat((1+16*30):(17*30),1:99);


SATNUMe100_withE300_cutoff = ...
    textscan(fopen('SATNUM_matE100_withE300_cutoff.DATA'), '%f'); %loading
% one value at the time, avoiding the "empty holes"
SATNUMe100_withE300_cutoff=SATNUMe100_withE300_cutoff{1}; % The data is
% organized correctly; the values are read row by row.

for i = 1:(length(SATNUMe100_withE300_cutoff))
```

```
    if SATNUMe100_withE300_cutoff(i)==0
        SATNUMe100_withE300_cutoff(i)=1;
    end
end


SATNUMe100_withE300_cutoff_Krzz = SATNUMe100_withE300_cutoff+18;

% ========================================================================
% Making E100 data with the cut-off-adjusted PERMZ values.
% ========================================================================

PERMZ_matE100_cutoff = vec2mat(PERMZe100,NXe100);
PERMZ_matE100_withE300_cutoff = PERMZ_matE100_cutoff;
PERMZ_LGR_mat = vec2mat(PERMZ_LGR,(339-241+1));

%Allocate the LGR values for PERMZ to the right place in the E100 grid.
%Place every 4th 30*99 value from PERMZ_LGR_mat. Because 4 and 4 layers are
%alike in the E300 LGR, as we have 5 groups (each divided into 4).

PERMZ_matE100_withE300_cutoff(a:b, c:d) = PERMZ_LGR_mat(1:30,1:99);
PERMZ_matE100_withE300_cutoff(a_2:b_2,c:d) = PERMZ_LGR_mat(1:30,1:99);

PERMZ_matE100_withE300_cutoff((a+NYe100):(b+NYe100), c:d)= ...
    PERMZ_LGR_mat((1+4*30):(5*30),1:99);
PERMZ_matE100_withE300_cutoff((a_2+NYe100):(b_2+NYe100), c:d)= ...
    PERMZ_LGR_mat((1+4*30):(5*30),1:99);

PERMZ_matE100_withE300_cutoff((a+2*NYe100):(b+2*NYe100), c:d)= ...
    PERMZ_LGR_mat((1+8*30):(9*30),1:99);
PERMZ_matE100_withE300_cutoff((a_2+2*NYe100):(b_2+2*NYe100), c:d)= ...
    PERMZ_LGR_mat((1+8*30):(9*30),1:99);

PERMZ_matE100_withE300_cutoff((a+3*NYe100):(b+3*NYe100), c:d)= ...
    PERMZ_LGR_mat((1+12*30):(13*30),1:99);
PERMZ_matE100_withE300_cutoff((a_2+3*NYe100):(b_2+3*NYe100), c:d)= ...
    PERMZ_LGR_mat((1+12*30):(13*30),1:99);

PERMZ_matE100_withE300_cutoff((a+4*NYe100):(b+4*NYe100), c:d)= ...
PERMZ_LGR_mat((1+16*30):(17*30),1:99);
PERMZ_matE100_withE300_cutoff((a_2+4*NYe100):(b_2+4*NYe100), c:d)= ...
    PERMZ_LGR_mat((1+16*30):(17*30),1:99);


PERMZe100_withE300_cutoff = ...
```

```
    textscan(fopen('PERMZ_matE100_withE300_cutoff.DATA'), '%f'); %loading
% one value at the time, avoiding the "empty holes"
PERMZe100_withE300_cutoff=PERMZe100_withE300_cutoff{1}; % The data is
% organized correctly; the values are read row by row.
```

Bibliography

Bachu, S. and Bennion, D. B. (2009). Dependence of co2-brine interfacial tension on aquifer pressure, temperature and water salinity. *Energy Procedia*, 1(1):3157–3164.

Benson, S., Pini, R., Reynolds, C., and Krevor, S. (2013). Relative permeability analysis to describe multi-phase flow in co2 storage reservoirs. Technical Report 2, Global CCS Inst.

Christie, M. A. (2001). Flow in porous media - scale up of multiphase flow. *Current Opinion in Colloid and Interface Science Volume*, 6(3):236–241.

Hansen, O., Gilding, D., Nazarian, B., Osdal, B., Ringrose, P., Kristoffersen, J.-B., Eiken, O., and Hansen, H. (2013). Snøhvit: the history of injecting and storing 1 mt co 2 in the fluvial tubåen fm. *Energy Procedia*, 37:3565–3573.

Jonoud, S. and Jackson, M. D. (2008). New criteria for the validity of steady-state upscaling. *Transport in Porous Media*, 71(1):53–73.

Krause, M. and Benson, S. (2015). Accurate determination of characteristic relative permeability curves. *Advances in Water Resources*, 83:376–388.

Kumar, A. T., Jerauld, G., et al. (1996). Impacts of scale-up on fluid flow from plug to gridblock scale in reservoir rock. In *SPE/DOE Improved Oil Recovery Symposium*. Society of Petroleum Engineers.

Martin, A. (2000). Flaser and wavy bedding in ephemeral streams: a modern and an ancient example. *Sedimentary Geology*, 136(1):1–5.

Morrow, N. R., Harris, C. C., et al. (1965). Capillary equilibrium in porous materials. *Society of Petroleum Engineers Journal*, 5(01):15–24.

Nilsen, H. M., Herrera, P. A., Ashraf, M., Ligaarden, I., Iding, M., Hermanrud, C., Lie, K., Nordbotten, J. M., Dahle, H. K., and Keilegavlen, E. (2011). Field-case simulation of co2 -plume migration using vertical-equilibrium models. *Energy Procedia*, 4:3801–3808.

Pham, T., Maast, T., Hellevang, H., and Aagaard, P. (2011). Numerical modeling including hysteresis properties for co2 storage in tubåen formation, snøhvit field, barents sea. *Energy Procedia*, 4:3746–3753.

Pickup, G. E., Ringrose, P. S., and Sharif, A. (2000). Steady-state upscaling: From lamina-scale to full-field model. *SPE Journal*, 5(02):208–217.

Pickup, G. E., Sorbie, K. S., et al. (1996). The scaleup of two-phase flow in porous media using phase permeability tensors. *SPE journal*, 1(04):369–382.

Pickup, G. E. and Stephen, K. D. (2000). An assessment of steady-state scale-up for small-scale geological models. *Petroleum Geoscience*, 6(3):203–210.

Reynolds, C. A. and Krevor, S. (2015). Characterizing flow behavior for gas injection: Relative permeability of co2-brine and n2-water in heterogeneous rocks. *Water Resources Research*, 51:9464–9489.

Ringrose, P., Sorbie, K., Corbett, P., and Jensen, J. (1993). Immiscible flow behaviour in laminated and cross-bedded sandstones. *Journal of Petroleum Science and Engineering*, 9(2):103–124.

Ringrose, P. S. and Bentley, M. (2015). *Reservoir Model Design*. Springer.

Singh, V. P., Cavanagh, A., Hansen, H., Nazarian, B., Iding, M., Ringrose, P. S., et al. (1981). Reservoir modeling of co2 plume behavior calibrated against monitoring data from sleipner, norway. In *SPE Annual Technical Conference and Exhibition*. Society of Petroleum Engineers.

Statoil ASA (2010). Snøhvit co2 tubåen fm. storage capacity and injection strategy study. http://www.miljodirektoratet.no/Global/dokumenter/horinger/Sladdet%20versjon%20-%20vedlegg%205%20-%20Technology%20Achievement%202010%20Sn%C3%B8hvit%20CO2%20storage.pdf?epslanguage=no. Accessed: 2017-03-09.

Virnovsky, G. A., Friis, H. A., and Lohne, A. (2004). A steady-state upscaling approach for immiscible two-phase flow. *Transport in Porous Media*, 54(2):167–192.

Wiki.opmproject.org (2017). Upscaling relative permeability in capillary limit. http://wiki.opm-project.org/index.php?title=Upscaling_relative_permeability_in_capillary_limit. Accessed: 2016-11-28.

Yokoyama, Y., Lake, L. W., et al. (1981). The effects of capillary pressure on immiscible displacements in stratified porous media. In *SPE Annual Technical Conference and Exhibition*. Society of Petroleum Engineers.

Zhou, D., Fayers, F., Orr Jr, F., et al. (1997). Scaling of multiphase flow in simple heterogeneous porous media. *SPE Reservoir Engineering*, 12(03):173–178.